NOTICE

AVIS

The quality of this microform is heavily dependent upon the quality of the original thesis submitted for microfilming. Every effort has been made to ensure the highest quality of reproduction possible.

If pages are missing, contact the university which granted the degree.

Some pages may have indistinct print especially if the original pages were typed with a poor typewriter ribbon or if the university sent us an inferior photocopy.

Reproduction in full or in part of this microform is governed by the Canadian Copyright Act, R.S.C. 1970, c. C-30, and subsequent amendments.

La qualité de cette microforme dépend grandement de la qualité de la thèse soumise au microfilmage. Nous avons tout fait pour assurer une qualité supérieure de reproduction.

S'il manque des pages, veuillez communiquer avec l'université qui a conféré le grade

La qualité d'impression de certaines pages peut laisser à désirer, surtout si les pages originales ont été dactylographiées à l'aide d'un ruban usé ou si l'université nous a fait parvenir une photocopie de qualité inférieure

La reproduction, même partielle, de cette microforme est soumise à la Loi canadienne sur le droit d'auteur, SRC 1970, c. C-30, et ses amendements subséquents

THE UNIVERSITY OF ALBERTA

A FLUID INCLUSION AND LIGHT STABLE ISOTOPE STUDY OF ANTIMONY-ASSOCIATED GOLD MINERALIZATION IN THE BRIDGE RIVER DISTRICT, BRITISH COLUMBIA, CANADA.

by

Pierre J. Maheux

A THESIS

SUBMITTED TO THE FACULTY OF GRADUATE STUDIES AND RESEARCH IN PARTIAL FULFILMENT OF THE REQUIREMENTS FOR THE DEGREE OF MASTER OF SCIENCE.

DEPARTMENT OF GEOLOGY

EDMONTON, ALBERTA

Spring, 1989

ISBN 0-315-52790-0

Canada

THE UNIVERSITY OF ALBERTA

RELEASE FORM

NAME OF AUTHOR: Pierre J. Maheux

TITLE OF THESIS: A FLUID INCLUSION AND LIGHT STABLE ISOTOPE

STUDY OF ANTIMONY-ASSOCIATED GOLD

MINERALIZATION IN THE BRIDGE RIVER DISTRICT,

BRITISH COLUMBIA, CANADA.

DEGREE: Master of Science

YEAR THIS
DEGREE GRANTED: Spring, 1989

Permission is hereby granted to THE UNIVERSITY OF ALBERTA LIBRARY to reproduce single copies of this thesis and to lend or sell such copies for private, scholarly or scientific research purposes only.

The author reserves other publication rights, and neither the thesis nor extensive extracts from it may be printed or otherwise reproduced without the author's written permission.
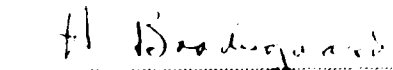
Pierre J. Maheux
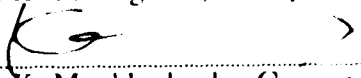
30 Paultiel Drive
Toronto, Ontario, CANADA
M2M 3P3
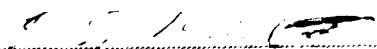
DATE: April 26, 1989.
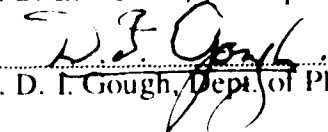
THE UNIVERSITY OF ALBERTA

FACULTY OF GRADUATE STUDIES AND RESEARCH

The undersigned certify that they have read, and recommend to the Faculty of Graduate Studies and Research, for acceptance, a thesis entitled *A Fluid Inclusion and Light Stable Isotope Study of Antimony-Associated Gold Mineralization in the Bridge River District, British Columbia, Canada*. submitted by Pierre J. Maheux in partial fulfilment for the requirements for the degree of Master of Science.

Dr. H. Baadsgaard, Examiner

Dr. K. Muehlenbachs, Co-Supervisor

Dr. B. E. Nesbitt, Co-Supervisor

Dr. D. I. Gough, Dept. of Physics

Date: *April 6, 1989*

To all graduate students for their efforts, but mostly
for my parents.

ABSTRACT

The Bridge River District is underlain by Mesozoic sedimentary and volcanic rocks that occur within a structurally complex, northwest-trending belt that flanks the eastern margin of the Coast Plutonic Complex. The Bridge River mining camp remains British Columbia's foremost historical gold producer. Most of the production was from mesothermal lode deposits in the southwest part of the camp. However, significant historical production of antimony-associated gold from hydrothermal vein and replacement deposits in the centre of the camp has prompted renewed interest in these smaller deposits.

Antimony-associated precious metal mineralization occupies shears in units of the Bridge River complex, a tectonostratigraphic assemblage of chert, greenstone, gabbro, serpentinite, limestone and clastic rocks ranging in age from at least Middle Triassic to Early Jurassic. The host rocks are hydrothermally altered to variable assemblages of carbonate-sericite±fuchsite-pyrite-arsenopyrite. Alteration envelopes may extend to 5 metres, but rarely exceed 1 metre in width.

Two styles of mineralization fall within the antimony metallogenetic zone in the district. Sb-Au-Ag±Hg is characterized by quartz-carbonate lodes and replacement bodies with massive stibnite and lesser amounts of pyrite and arsenopyrite. The paragenetic sequence can be divided into 2 to 3 stages. Quartz-ankerite±calcite with pyrite and arsenopyrite characterize the early stage. The main stage of mineralization is dominated by the deposition of quartz and massive stibnite. Main to late stage mineralization consists of open space-filling by quartz-carbonate with minor to accessory amounts of tetrahedrite, sphalerite, jamesonite, marcasite and cinnabar. Gold is a late phase and is most often associated with stibnite as fracture fillings and inclusions. Gold is also associated with pyrite, arsenopyrite and late cinnabar. Typical Au/Ag ratios range from 1.2 to 2.0.

Base metal-enriched Ag-Au±Sb mineralization also occurred through 2 to 3 stages. Quartz-ankerite (±calcite) lodes are dominated by early to main stage pyrite, arsenopyrite, chalcopyrite and sphalerite. Lesser amounts of jamesonite, stibnite, tetrahedrite, galena,

pyrrhotite and marcasite also characterize the main stage. Late stage mineralization consists of quartz, gold and minor base metal sulphides and possible tellurides. Gold is most commonly associated with jamesonite, galena, chalcopyrite and arsenopyrite. Typical Au/Ag ratios range from 0.2 to 0.35.

Fluid inclusion data indicate deposition from low-CO_2 ($X_{CO_2} = 0.05$), dilute (3-4 eq. wt. % NaCl) hydrothermal brines at temperatures around 300°C. Locally, data from base metal-enriched mineralization indicate CO_2-rich fluids ($X_{CO_2} = 0.9$) responsible for ore deposition. Fluid inclusion and light stable isotope data suggest .. Au-Ag±Hg mineralization formed at slightly lower temperatures (285° ±25°C) and at pressures (200 to 350 bars) than base metal-enriched mineralization, 310° ±15°C and 300 to 500 bars respectively.

Stable isotope analyses of oxygen, hydrogen and carbon in gangue minerals and inclusion fluids in quartz from both styles of mineralization show a large enrichment in $\delta^{18}O$ (ca. +20 to +24‰ SMOW, combined quartz and carbonate), and indicate no significant component of fresh meteoric water in the hydrothermal fluids. Water liberated from inclusions in quartz from Sb-Au-Ag±Hg mineralization is depleted in deuterium (-129 ±9‰ SMOW), which suggests derivation of the ore fluid from meteoric water with subsequent ^{18}O-enrichment. However, δD analyses of sericites from alteration assemblages have metamorphic values (-30 to 40‰ SMOW) but may reflect the latest pre-mineralization metamorphic event. Analyses of $\delta^{13}C$ in carbonates range from -12.5 to -5‰ (PDB) and probably reflect a heterogeneous source for carbon in the hydrothermal system.

The data in the present study support a model for district-wide Au-Sb-Hg mineralization from a unique meteoric-derived hydothermal fluid, highly enriched in ^{18}O that deposited mineralization in a sequence controlled by pressure and temperature. The resultant camp-scale metallogenetic pattern is elementally, mineralogically and isotopically zoned.

ACKNOWLEDGEMENTS

TABLE OF CONTENTS

TABLE OF CONTENTS (Continued)

TABLE OF CONTENTS (Continued)

TABLE OF CONTENTS (Continued)

TABLE OF CONTENTS (Continued)

LIST OF TABLES

xiv

LIST OF FIGURES

LIST OF FIGURES (Continued)

I. INTRODUCTION

1.0 General Statement

The Bridge River mining district in the southwestern Canadian Cordillera offers a unique opportunity to examine the genesis of gold mineralization within the context of a varied camp scale metallogeny and the context of a Cordilleran scale genetic model. This study attempts to clarify the role played by several antimony-associated gold deposits in the district within these contexts.

The Bridge River district, centered 180 km northeast of Vancouver (Figure 1-1), remains foremost in total gold production in British Columbia. Five of the 73 mineral localities in the camp achieved production. Of these five the Pioneer-Bralorne complex dominates with approximately 7.25 million tonnes of ore mined and in excess of 129,000 kg gold and 29,000 kg silver produced. The Wayside mine achieved a production of 166.0 kg gold and 26.0 kg silver from approximately 37,000 tonnes mined. The Minto mine attained figures of 546.0 kg gold and 1,573.0 kg silver from 79,073 tonnes mined, while the Congress mine produced 2.5 kg gold and 1.3 kg of silver from 943 tonnes of ore mined (Harrop and Sinclair, 1986).

Historically, principal interest has been in precious metals, but antimony, tungsten, and mercury deposits have all been found and worked to varying degrees suggesting the diversity of mineralization within the camp. This study focuses on a group of gold deposits and occurrences in the centre of the district, including: the past producers Minto and Congress; two newer discoveries adjacent to the Congress mine, the Howard and Lou zones; and lastly the Olympic prospect.

Rising gold prices stimulated renewed exploration activity in the district in the past several years. This activity in turn has recently prompted the Geological Survey Branch of the British Columbia Ministry of Energy, Mines, and Petroleum Resources to undertake
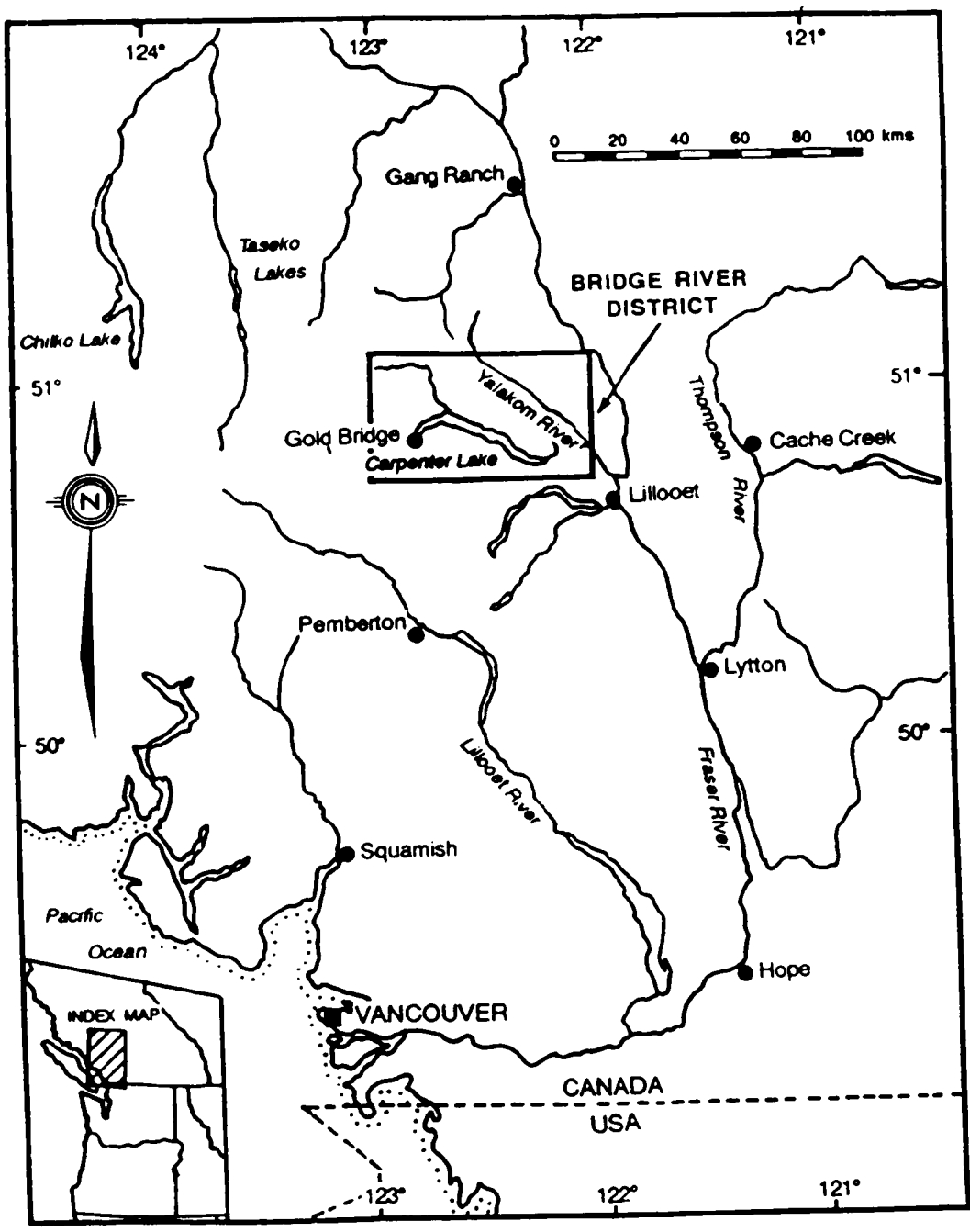
Figure 1-1. Location map.

regional mapping and property evaluations in the camp. Several companies were actively involved in exploration and development in the camp during the 1986 field season.

1.1 Location, Access, and Physiography

Location

The Bridge River mining camp lies about 180 kilometres nort'i or Vancouver, British Columbia, on the eastern flank of the Coast Rang· ͽ cov·ʼʼ᷈ng an ɑːʽɑ ᴐf mountainous terrain bounded roughly by Cadwallader C·ˀːₖ on the soɯ:ˑ ʌ ᴐd Tyaughton Creek on the north (Figure 3-1). The region is bounded by the quadrangle defined by latitudes 50°40' N and 51°05' N and longitudes 122°45' W and 123°00' W and is covered by parts of the Bralorne (92 J/15), Noaxe (92 O/2), Birkenhead (92 J/10), and Bridge River (92 J/16) NTS map sheets. Deposits and mineral occurrences investigated in this study are in the centre of the district east of the village of Gold Bridge, north and south of Carpenter Lake.

Access

Access to the district is by vehicle from Vancouver, 145 kilometres east on Highway 1 to Hope, 225 kilometres north on Highways 1 and 12 to Lillooet, and 100 kilometres west on gravel road to Gold Bridge. A more direct route follows Highway 99 north from Vancouver 150 kilometres to Pemberton, where a further 30 kilometres of hard surface road terminates at the Lillooet River. Access to the district from this point is by four-wheel-drive vehicle for 45 kilometres on a logging trunk road which traverses the divide between the Lillooet River and the Bridge River valley.

Within the Bridge River district good access is afforded by major gravel and logging roads. Four-wheel-drive is required to access the more remote occurrences logging and exploration tracks. Often a hike of some distance to a showing was necessary where the route had become impassable for a vehicle.

Physiography

The Bridge River district lies on the eastern flank of the Coast Range mountains, its northeastern corner forming a part of the transition belt of mountains separating the Coast Range proper from the Interior Plateau of British Columbia. A rugged topography persists with elevations ranging from 600 to 2600 metres. The valleys are steep walled and rise to narrow ridge tops. The northern slopes are generally more precipitous while southern slopes are more regular. Main tributaries to the Bridge River valley, most notably the Hurley River, Cadwallader Creek, and Tyaughton Creek, occupy valleys typically trough-shaped in profile. The tributaries enter the main valley through canyons that cut deeply into hanging valleys.

The higher, narrower ridge tops and the post glacial canyons along the main valley provide continuous exposures of bedrock for some distance. Elsewhere, however, much of the area is drift covered and outcrops are absent, or at best, small and scattered. Much of the lower valley slopes are mantled by glacial drift that supports forest vegetation which extends nearly to the summits of the less precipitous slopes. The valley bottoms are mostly formed of glacial, fluvioglacial, and recent stream deposits in places as much as tens of metres thick. Carpenter Lake presently occupies the valley of the Bridge River from Gold Bridge east approximately 45 kilometres. The lake was created by the construction of the Terzaghi Dam on the Bridge River in the early 1950's and subsequently flooded many of the lower workings on several properties.

1.2 Exploration History

McCann (1922) documents the history of mining in the Bridge River district as commencing in 1858, when placer miners, chiefly from California, prospected the area and recovered placer gold from the bed of the Bridge River near its confluence with the Fraser. In 1859 a discovery was made at Gun Creek just east of Gold Bridge. Good grades were also found on Tyaughton Creek and worked extensively by Chinese miners who followed the Californians.

In the 1880's gravels of the Hurley River were worked with fairly good returns. In 1886 gold was also found on Cadwallader Creek, a tributary of the Hurley. These discoveries diverted interest from the Bridge River valley and led to the discovery of gold-quartz lode deposits in 1896 on the east bank of the Hurley River, just below the mouth of Cadwallader Creek.

Development of the Cadwallader Creek gold belt progressed slowly through the turn of the century. As of 1915, C.W. Drysdale (1915, 1917) noted that in addition to the gold-quartz deposits, there were partly developed silver-copper and antimony veins, most notably on the north and south sides of Bridge River, east of Gold Bridge.

Minor production (ca. 7.5 kg gold) continued during and after the First World War. McCann (1922) observed that the mining properties in the district were still in the prospect stage, except those of the Cadwallader Creek gold belt, where there were a few well established mines, most notably the Wayside, Lorne, and Pioneer. He stated that no development work of any importance had been carried out on any other types of deposits other than the gold quartz veins.

These gold lodes continued to dominate the camp but by the Second World War Cairnes (1937, 1943) had included antimony, mercury, and tungsten as deposit classifications in their own right. The Minto, Congress, and Olympic deposits had all been initially developed between the years 1930 and 1937, but by 1943 only the Minto and the

Congress mines were producing with extensive underground development. The Olympic prospect had experienced considerable development work by this time but Cairnes suggested that neither quantity nor grade had yet afforded much likelihood of commercial production. Cairnes (1943) had also included the Dauntless prospect near the Minto mine, as a significant showing of gold mineralization .

Development of the Minto and Congress mines continued into the 1940's with production reaching 80,000 tonnes grading 6.8 g/t gold and 1,000 tonnes grading 2.7 g/t gold respectively. Production at the Congress mine was on a test scale only (Harrop and Sinclair, 1986).

The Howard vein was discovered in 1959, west of the Congress mine, and developed by Bralorne-Pioneer Mines Limited between 1960 and 1964. Exploration was renewed in the immediate area between 1976 and 1981 when two junior mining companies based in Vancouver drilled and drifted on the Howard zone. Surface surveys were extended in 1984 leading to the discovery of the Lou zone between the Howard vein and the Congress deposit. The same companies resumed surface exploration of the Minto mine, discovering several new showings in the past two years (Cooke et al., 1986).

While activity in the central part of the Bridge River camp was waning in the middle of the century the Pioneer-Bralorne, or Cadwallader Creek, gold belt had been gaining noteriety as the foremost gold producer in British Columbia and was to attain the rank of 6th largest in Canada by the close of production in 1971. Presently, many companies are investigating the potential for future gold production from this historically rich belt.

1.3 Previous Geologic Work

Exploration activity throughout this century and the development of the large gold mines in the upper Bridge River Valley stimulated several geologic studies. Early workers recognized that the Bridge River area formed an important link in Cordilleran structure as it

encompasses the transition zone of mountains connecting the Coast Range with the Interior Plateau of British Columbia. Similarily, modern workers have recognized its importance as the region falls within the boundary zone between crustal blocks that came to be called the Intermontane and Insular composite terranes (Terranes I and II).

The first reconnaissance reports on the geology of the Bridge River area were published by Camsell (1911) and Bateman (1912). A more comprehensive study was initiated by Drysdale (1915, 1917) and continued by McCann ('922). McCann's work represents the earliest comprehensive report on the area, including topographic and geologic maps. Economic sections of the report are devoted, mainly, to a discussion of the lode gold deposits of Cadwallader Creek in the southwest.

The next major contribution was that of C.E. Cairnes (1937). In a report on the geology of the Bridge River camp Cairnes modified the geology of McCann and Drysdale and provided a more rigorous classification of ore deposits in the camp. A second report by Cairnes (1943) further expanded his work of 1937 to include the Tyaughton Lake area in the central and northern part of the camp to secure more complete information on the sequence and age of the formations in the area.

More recent reconnaissance summaries of the geology of the district were provided by Roddick and Hutchison (1973) and Woodsworth (1977). The most recent work comprises regional mapping and property evaluations by provincial geologists (Church, 1987; Church et al., 1988).

More in-depth geologic studies are represented by C.J. Potter's (1983) and M.E. Rusmore's (1985) Ph.D. dissertations. Potter conducted a detailed structural and metamorphic study of the Bridge River complex, just east of the mining camp. In the west Rusmore (1985) investigated the geology and tectonic significance of the Upper Triassic Cadwallader Group and its bounding faults.

Several studies related to the economic geology of the district have been conducted to date. Pearson (1976) proposed that two mineralized centres are apparent in the camp; one

in the vicinity of the Bralorne-Pioneer mine complex, and the other in the area of the Minto mine. He reviewed the geologic associations of mineralization and attempted to date mineralization at both centres.

Pearson's work was inspired by that of Woodsworth *et al.* (1977) who had initiated a study of metal distribut' ins in the camp. Their work led to the identification of a generalized but systematic zoning pattern of mineralization on a camp scale.

Harrop and Sinclair (1986) undertook a re-evaluation of the production data from the Bridge River camp prompted by the resurgence of gold exploration ir the area. Their work echoes that of Pearson in that they outlined two types of precious metal-bearing mineralization in the district; the Bralorne and Congress types. According to their study Congress-type occurrences differ from the Bralorne-type in that they have less obvious geologic controls; they are not characterized by high gold to silver ratios; and they have greater concentrations of other metals, notably antimony.

While the studies mentioned above have included work on mineralization in the central part of the camp most, as well as others (Joubin, 1948; Bacon, 1978; Leitch and Godwin, 1987), have focused on the Pioneer-Bralorne centre due to its stature as a gold producer.

1.4 Purpose of the Study

While the recorded production from the Pioneer-Bralorne centre remains impressive, a significant potential for gold production has been recognized in several deposits in the centre of the Bridge River mining camp. These deposits, and other smaller occurrences, share general characteristics, including; geologic and structural setting, a large component of sulphide mineralization, and similar metal associations.

Previous workers (Woodsworth *et al.*, 1977) have documented a metal distribution pattern within the camp extending about 30 kilometres from gold in the southwest, through

a central antimony zone, to a mercury zone in the northeast. Others (Pearson, 1975; Harrop and Sinclair, 1986) have recognized a fundamental difference in precious metal occurrences in the camp, namely "gold zone" occurrences (Pioneer-Bralorne) versus "antimony zone" occurrences (Congress, Minto).

The purpose of this study is to investigate the geochemistry of the mineralizing fluids in several deposits and occurrences in the context of an antimony-gold association and in the context of a camp scale "antimony zone".

Specific objectives include:

(i) Determine the para,   esis of precious metals in the deposits;

(ii) Determine the physio-chemical conditions of min   , fluids;
    composition, temperature, and pressure;

(iii) Investigate the origin and evolution of mineralizing ".

(iv) Formulate a model for ore deposition.

Fieldwork was carried out over six weeks in the summer of 1986. Thirteen deposits and occurrences were sampled and a suite of host rocks and regional units was collected.

The mineralogy and paragenesis of ore mineralization were investigated through the examination of 40 thin sections, 60 polished-thin sections, and 13 polished blocks. The composition, temperature, and pressure of the mineralizing fluids were determined by fluid inclusion analyses of vein quartz and carbonate in 37 doubly polished sections. Light stable isotope analyses of oxygen, hydrogen, and carbon from over 220 samples of vein minerals and alteration phases were used to investigate fluid composition, origin, evolution, and temperature.

II. REGIONAL GEOLOGY

2.0 Introduction

The Bridge River mining district is in an area which occupies a unique tectonic and geologic setting in the southwest Canadian Cordillera. The district is situated in a complex boundary area between two large composite tectono-stratigraphic terranes, Terrane I and Terrane II. The boundary area is characterized by several smaller terranes not part of either composite terrane (Rusmore, 1987). The district incorporates portions of three of these smaller crustal fragments: the Bridge River terrane; the Cadwallader terrane; and the Methow-Tyaughton terrane.

The documentation of the Canadian Cordillera as a collage of distinct mappable "terranes" has evolved through the efforts of many workers (Tempelman-Kluit, 1979; Coney et al., 1980; Price et al., 1981,1985; Monger et al., 1982; Monger, 1984; Gabrielse, 1985). Each constituent terrane is delineated by an identifiable tectono-stratigraphic assemblage generated in a unique setting.

Pre-Cretaceous terranes in British Columbia compose two allochthonous composite terranes; Terrane I in the east and Terrane II in the west (Figure 2-1). Small, originally independent terranes are thought to have amalgamated by latest Triassic-earliest Jurassic time forming Terrane I prior to accretion to the ancient margin of the craton in the Jurassic. Terranes composing Terrane II coalesced by the Late Jurassic and were attached to the new continental margin during the Cretaceous (Monger et al., 1982; Monger, 1984). The eastern accretionary join is represented by the Omineca Crystalline Belt, while the Coast Putonic Complex represents the western join (Monger, 1984).

1 0
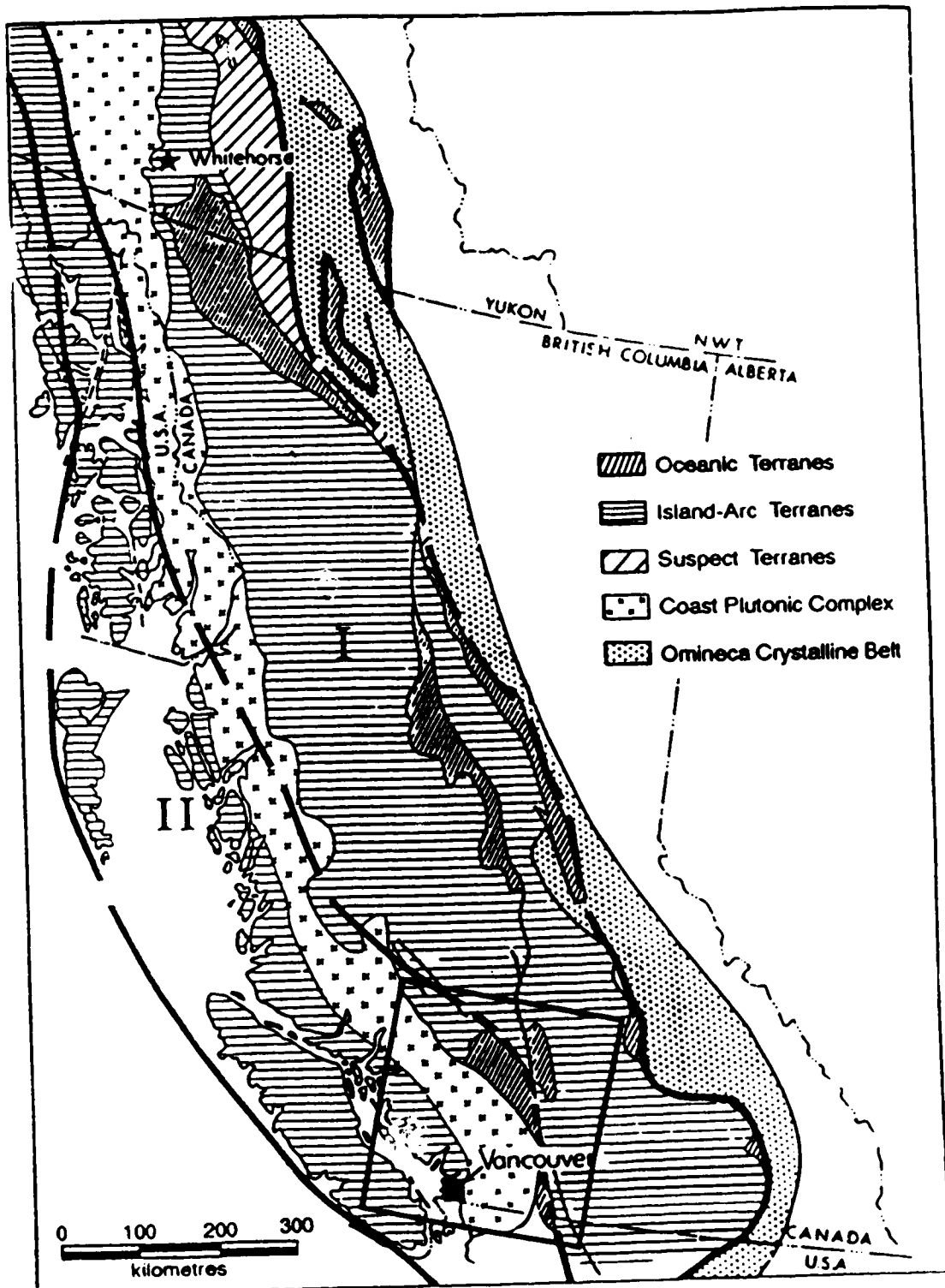
Figure 2-1. Distribution of allochthonous (or suspect) terranes in the Canadian Cordillera. Heavy lines enclose terranes (I, II) composed of small, originally independent terranes that amalgamated prior to accretion to the western margin of the North American craton. Box outlines the approximate boundaries of Figure 2-2. Modified from Monger (1984).

2.1 Tectonic Setting

In the northwestern Canadian Cordillera the Coast Plutonic Complex obscures the Terrane I-Terrane II boundary; in the southwest the boundary is obscured by several fault-bounded minor Mesozoic terranes (Rusmore, 1987). The Bridge River mining district is set amongst these smaller crustal blocks, straddling the boundary between the Bridge River terrane and the Cadwallader terrane, and bounded to the north by the Methow-Tyaughton terrane (Figure 2-2).

The Middle Triassic to Middle Jurassic Bridge River terrane became juxtaposed with the slightly younger Cadwallader terrane, to the west and northwest, in Middle Jurassic time, after which the terranes functioned as a single tectonic block (Rusmore, 1987). The present position and age of the Bridge River and Cadwallader terranes imply accretion later than Terrane I and earlier than Terrane II.

A portion of the Early to mid-Cretaceous Methow-Tyaughton terrane abuts the Bridge River and Cadwallader terranes in the north of the study are: This terrane straddles the Yalakom fault zone to the northeast and records only a fraction . entire dextral displacement the region has experienced (Kleinspehn, 1985).

The location of the Terrane I-Terrane II join in the region is the subject of some debate. Rusmore (1987) suggests that Wrangellia, the easternmost terrane within Terrane II, is separate from the Cadwallader terrane thereby placing the Terrane I-Terrane II join west of the Cadwallader terrane. Previously it was suggested that the Cadwallader terrane represents the eastern edge of Wrangellia that was faulted against Terrane I (Tipper et al., 1981; Tipper, 1984; Kleinspehn, 1985). In either case, the Cadwallader terrane and the Bridge River terrane are intruded by the easternmost elements of the Coast Plutonic Complex. Results of paleomagnetic studies of the plutonic rocks suggest that Terrane II and the Coast Plutonic Complex may have been displaced northward relative to North America by about 2400 kilometres since the mid-Cretaceous (Irving et al., 1985).
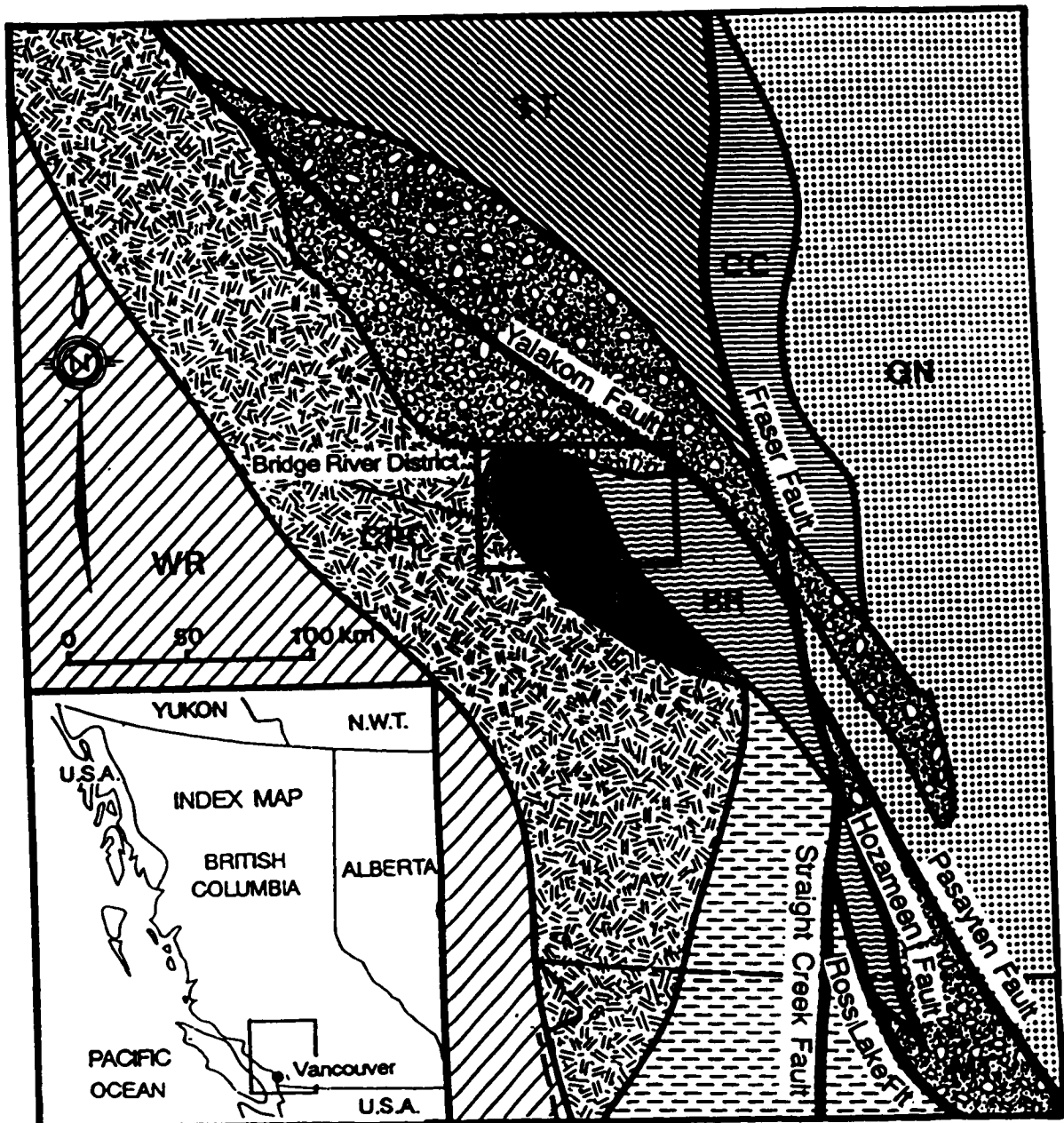
Figure 2-2. Location of the Bridge River Mining District relative to tectono-stratigraphic
terranes in the southwest Canadian Cordillera. Nomenclature and modified map from
Monger *et al.* (1982), Monger (1984), Kleinspehn (1985), and Rusmore (1987). Terranes:
BR=Bridge River, CC=Cache Creek, CD=Cadwallader, CPC=Coast Plutonic Complex,
MT=Methow-Tyaughton, QN=Quesnellia, ST=Stikinia, WR=Wrangellia. Horizontal
dashed pattern denotes other terranes exposed between composite Terranes I and II. Late
Cretaceous to Early Tertiary faults are labelled.

2.2 Bridge River Terrane

Three major elements of the Bridge River terrane are present in the vicinity of the Bridge River district. Potter (1986) has designated these the Carpenter Lake assemblage, the Bridge River schists, and the Shulaps ultramafic complex (Figure 2-3). The first two units together compose the "Bridge River complex". The Carpenter Lake assemblage is the most extensive and is essentially equivalent to the Fergusson Group of Cairnes (1943) and the Bridge River Group of Roddick and Hutchison (1973). The Carpenter Lake assemblage is the oldest known unit in the area consisting of a Middle Triassic through Middle Jurassic sequence of thinly bedded radiolarion chert, argillite, intercalated basaltic flows, and minor limestone. Locally abundant volcaniclastic flows are present and serpentinite is exposed along some fault zones. Nowhere is the base of the unit exposed.

The Carpenter Lake assemblage and the Bridge River schists to the north are juxtaposed by the high angle Marshall Creek fault. The Bridge River schists are thought to be the metamorphic equivalent of the Carpenter Lake assemblage. The metamorphic grade of the schists ranges from prehnite-pumpellyite to lower amphibolite facies (Potter, 1983).

The allochthonous Shulaps ultramafic complex was thrust over the Bridge River schists in the Mesozoic. The Shulaps thrust is marked by extensive schistose serpentinite and a metamorphic aureole developed in the schists (Potter, 1983). The ultramafic complex is exposed over 180 square kilometres and consists mainly of variably serpentinized harzburgite. A Mesozoic phase of deformation and metamorphism was related to the emplacement of the Shulaps complex. Tertiary deformation resulted in recumbent folding of the earlier thrust related fabric (Potter, 1983). Early phases of deformation in all elements of the Bridge River terrane are thought to record accretion. Potter (1986) notes that the location of the Bridge River terrane, inboard of the eastern extent of Wrangellia, suggests that the deformation of the terrane, and the Cadwallader terrane, represents the closing of a sea and an adjacent arc in response to the approach and collision of Wrangellia.

2.3 Cadwallader Terrane

The Bridge River complex and the coeval Cadwallader terrane to the west are juxtaposed by the Eldorado fault zone. The most recent work on the Cadwallader terrane (Rusmore, 1987) recognizes two stratigraphic units: the Tyaughton Group and the Cadwallader Group (Figure 2-3). Together these groups are interpreted as an arc-related terrane with the thrust presently separating them representing internal disruption of a coherent stratigraphic sequence.

The Upper Triassic Cadwallader Group is the older of the two; the younger clastic rocks of the late Triassic to middle Jurassic Tyaughton Group are not significantly represented within the study area. The Cadwallader Group comprises three formations according to Roddick and Hutchison's (1973) work: the Noel, the Pioneer, and the Hurley. The Noel Formation was dropped in Rusmore's (1985) revised stratigraphy.

The Pioneer Formation comprises greenstone breccias, pillow basalts, flows and minor diabasic gabbro. Minor andesite and rhyolite are also present. The rocks were metamorphosed to sub-greenschist facies and lack a penetrative fabric. The ages of these rocks are unknown, but they may have been the source of andesite and rhyolite clasts in the overlying early Norian Hurley Formation (Rusmore, 1985).

The Hurley Formation comprises two members: a local, lower volcaniclastic member and a widespread turbidite member. Interbedded basalt and sedimentary rocks characterize the volcaniclastic member of the Hurley. Tuffaceous sandstone is the most comm sedimentary rock type, but conglomerate, sandstone, and minor limestone also Estimates of the true thickness of the Cadwallader Group are uncertain but it is 2,000 metres thick (Rusmore, 1985).
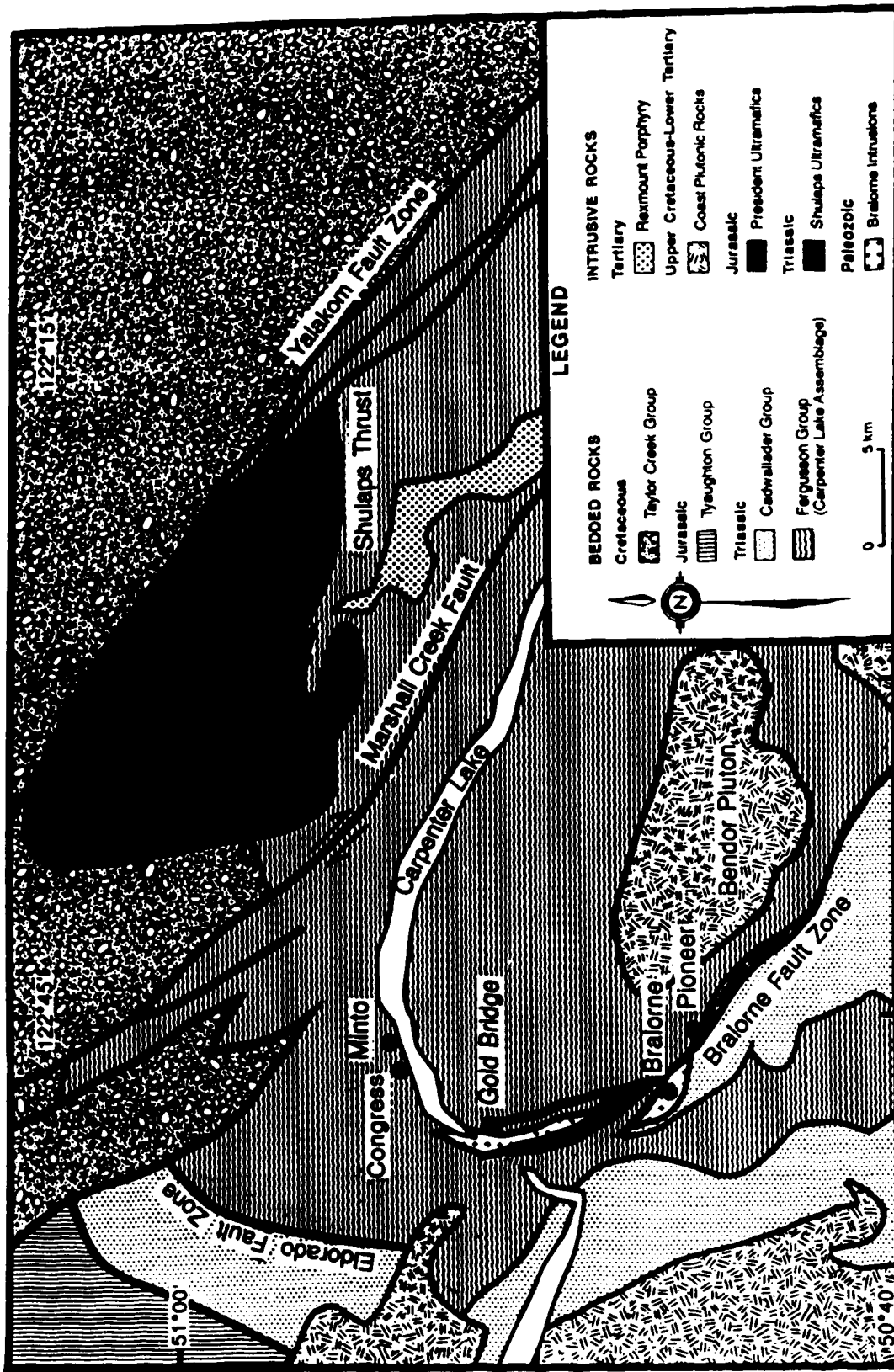
Figure 2-3. Generalized geology of the Bridge River District. Modified from Caimes (1943), Roddick and Hutchison (1973), Potter (1983), Rusmore (1985), and Church (1987).

Two phases of deformation affected the Cadwallader Group; the north-northeast trending Eldorado fault zone, which juxtaposes the Cadwallader Group with the Bridge River complex to the east is thought to be a D_1 structure (Rusmore, 1987). The fault is truncated in the south by the Bralorne fault zone. The second phase of deformation produced northward verging thrusts and folds which Rusmore suggests may have formed in a transpressive regime accompanying Cretaceous-Tertiary displacement along the Yalakom and Fraser fault systems.

2.4 Methow-Tyaughton Terrane: Taylor Creek Group

The Methow-Tyaughton terrane is represented in the study area by the Aptian-Albian Taylor Creek Group (Figure 2-3), which is in fault contact with the Cadwallader Group and the Bridge River complex to the south. The Taylor Creek Group consists mainly of black to dark grey shale and sub-greywacke. Chert pebble conglomerate and interbeds of tuff, breccia, and dark green to purple basaltic flows are characteristic. The source of fragments in the clastic rocks is believed to be the Hurley Formation and the Carpenter Lake assemblage. The thickness is estimated at 1,300 metres near the north edge of the district (Roddick and Hutchison, 1973).

2.5 Intrusive Rocks

The main igneous intrusions in the area are the Paleozoic Bralorne diorite, the Mesozoic President ultramafic rocks and Coast Plutonic rocks and the Tertiary Rexmount porphyry (Figure 2-3). In addition, throughout the map area there is a variety of Mesozoic and Tertiary dykes and sills (Church, 1987).

The Bralorne diorite is a very fine to coarse-grained dark greenish-gray rock. The composition of the rock ranges to gabbro, especially where coarse-grained. The diorite is

gradational to trondhjemite in places. These rocks have been dated as Early Permian by

uranium-lead on zircons (minimum age 270 ±5 Ma; Leitch and Godwin, 1988).

The Early Permian President ultramafic rocks form lenticular bodies within the

Bralorne fault zone. Other major zones of ultramafic rocks are coincident with major faults,

notably the Eldorado fault zone. Sever?! smaller ultramafic bodies, for the most part

converted to serpentinite, are common throughout the Carpenter Lake assemblage

coincident with more local shears.

The Coast Plutonic rocks comprise an assortment of Upper Cretaceous to Lower

Tertiary granitic plutons in the w.:st. The Bendor stock south of Carpenter Lake and east of

the Pioneer-Bralorne gold belt is the \oun,.-st of these. The rocks are mostly hornblende

granodiorite with accessory biotite and :)I...ne.

Mesozoic and Tertiary dykes and sills throughout the area are mafic to intermediate

in composition . They are commonly fine-grained and massive and less deformed than their

hosts (Church, 1987).

2.6 Regional Structure

The most prominent structural characteristics of the region are major faults marking

the boundaries of principal structural regimes. The regional trend is north-northwest, with

the Eldorado fault a notable exception trending north-northeast. On a local scale the rocks

are structurally chaotic. Potter (1986) suggests that the northwest regional trend records

deformation associated with synaccretion shearing along transcurrent faults which

juxtaposed the Bridge River complex and the Cadwallader Group with other Mesozoic

elements in the southwest Canadian Cordillera. Early structures have been strongly over-

printed during late Cretaceous and early Tertiary northwest transport (Potter, 1986).

Within the Bridge River Group repeated cycles of folding and faulting are recorded

but obscured by slump structures and repeated faulting. The Hurley beds in the

Cadwallader Group to the west record only part of this history; only two periods of 1 . rmation have been identified by Rusmore (1985).

Broad throughgoing structures within the Bridge River terrane and the Cadwallader terrane (Bralorne fault zone, Eldorado fault zone, Marshall Creek fault) are mimicked on a smaller scale and commonly serve as loci for mineral deposits in the region (Cairnes, 1943).

2.7 Summary

The Bridge River district lies at the junction of two allochthonous, tectono-stratigraphic terranes located between two larger composite terranes in the southwest Canadian Cordillera. Knowledge of the timing of accretion of these crustal blocks, their subsequent deformation and later dextral strike-slip translations is necessary to understand the setting into which mineralization in the Bridge River district was emplaced.

The two major units represented in the district, the Bridge River terrane and the Cadwallader terrane, are thought to have acted as a single block sometime after their amalgamation in Middle Jurassic time. Their present position and age imply accretion later than the accretion of Terrane I and earlier than Terrane II. The controversy as to whether the Cadwallader terrane represents the eastern margin of Terrane II or lies inboard of that margin speaks to the timing of emplacement of the Bridge River-Cadwallader block and by extension, to the paleogeographic position of mineralization hosted in these crustal blocks.

III. MINERAL DEPOSITS AND OCCURRENCES

3.0 Introduction

Mineral deposits and occurrences in the Bridge River mining district have been characterized as part of a regional metallogenetic zonation pattern across 35 kilometres in a northe. terly direction (Figure 3-1). Woodsworth *et al.* (1977) documented that a gold zone in the southwest is overlapped to the northeast by an antimony zone which extends to the northeast and, in turn, is partially overlapped by a mercury zone. Specifically, two dominant styles of mineralization have been described within this pattern; the Bralorne-Pioneer, versus the Congress-type of deposits (Pearson, 1976). Deposits and occurrences considered in the present study; Congress, Howard, Lou, Dauntless, Minto, Olympic, are Congress-type deposits and fall within a central Au-Ag-Sb±Hg zone in the district. Table 3-1 summarizes the characteristics of the deposits and occurrences included in this study and compares them with those of three Bralorne-Pioneer-type deposits. Congress-type deposits have lower gold to silver ratios than Bralorne-Pioneer-type deposits and they are characterized by abundant mixed sulphides and a high antimony content.

In this study the Congress-type classification is subdivided into two categories on the basis of differences in ore mineralogies, Au/Ag ratios and base metal concentrations among the deposits (Table 3-1). The Congress, Howard, Lou, and Dauntless occurrences are grouped into a Sb-Au-Ag±Hg category while the Minto and Olympic deposits are grouped into a base metal-enriched Ag-Au±Sb category.

Cairnes (1937) was the first to record that in some deposits stibnite is the abundant sulphide phase associated with minor gold mineralization while in other deposits a variety of ore minerals are present and the value of the deposits rests on the combined gold and antimony content. The Sb-Au-Ag±Hg deposits have fewer sulphide phases, higher gold to silver ratios, and lower base metal values. The base metal-enriched Ag-Au±Sb deposits

20
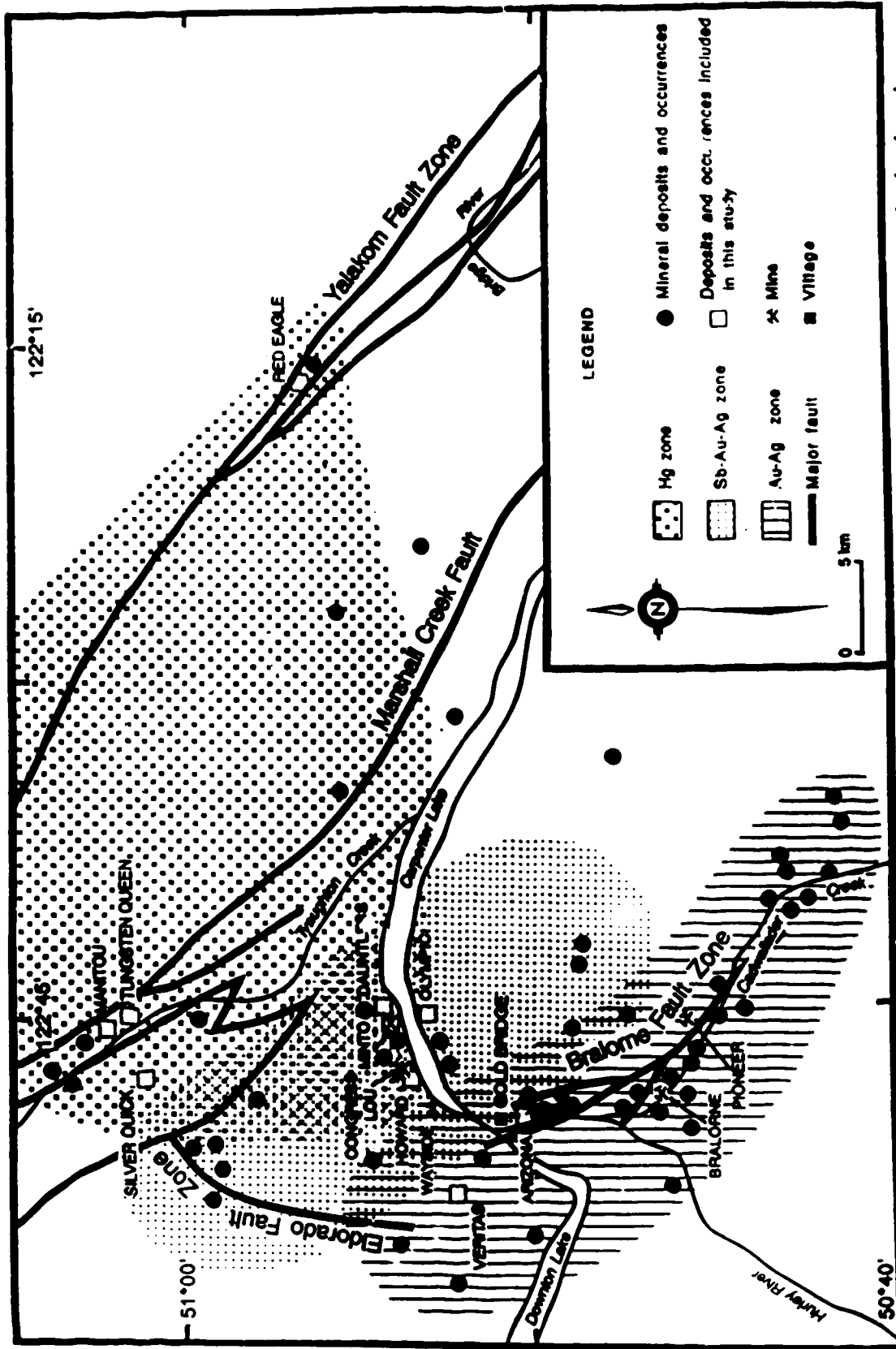
Figure 3-1. Generalized metal zoning pattern in the Bridge River Mining District showing mineral deposit and mine locations. Modified from Woodsworth *et al.* (1977) and Pearson (1977).

Table 3-1. Summary of deposit characteristics of Congress-type occurrences compared to the three largest Bralorne-type deposits. CLA= Carpenter Lake Assemblage of Potter (1983). Sources of data; Harrop and Sinclair (1986), and Cooke et al. (1986).

	BRALORNE-TYPE Au-Ag±W			CONGRESS-TYPE					
				Sb-Au-Ag±Hg				Base Metal-Enriched Ag-Au±Sb	
	BRALORNE	PIONEER	WAYSIDE	CONGRESS	HOWARD	LOU	DAUNTLESS	MINTO	OLYMPIC
HOST LITHOLOGY	-Bralorne intrusives -Pioneer Fm.	-Bralorne intrusives -Pioneer Fm.	-Pioneer Fm.	-CLA -dyke	-CLA -dyke	-CLA -dyke	-CLA	-CLA -dyke	-CLA -dyke
TONNES MILLED	4,984,469	2,313,552	39,094	943	reserves 610,000	---	---	80,650	---
GRADE (g/t)	Au 17.6 Ag 4.4	Au 17.9 Ag 3.3	Au 4.2 Ag 0.67	Au 2.7 Ag 1.4	Au 10.2 Ag ~6.0	Au 11.5 Ag 10.0	Au 5.1 Ag 3.0	Au 6.8 Ag 19.5	Au 3.1 Ag 15.3
Au/Ag	5.4	4.0	6.4	2.0	1.7	1.2	1.2	0.35	0.20
OTHER METALS	W, As	W, As	W, As	Sb, As, Hg	Sb, As, Hg	Sb, As, Hg	Sb	Cu, Zn, Pb As, ±Sb	Cu, Zn, Pb, ±Sb

exhibit a more abundant and varied sulphide mineralogy, lower gold to silver ratios, and lack any mercury mineralization.

3.1 Sb-Au-Ag±Hg Deposits

Congress Mine

The Congress mine is located on the north shore of Carpenter Lake appro' mately 6 kilometres northeast of Gold Bridge (Figure 3-1). The Congress was the first mi   in the area to establish considerable bodies of ore carrying gold as well as antimony. The earliest workings developed a mineralized shear zone for a vertical distance of 200 metres through three adit levels.

Stratigraphic trends in the area are north to northwest with steep west to east dips. Porphyry dykes and mineralized shears in the area are northwest to northeast-trending and steeply dipping. Antimony-gold±mercury mineralized shear zones follow the intrusive contacts of feldspar porphyry dykes or the stratigraphic contacts of sedimentary and volcanic units of the Carpenter Lake assemblage. Three main fault ages have been identified: 1) Early Jurassic? thrust faults within the Carpenter Lake assemblage; 2) later mineralized shear zones crosscutting elements of the Carpenter Lake assemblage and; 3) Late Tertiary?, dominantly strike-slip faults, which offset mineralization (Cooke *et al.*, 1986).

The main structure at ... Congress mine strikes northeast across argillaceous and chert sediments, greenstones, and a late feldspar porphyry dyke about 20 metres wide. It dips northwest approximately 45° and is well defined in greenstone and dyke units, less so in the sedimentary rocks. Mineralization along the near is discor...inuous and comprises fissure fillings and replacement bodies with widths from a few centimetres to over 4.5 metres (Cooke *et al.*, 1986). Wall rocks on either side of the principal fissure are replaced

by ankeritic carbonate (±calcite) and sulphide minerals, dominantly pyrite and arsenopyrite. Sericite and minor kaolinite alteration of wall rock is common for several centimetres on either side of a mineralized fissure. The most abundant sulphide is stibnite, which occurs in prominent replacement bodies and veins. In veins it occurs as irregular masses of nearly solid sulphide together with pyrite, arsenopyrite, and sphalerite. Less common minerals include galena, tetrahedrite, jamesonite, chalcopyrite, pyrrhotite, cinnabar, and native gold. Native bismuth and telluride minerals have also been documented (Cairnes, 1943). Quartz dominates the gangue r .neralogy which includes ankerite, calcite and rare fuchsite.

Howard Vein Deposit

The Howard vein deposit lies about 1.5 kilometres west of the Congress mine and has a geologic setting similar to that deposit (Figure 3-1). The main structure strikes N 35° E to N 35° W and dips 75° E to 55° W. Veins tend to be irregularly splayed in basalt flows and in dyke rocks but are more continuous where hosted in more competent basalt and gabbro. The Howard deposit displays a pattern of alteration and mineralization similar to the Congress deposit. Early ankerite-sericite±kaolinite alteration with disseminated pyrite and arsenopyrite is followed by one or two stages of quartz-ankerite veining with arsenopyrite and stibnite as the dominant sulphides hosting microscopic blebs of native gold.

Lou Zone

The Lou zone which lies approximately 750 metres to the northwest, is most likely an extension of Congress mineralization (Cooke *et al.*, 1986). The geologic setting is that of the Congress deposit with the exception that mineralization is spatially associated with a feldspar porphyry dyke-volcanic contact, which strikes northeasterly and dips steeply to the

northwest. The zone, up to 3.5 metres wide, is well exposed in surface trenching over an 800 metre strike length.

Mineralization in the Lou zone is identical to that of the Congress deposit with massive stibnite pods and lenses. Late quartz, minor calcite and associated cinnabar vein earlier quartz and associated stibnite.

Dauntless Prospect

The Dauntless prospect lies about 1 kilometre north of the Minto mine (Figure 3-1) and consists of a mineralized shear zone striking southwesterly across argillaceous and cherty sedimentary rocks of the Carpenter Lake assemblage. The shear zone averages 3 metres in width with a steep dip to the northwest. It is mineralized with disseminated arsenopyrite, pyrite, and stibnite in a gangue of quartz and calcite and altered sedimentary rock fragments.

3.2 Base Metal-Enriched Ag-Au±Sb Deposits

Minto Mine

The Minto mine is situated on the north shore of Carpenter Lake about 3.5 kilometres east of the Congress mine (Figure 3-1). Little work was done on the property proir to 1930. From that time to 1943 the principal vein showings were developed from four adits and a winze to three lower levels. The lowest four levels are now flooded by Carpenter Lake. The remaining levels were not accessible during the 1986 field season and sampling was relegated to two ore dumps and a caved stope. Mineralization has been developed to a vertical depth of 250 metres and a length of over 300 metres.

The geological formations hosting the ores comprise greenstones and sedimentary rocks of the Carpenter Lake assemblage with local, serpentinized, ultramafic intrusions and feldspar porphyry dykes. The general structural trend is north to north-northwest with subvertical to intermediate dips. The local setting is structurally complicated by faulting and deformation as well as by the irregularly intercalated sedimentary and volcanic rocks.

The principal vein structure strikes northerly and dips ~75° E. It follows closely the contact between an argillaceous and cherty sedimentary unit with a feldspar porphyry diorite dyke. Cairnes (1943) recorded that through the productive length of the vein the immediate hanging wall is the dyke. Shearing in other lithological settings does not appear to be favourable for vein formation. A major barren fault, therefore thought to be post-mineralization, offsets the dyke and principal vein. The fault strikes N 75° W and dips 45° W and offsets the vein to the west about 80 metres in a horizontal sense.

As described by Cairnes (1943) the principal mineralized fissure, for over a strik-- length of 150 metres and from the uppermost to the lowest mine levels, is occupied by a continuous, well-defined vein up to 1.4 metres wide. The vein carries a high proportion of sulphides in a gangue of quartz, ankerite±calcite, and locally, fuchsite. The principal sulphides are arsenopyrite, pyrite, sphalerite, and jamesonite. Smaller amounts of galena, tetrahedrite, chalcopyrite, pyrrhotite and stibnite are present. Native bismuth has also been recorded (Cairnes, 1943). Gold occurs as microscopic blebs in quartz and associated with pyrite and arsenopyrite. Sulphides are generally coarse and occur as solid masses. This is especially true of arsenopyrite. Though vein material could not be sampled in s.′.u, the banded structure of the vein is apparent in larger hand specimens.

Cairnes (1943) reported that wall rock alteration is not a pronounced feature in the deposit; however, wall rock fragments included in the vein are pervasively altered, typically carbonate flooded and silicified to varying degrees.

Olympic Prospect

The mineral showings which constitute the Olympic prospect are located on the south side of Carpenter Lake directly opposite the Minto mine. The principal workings were near river level and were subsequently flooded on the completion of the Terzaghi Dam on the Bridge River. The uppermost of several adits is about 50 metres above peak lake level and is caved. However, a large dump at the portal provides an opportunity to sample what is thought to be a partial cross-section of mineralization based on descriptions in the literature.

The Olympic workings exposed mineralization in sedimentary and volcanic rocks of the Carpenter Lake assemblage intruded by mafic and ultramafic rocks and a variety of dykes. The most prominent dykes are two broad belts of very fine grained felsite on either side of the lower workings.

Adits have been driven along a mineralized shear zone that extends southwesterly within a belt of partly serpentinized ultramafic rocks. On the northeast a massive, lenticular, medium to coarse grained gabbro body borders the host peridotite. Further to the northeast the gabbro is intruded by a broad felsic dyke. To the southwest a similar dyke intrudes the peridotite.

The shear zone is up to 1.5 metres wide and strikes N 25° W, dips 55° SW, and is continuously and heavily mineralized for over 20 metres of strike length. For another 70 metres the shear zone is less well developed and mineralization is more sporadic (Cairnes, 1943). Ore minerals include arsenopyrite, pyrite, chalcopyrite, sphalerite, galena, and tetrahedrite. More local masses of jamesonite and stibnite have been observed in some ore samples. Accumulations of magnetite and pyrrhotite are present in some specimens. Gold, where observed, is in microscopic amounts associated solely with chalcopyrite, though historically, stronger grades are associated with pyrite and arsenopyrite. Quartz is the principal gangue mineral with lesser amounts of calcite, sericite, and minor fuchsite.

Alteration is not exposed to a large degree but on a local scale consists of pervasive sericitization and carbonatization of included wall rock fragments.

IV. PETROGRAPHY OF MINERAL DEPOSITS AND OCCURRENCES

4.0 Introduction

Antimony-associated, precious metal deposits in this study have been grouped into two categories reflecting their respective ore mineralogies; those with a significant base metal content versus deposits with fewer base metals. The Congress, Howard, Lou, and Dauntless occurrences exhibit characteristics of the latter group while the Minto and Olympic deposits, those of the former. In all cases the current or potential value of the deposits lies in their gold content.

The following description of mineralogy and petrology of the mineral occurrences focuses primarily on ore petrology and ore mineral paragenesis. This work is the first in-depth petrographic study of these deposits. Earlier workers (McCann, 1922; Cairnes, 1937, 1943) included petrographic data, which are for the most part corroborated by the present study, though in some instances information presented here differs from the historical record.

All of the deposits are hosted by the Carpenter Lake assemblage of Potter (1983). The volcanic units of the Carpenter Lake assemblage comprise basalt, tuff, gabbro, and serpentinite, while sedimentary rocks include chert, argillite, siltstone, sandstone, minor limestone, and minor melange breccia. The mineralized shear zones in the area generally follow intrusive contacts of porphyry dykes or stratigraphic contacts of sedimentary and volcanic units. The majority of mineralized shears are hosted in igneous rocks which are structurally more competent.

The abbreviations used in the photomicrographs are as follows: ank = ankerite, apy = arsenopyrite, Au = gold, cal = calcite, carb = carbonate, cin = cinnabar, cpy = chalcopyrite,

ga = galena, jam = jamesonite, mag = magnetite, py = pyrite, qz = quartz, sb = stibnite,

sp = sphalerite, tet = tetrahedrite.

4.1 Host Rock Petrography

Basalt

Amygdaloidal and pillow basalt are typical host rocks at the Congress mine. The

original texture of the rock is recognizable but a pervasive alteration has affected all

minerals to some degree. The rock is composed of a felted mass of plagioclase laths,

averaging 0.2 mm in length, in an altered groundmass of sericite, kaolinite, ankerite, and

quartz. The plagioclase has been largely altered to sericite. Amygdules are common and

consist of extremely fine-grained quartz and ankerite. The rock is up to 30% veined by

fine-grained ankerite, minor hematite, and later quartz. Early, very fine-grained quartz

veinlets up to 1 mm wide are common.

Porphyrytic basalt also hosts mineralized shears. The rock contains scattered

phenocrysts of plagioclase in a groundmass containing abundant plagioclase laths and

scattered grains of possible clinopyroxene. Plagioclase forms equant, subhedral

phenocrysts averaging 1 mm in size. Alteration is dominated by extremely fine-grained

sericite with minor kaolinite. Some spotty replacement by ankerite occurs as well. Possible

relict clinopyroxene phenocrysts form patches approximating subhedral to anhedral outlines

averaging 0.2 mm in size. These are completely replaced by extremely fine-grained sericite.

The groundmass is dominated by (20-30%) unoriented, prismatic, plagioclase

grains averaging 1 mm in length. Alteration is similar to that in the phenocrysts. Interstitial

to the plagioclase laths is anhedral, very fine-grained plagioclase, intergrown with altered

mafic material and ilmenite. Both the mafic minerals and the plagioclase are strongly altered

to sericite and minor ankerite. Ilmenite occurs in aggregates up to 0.2 mm intergrown with plagioclase and locally moderately altered to leucoxene.

Extremely fine-grained pyrite, and smaller amounts of marcasite, are disseminated in the rock as irregular aggregates up to 0.5 mm. Chalcopyrite is present in trace amounts as scattered grains averaging 0.02 mm in size.

Throughout the rock are patches of sericite averaging 0.05 to 0.1 mm in size. These patches are rimmed by optically continuous grains of quartz and most likely represent amygdules. Minor veinlets of ankerite and/or hematite are present throughout the rock.

Gabbro

Mineralization in the Howard vein deposit, as well as showings at the Olympic prospect, are partly hosted by massive gabbro. The rock is dark green, medium-grained containing up to 50% plagioclase nd two mafic minerals, together with ilmenite and minor apatite. Textures suggest the mafic phases were originally biotite and pyroxene. Together the two mafic phases constitute up to 40% of the rock. One phase forms equant subrounded grains averaging 1 mm in size; a few grains are elongate. The second mafic phase commonly forms interstitial grains between subhedral to euhedral plagioclase grains.

Plagioclase forms anhedral to euhedral, prismatic to equant grains averaging 1 mm in size. Pericline and albite twins are common while Carlsbad twinning is rare. Combined albite-Carlsbad twin determinations yield a range of composition of labradorite-bytownite (An_{65-75}). Ilmenite forms subhedral grains averaging 0.3 mm and is usually replaced by leucoxene. Trace apati. forms scattered, irregular, subhedral prismatic grains to 0.2 mm in length. Arsenopyrite forms fairly abundant (1%) aggregates of extremely fine-grained subhedral to euhedral crystals scattered throughout the rock.

Veining in the rock is common and of two types: 1) ankerite-arsenopyrite-quartz and; 2) ankerite-pyrite-arsenopyrite.

Feldspar Porphyry Dykes

Feldspar porphyry dykes of variable composition also host significant mineralization among the deposits. The dykes vary from gabbro to dacite in composition. The rock is slightly porphyritic with a variable extremely fine to fine-grained groundmass. Plagioclase and biotite phenocrysts together make up approximately 10% of the rock. Plagioclase forms subhedral to euhedral, equant to slightly prismatic phenocrysts averaging 0.5 mm in size. Biotite forms equant to elongate phenocrysts from 0.7 to 2 mm in length. Groundmass material averages 0.1 mm , and is dominated by equant plagioclase and ankerite with sericite as replacement patches, totalling about 10% of the rock.

Ilmenite forms scattered equant to slightly elongate patches up to 0.1 mm in size and totals less than 1% of the rock. Leucoxene often replaces ilmenite. Pyrite, and lesser amounts of arsenopyrite, occur as grain clusters and disseminations up to 0.1 mm in size. Pyrite is equant while arsenopyrite displays characteristic subhedral to euhedral rhombohedral outlines. Trace apatite forms a few anhedral to subhedral grains to 0.15 mm in size.

Serpentinite

Serpentinite occurs as lenticular pods and is a relatively common lithology in the Carpenter Lake assemblage. Where serpentinite is in close proximity to mineralization it is typically altered to listwaenite (Buisson and Leblanc, 1985), an asssemblage of Mg-Fe-Ca carbonate, quartz, fuchsite (mariposite), talc, lizardite serpentine, with accessory chlorite, pyrite, magnetite, and chromite. The rock contains extremely fine-grained patches of quartz and fuchsite (±sericite), which imparts a bright green colour. The remainder of the rock is a

dominantly very fine to fine-grained aggregate of Mg-Fe-Ca carbonate and quartz with minor pyrite.

Veins of quartz-pyrite and pyrite account for 1-5% of the rock. Relict chromite grains and grain fragments average 0.2 mm in size and are present in very minor amounts. Pyrite and pyrrhotite form scattered, anhedral grains 0.1 mm across in trace amounts.

4.2 Ore Petrography and Mineralogy

4.2.1 Sb-Au-Ag±Hg Deposits

Between all deposits of this type a recognized pattern of alteration and mineralization is observed. This pattern encompasses three events: 1) early ankerite-sericite-quartz ±kaolinite flooding with attendant pyrite and arsenopyrite disseminations; 2) major quartz, ankerite, stibnite, arsenopyrite veining; and 3) late ankerite±calcite, quartz, stibnite ±tetrahedrite and cinnabar veining. The ore minerals include, in order of their abundance, pyrite, arsenopyrite, stibnite, jamesonite, sphalerite, tetrahedrite, marcasite, pyrrhotite, cinnabar, gold, ± possible tellurides.

Congress Mine

Alteration and mineralization at the Congress mine conforms to the paragenesis described above (Figure 4-1). Pyrite, arsenopyrite, stibnite, sphalerite, pyrrhotite, tetrahedrite, cinnabar, and gold are present in that order of abundance. A very minor amount of marcasite, jamesonite, and possibly trace native bismuth were identified as well. Gangue mineralogy is relatively simple with quartz dominating all three stages of veining and replacement. Ankerite is next in abundance, particularly in the early and late

Figure 4-1. Summary of idealized paragenetic sequences for the Congress, Lou. Howard, and Dauntless deposits and occurrence.

paragenetic stages. Sericite and kaolinite, present in vein material, are more prominent as pervasive alteration phases of host rocks and wall rock fragments in veins.

The deposition of pyrite and arsenopyrite   isseminations in altered wall rock and associated with grey quartz and carbonate flooding is characteristic of the early stage of mineralization in these systems. These sulphides occur as fine subhedral to euhedral discrete grains or intergrown aggregates up to 0.4 mm in size (Figure 4-2).

The main stage of mineralization at Congress is characterized by large irregular masses of unoriented stibnite crystals veining and replacing quartz (Figure 4-3 and 4-4). Stibnite represents up to 80% of vein and replacement material in some samples. Stibnite contains rare inclusions of euhedral arsenopyrite grains and in places displays intergrowths with small amounts of jamesonite. Where arsenopyrite and pyrite occur in the main stage of mineralization they are closely a   ciated in masses in which the former appears to rim the latter. In two samples gold occur   /ery rare, 1 to 10 μm blebs isolated in stibnite and in quartz associated with stibnite   urrence of gold in the deposits is summarized in Table 4-1.

Late stage vein material comprises milky quartz that carries very minor amounts of sphalerite, arsenopyrite, pyrite, and tetrahedrite. Sphalerite and tetrahedrite occur as small (100 μm) grains sharing grain boundaries with pyrite and arsenopyrite and as disseminations in quartz. Kermesite (Sb_2S_2O) is present as a secondary replacement along microfractures in stibnite.

Ankerite, minor calcite, and later quartz are the dominant replacement phases in areas adjacent to mineralization. These minerals occur as pervasive floodings of wall rock and are accompanied by up to 2% arsenopyrite and 5% pyrite as subhedral to euhedral disseminations averaging 0.01 to 0.02 mm in size. Closer to mineralization plagioclase crystals are altered to quartz and sericite and mantled by an extremely fine-grained green-grey phase outlining their relict texture; possibly a graphite-chlorite mixture. Trace epidote replaces the cores of plagioclase laths. Vesicules are variably filled with fine-grained
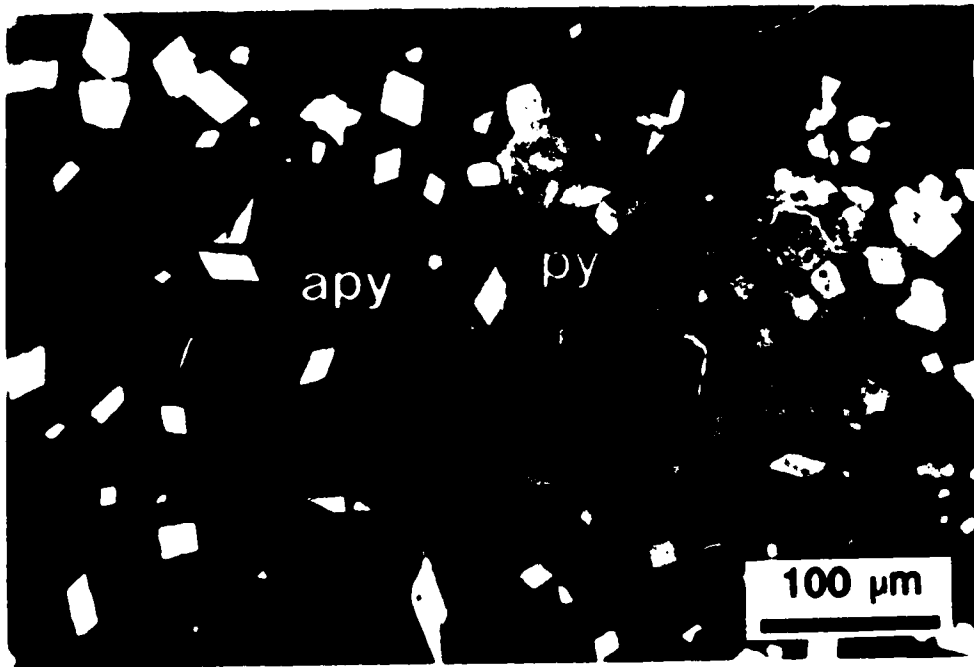
Figure 4-2. Polished thin section, CON 16. Plane polarized light. Pyrite and arsenopyrite disseminations in altered basalt.
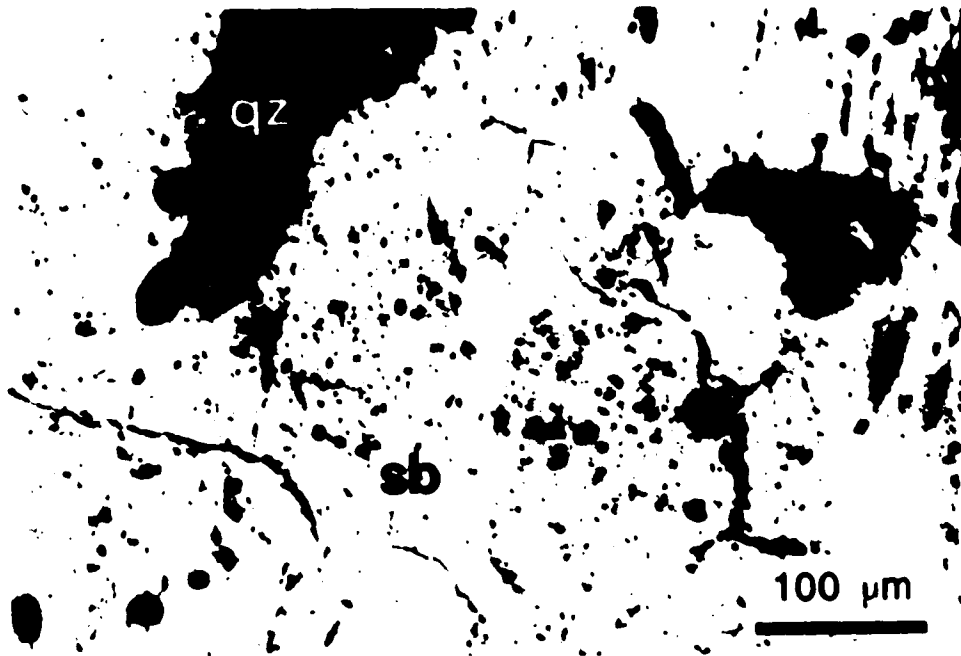
Figure 4-3. Polished section, CON 16. Plane polarized light. Massive stibnite replacing quartz.

Figure 4-4. Polished section, CON 16. Crossed polars. Massive stibnite replacing quartz.

Table 4-1. Summary of gold localization in Congress-type deposits included in the study.

Number of occurrences of gold as inclusions, veins, or replacements in sulphide and gangue phases.

Sb-Au-Ag±Hg

CONGRESS, LOU, HOWARD

stibnite	10
cinnabar	4
quartz	4
stibnite/arsenopyrite	1

Base Metal-Enriched Ag-Au±Sb

MINTO, OLYMPIC

galena	40
pyrite	18
jamesonite	10
quartz	10
chalcopyrite	3
arsenopyrite	2
tetrahedrite	1

granular quartz, epidote, chlorite, and pyrite. Late quartz-kaolinite-epidote veinlets up to
0.5 mm in width are common.

As much as 40% of the immediate wall rock is replaced by ankerite and quartz.
Ankerite occurs in patches to a few centimetres across with subordinate amounts of cherty
quartz and minor sericite. Quartz also forms irregular interstitial patches in the groundmass.

Lou Zone

The Lou zone is thought to be a continuation of the Congress deposit. The style of
mineralization in both occurrences is quite similar. Three readily identifiable stages of
mineralization are present (Figure 4-1). An early stage of grey quartz flooding of the wall
rock carries a significant amount of pyrite (± marcasite) and arsenopyrite as disseminated
grains and grain aggregates. Quartz of this stage grades into a second generation of quartz
of subhedral to euhedral interlocking grains averaging 0.5 cm in size. This quartz mat
wall rock fragments in a cockade pattern with crystals exhibiting euhedral terminations.

Stibnite is the dominant ore mineral in the second stage of mineralization with
subordinate amounts of pyrite and arsenopyrite. The phase constitutes up to 75% of vein
and replacement material as irregular masses up to several centimetres in size. Individual
stibnite crystals average 0.5 cm in length. Stibnite shares simple grain boundaries with and
contains inclusions of pyrite and arsenopyrite and infills the bulk of open spaces in second
generation quartz.

Ankerite and minor calcite constitute the remainder of gangue in the second and
final stages of mineralization. Carbonate is linked to the main stage of mineralization by its
coeval deposition with cockade patterned quartz, and to the final stage by its close
association with sphalerite and tetrahedrite. Ankerite generally occurs as open space-filling
material as veinlets and as interlocking grains with euhedral terminations. Minor calcite

occurs as penecontemporaneous veinlets and patches with ankerite. Carbonate in the main and late stages totals about 15% of vein material.

Sphalerite, tetrahedrite, and cinnabar define the late stage of mineralization. The first two phases are present in trace amounts as anhedral, equant, isolated bodies with highly embayed grain boundaries with quartz. In a few instances, tetrahedrite was observed as very small (~10 μm) inclusions in sphalerite. Cinnabar occurs in minor amounts as small replacement bodies and fracture coatings in stibnite (Figure 4-5 and 4-6). Covellite and kermesite occur as as secondary alterations along grain boundaries and fractures in tetrahedrite and stibnite respectively. No free gold was observed in any mineralization from the Lo zone.

The hanging wall of the Lou zone deposit consists of an altered porphyritic dacite dyke and is the best example of the close association of mineralization with dyke rocks. Plagioclase phenocrysts are typically completely replaced by extremely fine-grained sericite. A sericite, minor ankerite and leucoxene assemblage partially pseudomorphs biotite.

Howard Vein Deposit

Two stages of mineralization have been identified in samples from this occurrence (Figure 4-1). Early pervasive quartz flooding with a pyrite-arsenopyrite-stibnite assemblage dominates vein and replacement material. A late quartz-stibnite-gold-cinnabar assemblage defines a stockwork breccia.

Alteration is similar to that of other deposits in the group. Extremely fine-grained, abundant quartz in wall rock with pyrite and arsenopyrite typifies early alteration. Plagioclase in gabbro is strongly, and in places, completely replaced by extremely fine-grained sericite with minor kaolinite. Mafic phases are completely replaced by a very fine-grained aggregate of muscovite-sericite with minor amounts of ankerite and leucoxene.
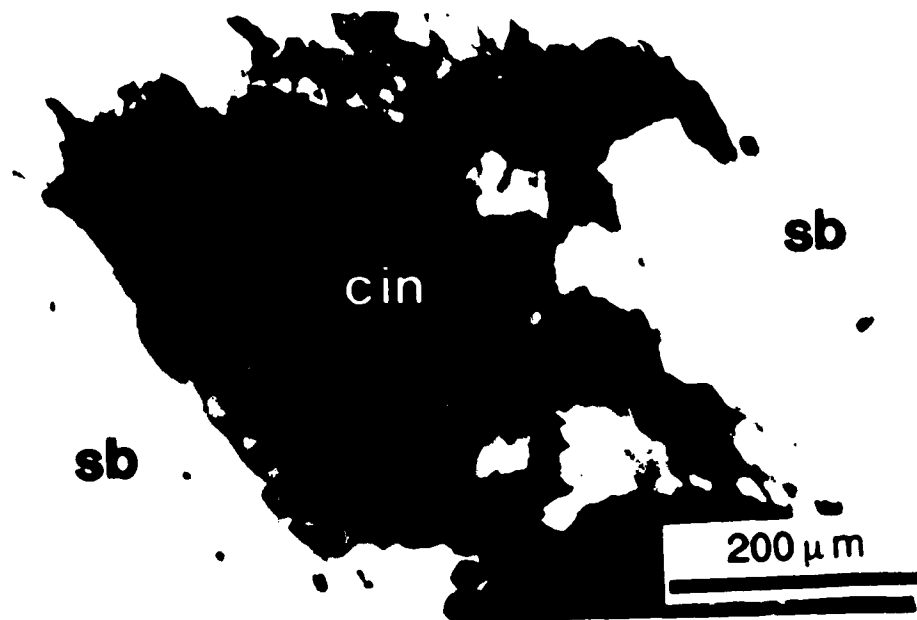
Figure 4-5. Polished section, LOU 16. Plane polarized light. Cinnabar replacing stibnite along fractures.
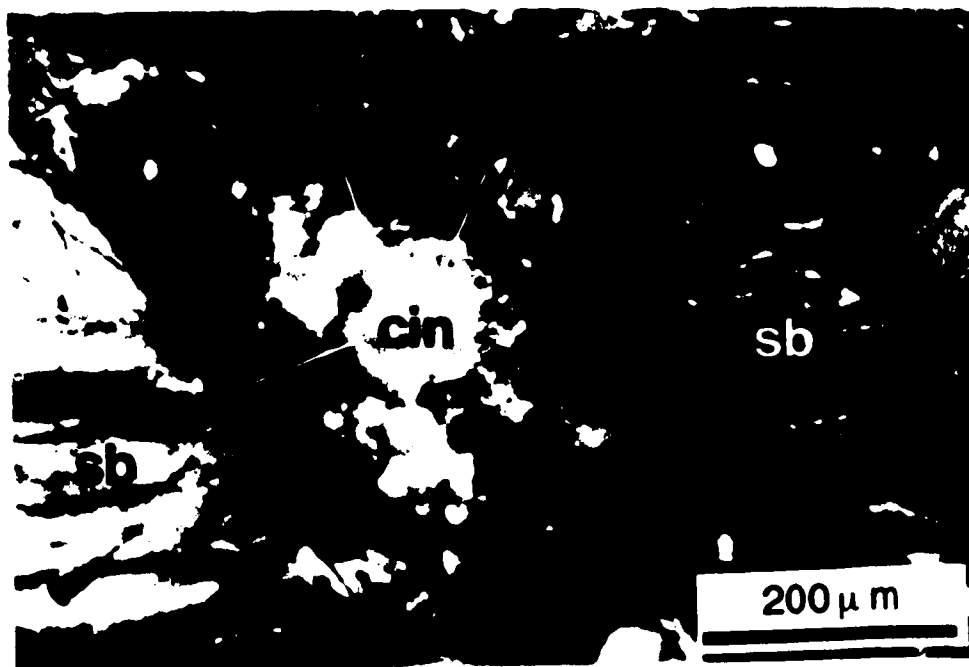
Figure 4-6 Polished section, LOU 16. Crossed polars. Cinnabar replacing stibnite along fractures.

Disseminated grains of ankerite and patches of possibly secondary plagioclase intergrowths are common. In places that were not silicified an assemblage of sericite and ankerite dominates the altered rock. Pervasive, extremely fine-grained sericite, together with fine-grained ankerite in replacement patches up to 1 cm constitute up to 40% of the rock locally.

The alteration described above is succeeded by the deposition of relatively coarse grained quartz with stibnite and other minerals as open space fillings during brecciation. The stibnite, highly corroded with numerous pits and gangue inclusions, occurs as randomly oriented grains and aggregates among masses (~100 μm) of euhedral arsenopyrite. Gold shares grain boundaries with and is included in stibnite (Figure 4-7). In several instances gold was observed to straddle the stibnite grain boundaries suggesting replacement of stibnite by gold (Figure 4-8). Gold is also associated with arsenopyrite where the latter occurs in close association with stibnite. Blebs of gold 1-40 μm in size are commonly surrounded by i .ny subhedral, highly fractured grains of ...senopyrite (Figure 4-9). Arsenopyrite in turn shares sutured grain boundaries with strc 'gly corroded stibnite, itself riddled with gold. (innabar, in trace quantities, fills fractures that can be traced to stibnite grains which host gold; yet in no instance was gold observed to be in contact with cinnabar (Figure 4-10).

Zones of late brecciation serve to concentrate quartz-stibnite-cinnabar mineralization. Stibnite grains in this assemblage are larger and less corroded. The stibnite, together with late quartz, fills open spaces in early coxcomb quartz. Late cinnabar mineralization occurs as microfracture fillings in stibnite. In summary, two generations of quartz-stibnite-cinnabar mineralization have been documented with the introduction of gold occurring between them.
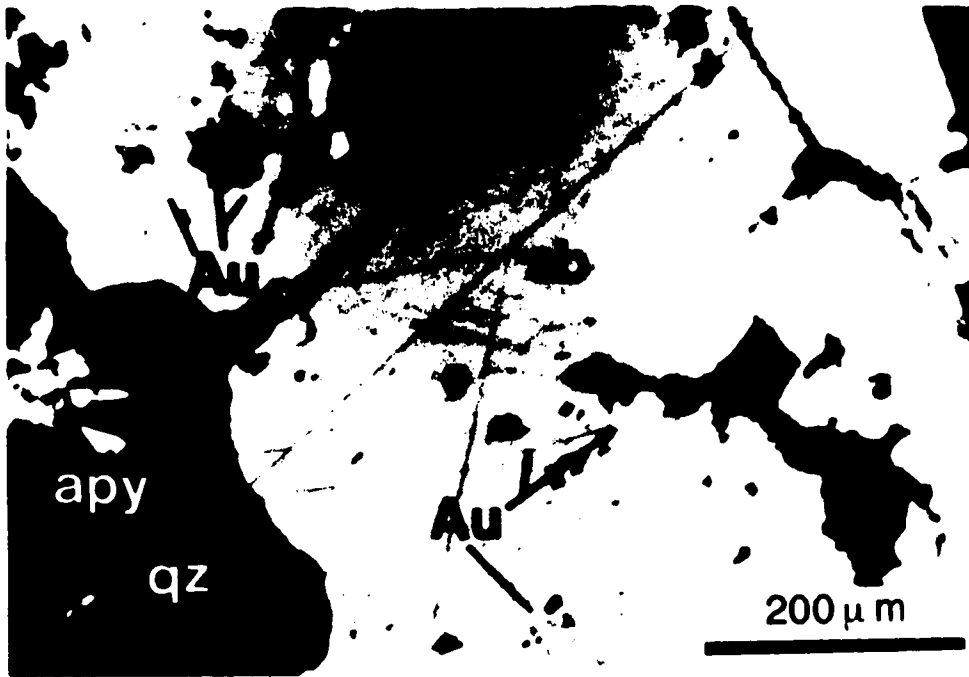
Figure 4-7. Polished section, HOW 08. Plane polarized light. Gold inclusions in stibnite.

Figure 4-8. Polished section, HOW 08. Plane pola red light. Gold replacing stibnite.
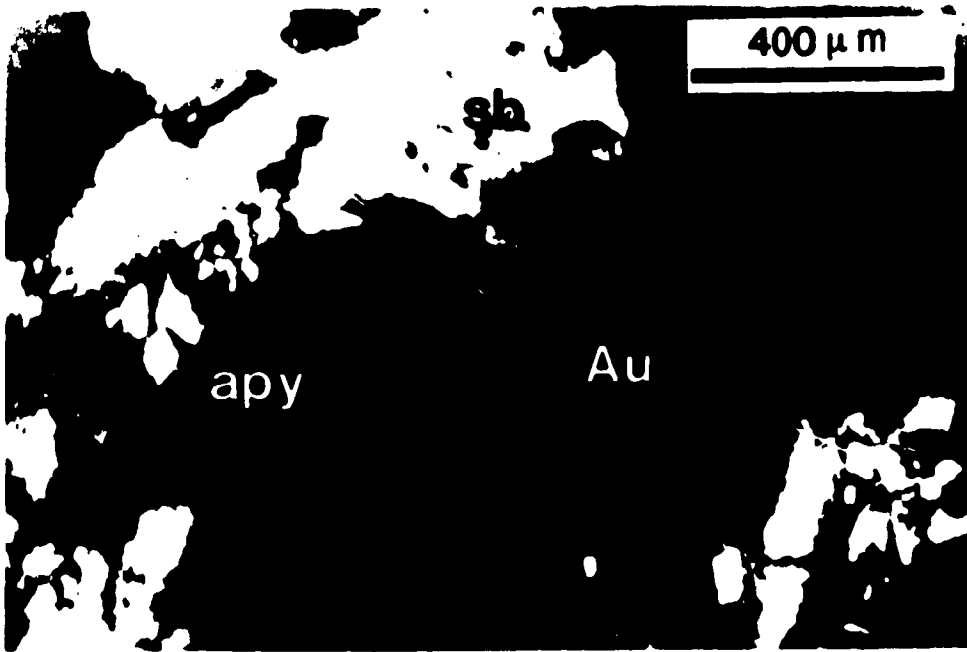
Figure 4-9. Polished section, HOW 08. Plane polarized light. Gold replacing stibnite in association with arsenopyrite.
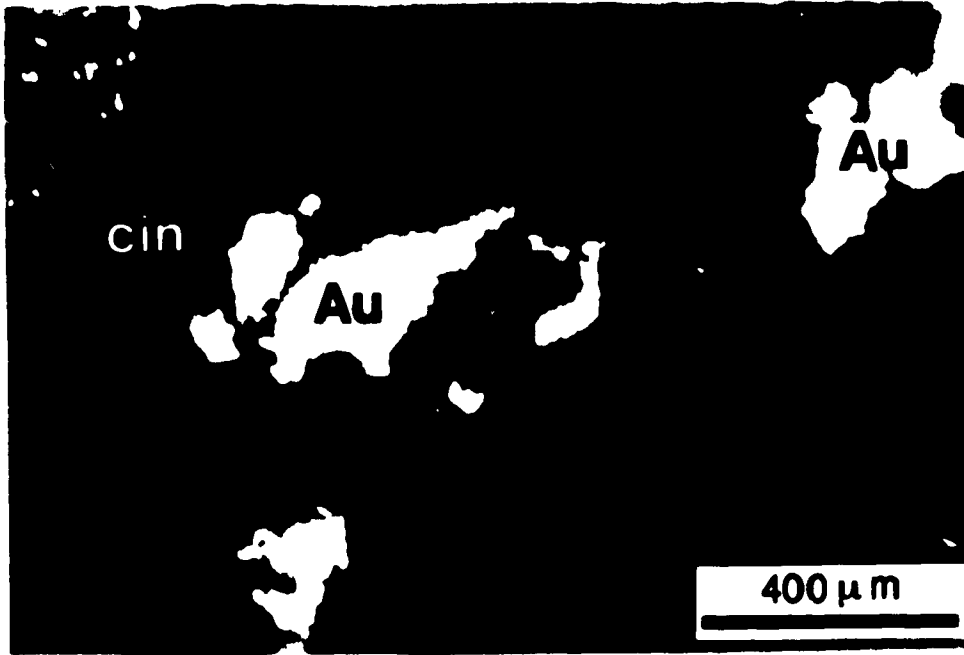
Figure 4-10. Polished section, HOW 08. Plane polarized light. Late gold and cinnabar in quartz.

Dauntless Prospect

The mineralogy of this occurrence is the simplest among the deposits studied. A gangue assemblage of quartz-ankerite-calcite occurs as vein breccia material in alternating bands. Quartz dominates (70%) with lesser amounts of calcite (15%) and ankerite (5%). The ore mineral assemblage is simple as well; pyrite, arsenopyrite, stibnite, sphalerite, and trace tetrahedrite and pyrrhotite total less than 10% of the vein material.

Two generations of veining are present. Early quartz comprises fine to medium-grained, anhedral interlocking grains with interspersed patches of sericite and minor chlorite. Brecciation was followed by the deposition of a second generation of coxcomb quartz on fracture walls. The quartz grains average 0.2 mm in size and exhibit euhedral terminations. Deposition of ankerite followed as symmetric bands up to 1 cm in width. Bands of ankerite are composed of subhedral grains averaging 0.1 mm in size. The ankerite is crosscut by veinlets of calcite that fill the remaining open space in the rock.

Pyrite and arsenopyrite are disseminated throughout the rock but are in highest concentrations as very fine disseminations and aggregates in altered wall rock fragments. The remaining sulfide phases are associated with the second generation of quartz veining. Stibnite occurs as disseminations, irregular lenses (*ca.* 1 cm) and veinlets in quartz. Sphalerite occurs as small (20 μm) irregular inclusions in and intergrowths with pyrite. These phases total no more than 5% of the vein material. Tetrahedrite and pyrrhotite are present in trace amounts associated with pyrite and arsenopyrite. Pyrrhotite occurs as irregular grains averaging 2-5 μm in size that mantle pyrite-arsenopyrite aggregates while tetrahedrite fills microfractures in pyrite-arsenopyrite and pyrite-pyrrhotite aggregates.
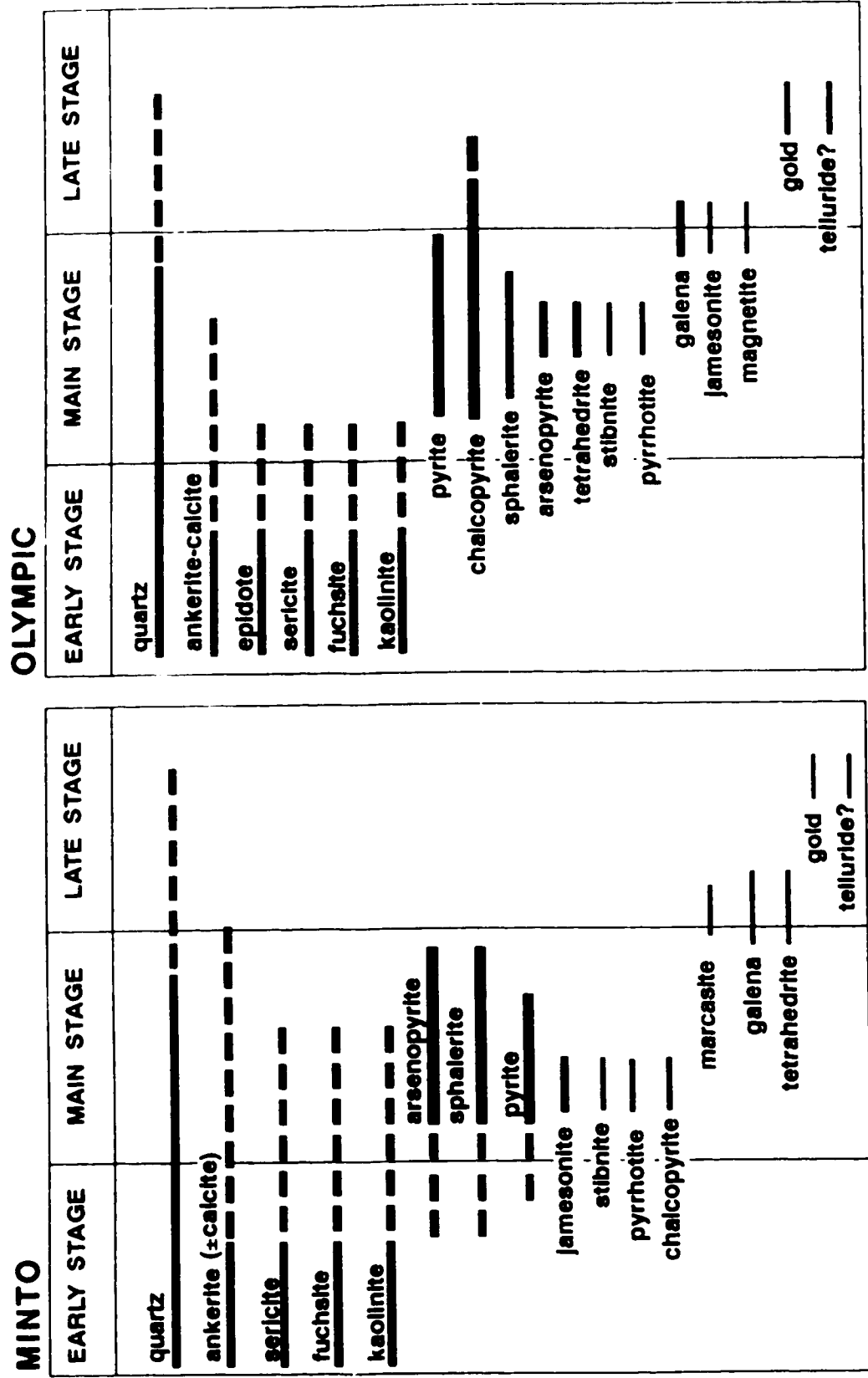
Figure 4-11. Summary of idealized paragenetic sequences for the Minto deposit and the Olympic showing.

4.2.2 Base Metal-Enriched Ag-A'u±Sb Deposits

The Minto deposit and the mineral showings of the Olympic occurrence are mineralized shear systems that carry a high proportion of sulphides, and have low gold to silver ratios. These characteristics distinguish the two deposits from the Congress mine and deposits similar to it.

Mineralization conforms to two and locally, three events (Figure 4-11). The early stage in each system is characterized by the emplacement of a quartz-carbonate-sericite-fuchsite-kaolinite alteration and gangue assemblage. Main stage sulphide deposition including arsenopyrite, pyrite, sphalerite, galena, chalcopyrite, tetrahedrite, jamesonite, stibnite, marcasite, and pyrrhotite in roughly that order of abundance was succeeded by the introduction of gold and possible tellurides.

Minto Mine

Gangue mineralogy in the Minto deposit is dominated by ankerite (30%) as gra... ... masses with grains averaging 1 mm in size. Up to 15% of gangue material is quartz intergrown with carbonate. Quartz occurs as anhedral to subhedral grains in irregular masses and rarely displays a coxcomb texture. Quartz-rich patches occur surrounded by intergrowths of quartz and ankerite. Wall rock fragments included in vein material are altered to one of two assemblages; they display either a pervasive carbonate flooding or a quartz-fuchsite (± sericite)-sulphide assemblage. The sulphide phases pyrite, arsenopyrite, and sphalerite occur as extremely fine-grained anhedral to subhedral grains disseminated throughout the rock fragments in which they occur. Sericite is extremely fine-grained in small (0.5 cm) replacement patches. The bulk of the remaining material is interstitial, extremely fine to fine-grained quartz.

The main stage of mineralization resulted in quite massive, local accumulations of sulphide minerals in a gangue of quartz and carbonate. Sphalerite and arsenopyrite dominate the sulphide mineralogy followed by moderate amounts of pyrite, tetrahedrite, galena, and jamesonite. Minor concentrations of stibnite, marcasit , pyrrhotite, and chalcopyrite complete the main stage sulphide assemblage

Sphalerite and arsenopyrite occur as massive accumulations up to tens of centimetres in size consisting up to 30% and 80% of vein material respectively. Arsenopyrite tends to occur as highly fractured aggregates (ca. 0.5 cm) of grains up to 0.3 mm in size (Figure 4-12) and small subhedral to euhedral crystals as inclusions in the other sulphide phases. Sphalerite occurs as irregular masses up to 5 mm in size closely associated with pyrite, galena, tetrahedrite, jamesonite, and chalcopyrite (Figure 4-13). Other than sphalerite, pyrite's closest association is with arsenopyrite as irregular inclusions and fracture-fillings. Pyrite in any one sample can constitute up to 15% of vein material.

Tetrahedrite, galena, and jamesonite occur in relatively equal amounts each totalling anywhere from 1 to 8% of vein material. In the literature (Cairnes, 1937; 1943) jamesonite is not reported as occurring in ores from the Minto mine, while mention is made of significant concentrations of stibnite. Though stibnite is present as a minor phase, the dominant antimony-bearing mineral identified in this study is jamesonite (Figure 4-14),. Tetrahedrite is most closely associated with sphalerite as fracture-fillings and included masses (Figure 4-15). In some instances textures suggest that tetrahedrite has replaced sphalerite along cleavage planes resulting in a distinctive triangular pattern of tetrahedrite lamellae in sphalerite. Tetrahedrite is also present in close association with pyrite. Where the two minerals share grain boundaries, a possible reaction rim of rnite was observed suggesting replacement of pyrite by tetrahedrite.

Galena shares simple grain boundaries with sphalerite but is more closely associated with jamesonite in complex intergrowths (Figure 4-16 and 4-1). Aggregates of

Figure 4-12. Polished section, MINTO 05. Plane polarized light. Aggregate of highly fractured arsenopyrite.

Figure 4-13. Polished section, MINTO 01. Plane polarized light. Typical sulphide assemblage in Minto ore.

Figure 4-14. Polished section MINTO 02. Plane polarized light. Typical occurrence of jamesonite, the major antimony-bearing mineral, in Minto ore.
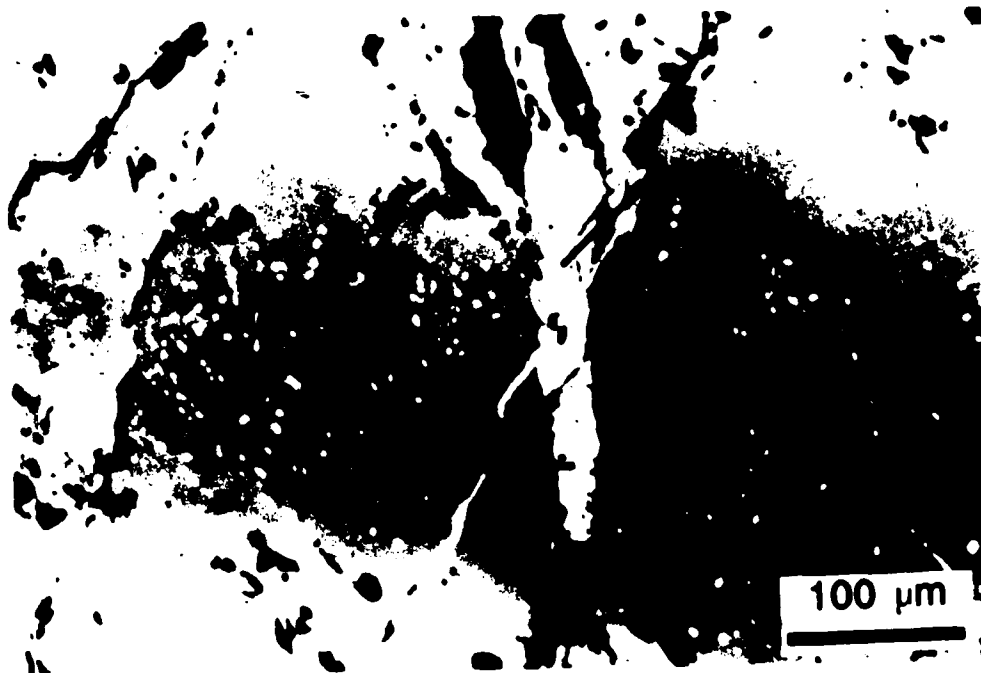
Figure 4-15. Polished section, MINTO 02. Plane polarized light. Association of sphalerite, tetrahedrite, and galena.
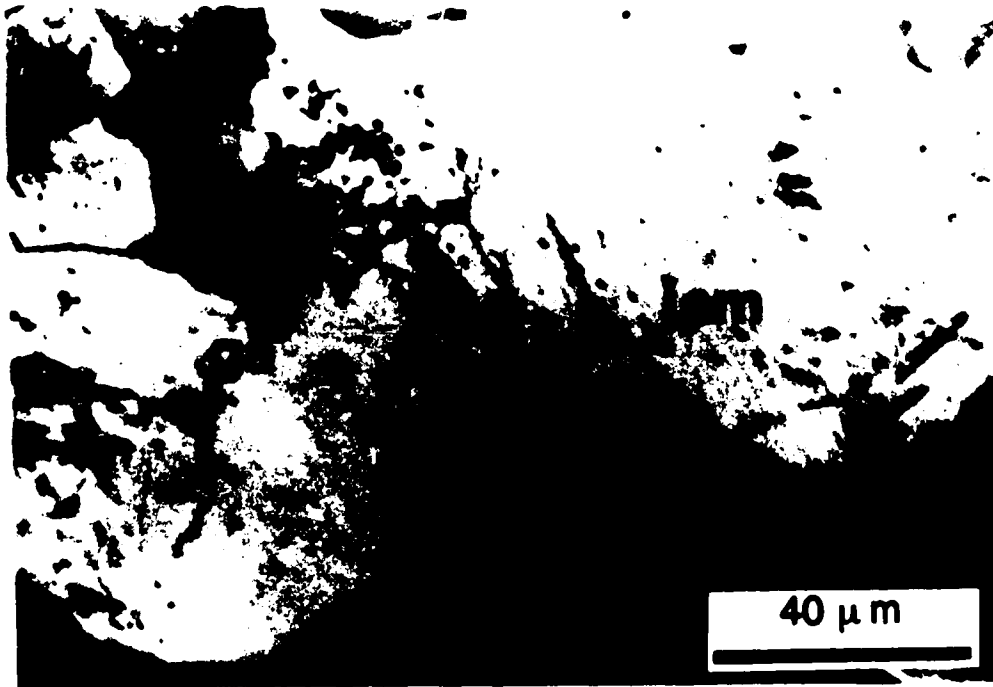
Figure 4-16. Polished section MINTO 01. Plane polarized light. Jamesonite replacing galena which shares simple boundaries with sphalerite and pyrite.
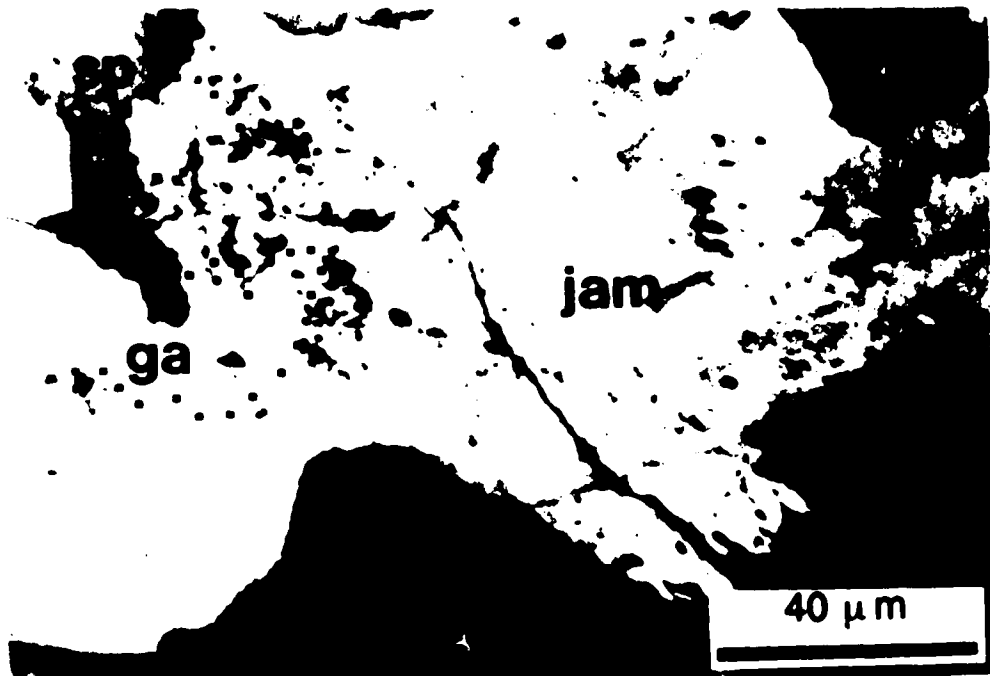
Figure 4-17. Polished section, MINTO 01. Crossed polars. Jamesonite replacing galena which shares simple boundaries with sphalerite and pyrite.

subhedral needle-shaped crystals of jamesonite with euhedral terminations project from masses of irregular galena grains. The cusp and vane nature of the galena-jamesonite boundaries suggests the replacement of jamesonite by galena. Jamesonite also occurs as isolated needle-shaped crystals in quartz that veins arsenopyrite.

Marcasite occurs in very small amounts (<1%) as anhedral grains, less than 0.1 mm in size, in pyrite grains. Pyrrhotite is present in a few ore samples in even smaller concentrations as fracture-coatings and inclusions intergrown with arsenopyrite. Chalcopyrite occurs as a multitude of submicron- to micron-sized blebs concentrated along rims and fractures of sphalerite crystals. It has recently been suggested that this common ore texture known as chalcopyrite disease represents the earliest stages of replacement of sphalerite by chalcopyrite (Eldridge *et al.*, 1988).

The final stage of mineralization in the Minto deposit is the introduction of gold and an unknown phase, possibly a gold-bearing telluride mineral. Gold occurs as blebs, infillings, and microveinlets in sulphide minerals (Table 4-1). The most common morphology of gold is as blebs averaging 30 to 50 μm in size but grains up to 250 μm occur, most often as replacements along cleavage traces in galena (Figure 4-18). Other phases which host gold are pyrite, jamesonite, arsenopyrite, and tetrahedrite. Gold also occurs as discrete grains interstitial to quartz gangue. Pyrite is the second most common host to gold which occurs as blebs and replacements along fractures. Gold occurs similarily in arsenopyrite to a lesser extent.

Highly corroded jamesonite, closely associated with arsenopyrite, is a common host to gold (Figure 4-19). Gold grains and blebs in these circumstances have a spongy texture and appear to have infilled corrosion pits in the jamesonite. Free gold in quartz is the next most common occurrence as irregular interstitial blebs up to 30 μm in size. A single occurrence of gold associated with tetrahedrite was recorded where both phases were included in pyrite.

Figure 4-18. Polished section, MINTO 02. Plane polarized light. Gold replacing galena along cleavage planes.
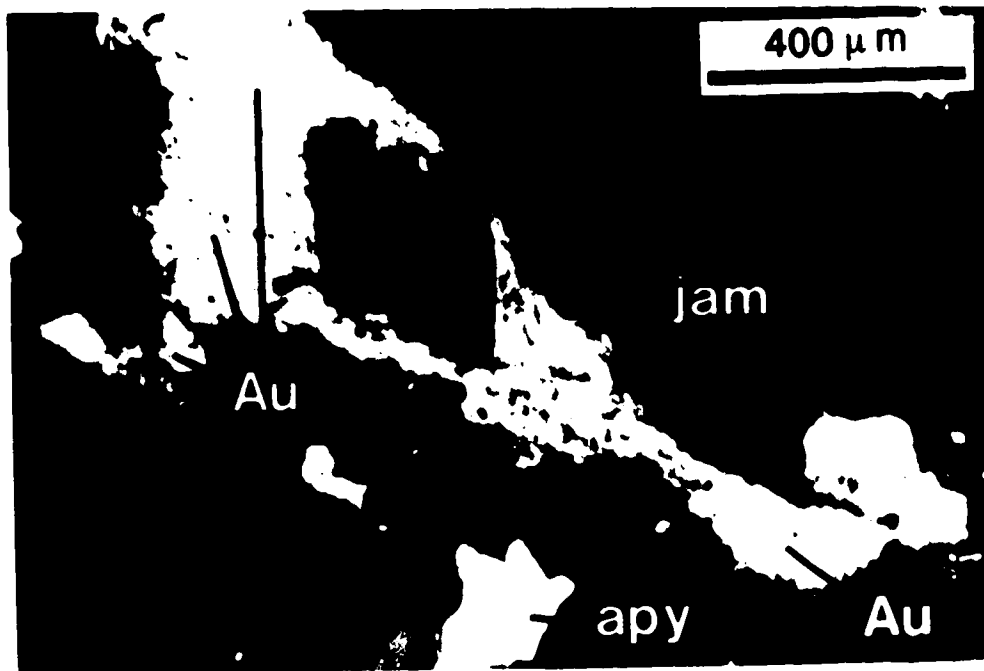
Figure 4-19. Polished section, MINTO 04. Plane polarized light. Gold infilling pits in highly corroded jamesonite.

A few isolated occurrences of a highly reflective, white phase associated with jamesonite were recorded. The phase occurs as wire-like bodies up to 100 μm in length coating stibnite and interstitial to quartz. In one location the material includes a small (<5 μm) bleb of gold . The phase's reflectance is too great to be that of silver and based on the limited textural and paragenetic evidence it is proposed that the phase is one of the gold-bearing tellurides.

Of the phases which host gold, galena appears to be the freshest, while pyrite and arsenopyrite are greatly pitted and fractured. The implication is that galena is most closely associated with the introduction of gold.

Olympic Prospect

The showings of the Olympic prospect display as varied a mineralogy as the Minto deposit. The early stages of gangue deposition and alteration included quartz, calcite (±ankerite), epidote, kaolinite, and sericite in variable amounts as replacement material in wall rock. Main stage mineralization is dominated by pyrite, chalcopyrite, and sphalerite. There are smaller concentrations of arsenopyrite, tetrahedrite and minor galena, jamesonite, magnetite, pyrrhotite, and marcasite. Trace amounts of gold complete the assembiage. Gold deposition is the final event in a somewhat protracted main stage of mineralization (Figure 4-11).

Pyrite, in concentrations up to 70%, dominates the sulphide mineralogy. Large irregular masses of anhedral to subhedral crystals up to several centimetres in size occur intergrown with quartz and calcite. The pyrite is highly fractured and corroded, particularily along fractures. Pyrite is most closely associated with chalcopyrite which occurs as irregular masses intergrown with it. Chalcopyrite represents up to 30% of mineralization. Pyrrhotite and marcasite are present in small amounts, less than 1% each as irregular grains averaging 0.3 mm in size, completely intergrown with pyrite.

Sphalerite, tetrahedrite and arsenopyrite occur in roughly equal (5-10%)

concentrations but, in total, are subordinate to pyrite and chalcopyrite (Figure 4-20). The

three phases exhibit similar morphologies as micron-sized blebs and irregular masses up to

1 mm in size sharing simple grain boundaries with and veining chalcopyrite and pyrite.

Tetrahedrite is most closely associated with chalcopyrite; both phases occur as inclusions in

one another. Star-shaped exsolution? bodies (~4 μm) of tetrahedrite are quite common in

individual chalcopyrite grains. Arsenopyrite and sphalerite share simple grain boundaries

with each other and chalcopyrite. They occur in irregular, highly fractured and corroded

masses to 1 cm in size. Sphalerite exhibits characteristic oriented intergrowths of

chalcopyrite.

The three sulphide phases, sphalerite, tetrahedrite, and arsenopyrite, are closely

associated with each other and pyrite, which texturally appears to be an earlier phase. The

three slightly later phases are included within and vein one another. Chalcopyrite has a

prolonged depositional history as it occurs associated both with early pyrite and veins the

later phases.

The deposition of galena, jamesonite, magnetite, and gold, together with late

chalcopyrite represents the waning of the main stage of mineralization. Galena occurs in

concentrations up to 5% as replacement blebs and irre   nclusions in chalcopyrite and

sphalerite and as masses sharing boundaries with arsenopyrite (Figure 4-21). Subhedral

needle-shaped crystals of jamesonite interstitial to and replacing quartz average 0.1 mm in

size. Irregular granular masses of magnetite totalling less than 1% of mineralization occur

up to 2 mm in size and often include individual octahedral crystals to 300 μm (Figure 4-

22). The magnetite is isolated in carbonate gangue and rarely shares simple grain

boundaries with chalcopyrite (Figure 4-23). Native gold was rarely observed. In the few

occurrences documented, gold was completely included in chalcopyrite as irre lar blebs

(ca. 20 μm) filling corrosion pits (Figure 4-24). A single occurrence of a highly reflective

phase, similar to that tentatively identified as a telluride in Minto ore, was noted. The phase
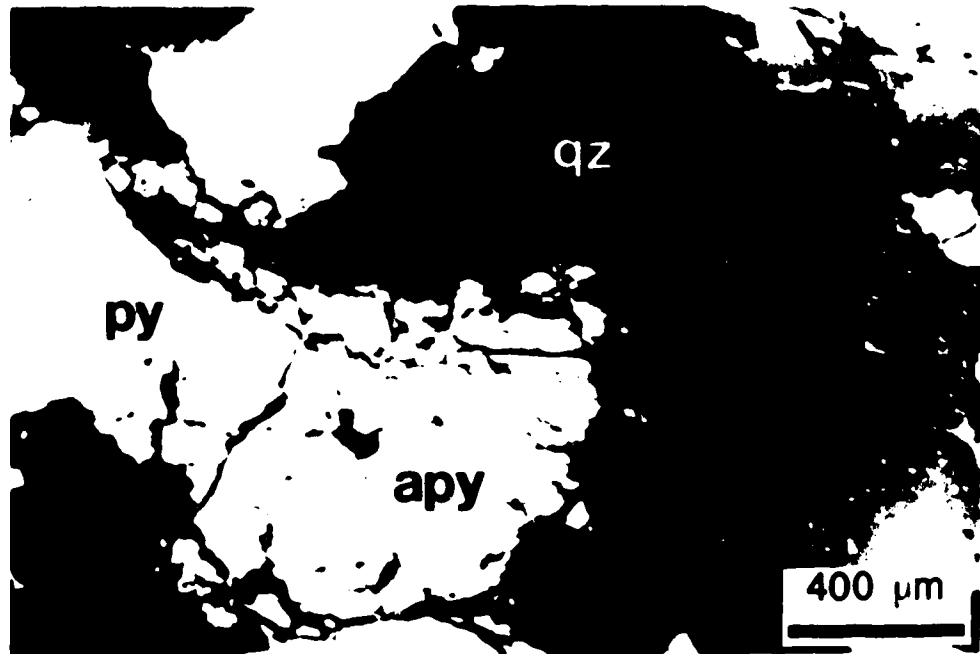
Figure 4-20. Polished section, OLY 07. Plane polarized light. Typical occurrence of sphalerite, tetrahedrite, pyrite, and arsenopyrite in Olympic ore.
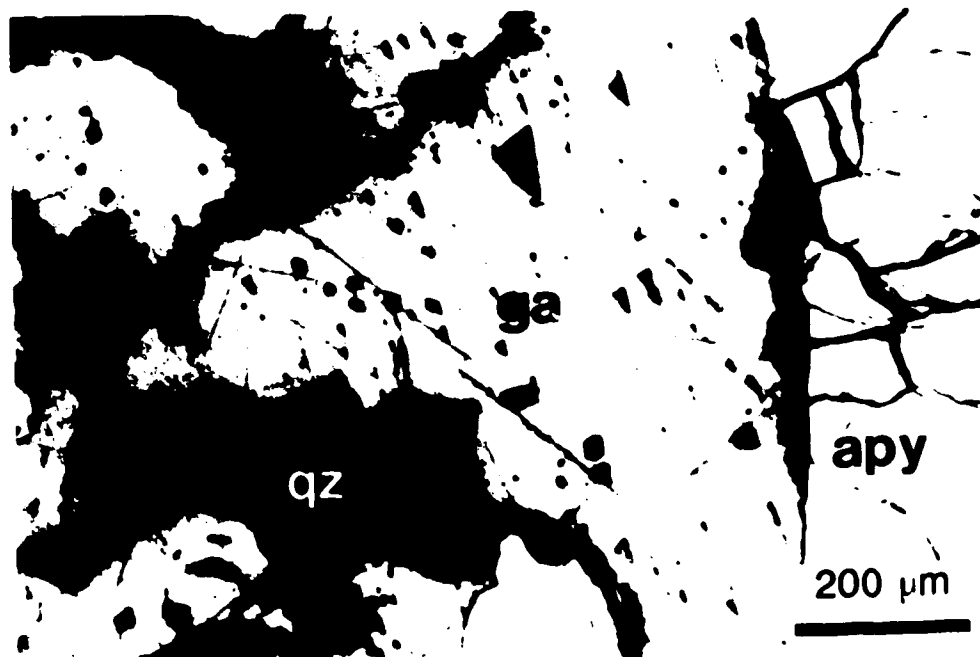
Figure 4-21. Polishe ection, OLY 07. Plane polarized light. Galena sharing simple boundary wi:h early arsenopyrite.
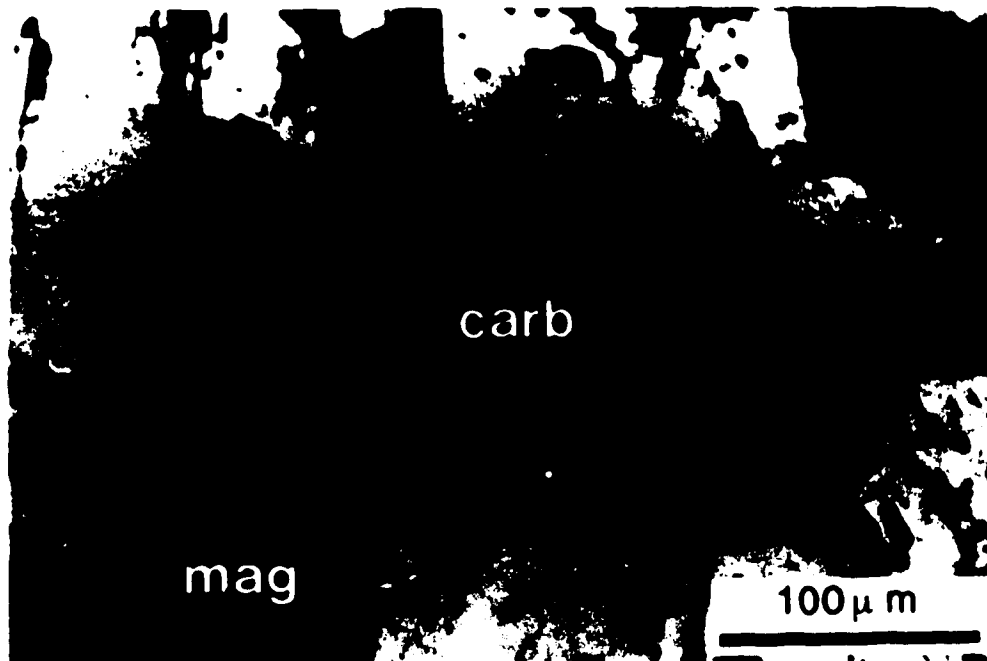
Figure 4-22. Polished section, OLY 01. Plane polarized light. Subhedral magnetite in carbonate gangue.
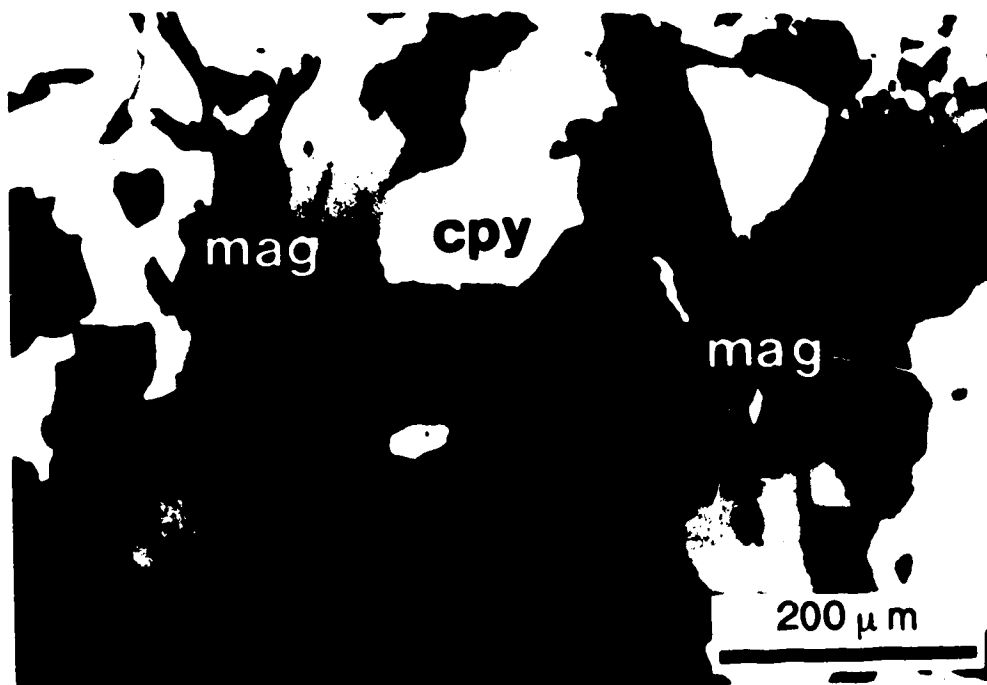
Figure 4-23. Polished section, OLY 01. .e polarized light. Typical occurrence of chalcopyrite and magnetite in Olympic ore.
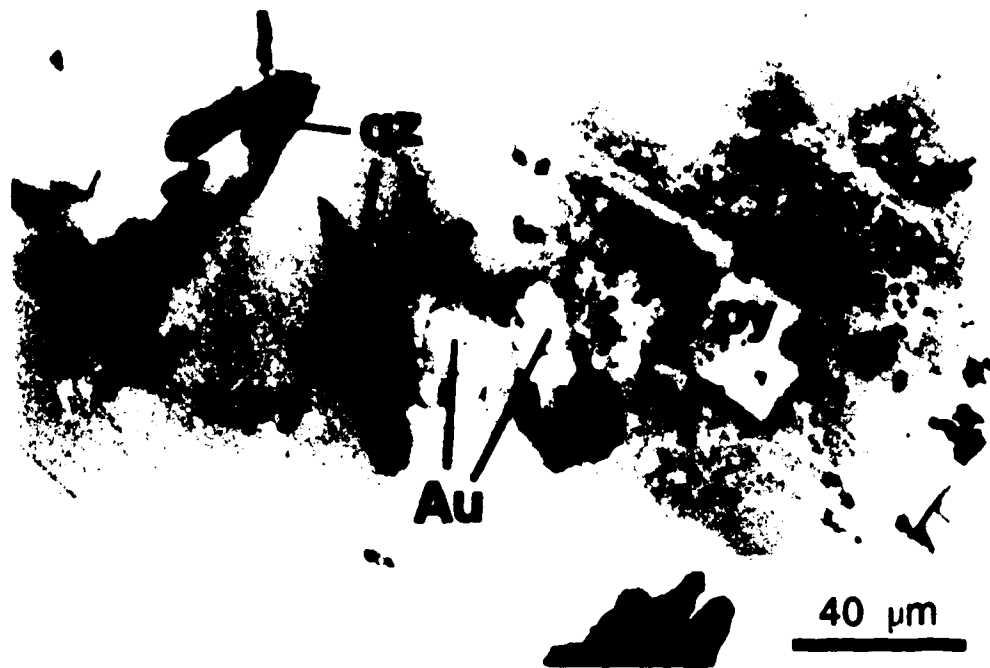
Figure 4-24. Polished section, OLY 03. Plane polarized light. Gold inclusions in chalcopyrite.

is associated with sphalerite as inclusions and fracture coatings and occurs as isolated blebs less than 5 μm interstitial to late quartz.

Secondary phases include covellite as an alteration of chalcopyrite along fractures and grain walls and much goethite as an alteration of iron-bearing phases.

4.3 Summary of Ore Petrography

Mineralization within all the deposits occurred during two to three events, which were not necessarily temporally discrete. Evidence of a protracted main stage of mineralization is present in the Minto and Olympic ores.

Though deposit mineralogies are grossly similar, and unique within the camp context, mineralogical differences are notable. Both categories of mineralization described in the previous sections contain significant concentrations of sulphides associated with gold-antimony mineralization. The Minto and Olympic deposits are noteworthy because of their even larger base metal concentrations. A less obvious difference is the association among mercury, antimony, and gold in the Congress deposits versus a strong gold-base metal association with lesser amounts of antimony in the Minto and Olympic ores. In each instance the texture of gold implies a late timing for deposition.

Cairnes (1943) suggested that both ore types within the antimony associated classification had originated from "the same magmatic source". He further proposed that evidence pointed to the influence of a temperature gradient in controlling mineral deposition, with antimony mineralization dominant at surface and other sulphides increasing in proportion at depth. In addition Cairnes documented a gold-arsenopyrite association, that is, with gold increasing at depth. Due to the lack of access, a three dimensional *in situ* survey of the deposits could not be undertaken in the present study to more fully investigate the potential for a vertical zonation in the deposits. However, samples of characteristic mineral assemblages were studied and, contrary to Cairnes earlier

findings, the strongest association for gold is with antimony and occasionally mercury mineralization in the Congress and related higher Au/Ag deposits and with base metal-antimony mineralization at Minto and Olympic (Table 4-1).

The question as to whether deposition was from an evolving hydrothermal fluid under the influence of a temperature gradient can be addressed through the study of inclusion fluid chemistry, geothermometry, geobarometry and through an investigation of the light stable isotope geochemistry of the gangue and alteration mineralogy associated with ore deposition.

The following chapters present the results of such a study and an attempt is made to synthesize the findings in a genetic model for antimony-associated gold mineralization in the Bridge River district.

V. FLUID INCLUSION STUDY

5.0 Introduction

Analyses of fluid inclusions in quartz and carbonate vein material associated with mineralization in five deposits were carried out to obtain information on the nature of the ore forming fluids and to determine if the thermal and chemical character of the hydrothermal fluids varied as a function of time and space. Specific objectives include ascertaining the temperature of formation (trapping temperatures), pressures at the time of trapping, and fluid compositions. This information, coupled with light stable isotope data could potentially indicate the origin of the ore fluids and limit the conditions of ore deposition.

Material was selected for inclusion study based on its paragenetic association with the main stage of mineralization in each occurrence and/or that stage which hosts gold. In many instances this criterion could not be satisfied as the material was of poor optical quality or the inclusions were not useable because of small size or evidence of leakage. In such a case material that provided useable inclusions, but could not be unequivocally associated with main stage mineralization, was analysed.

Fluid inclusions observed are of two types: Type 1 inclusions are dilute salt-H_2O inclusions; Type 2 inclusions are CO_2 with possibly up to a 5% CH_4 component.

Salinities in Type 1 inclusions range between 2.9 and 4.2 equivalent weight percent (eq. wt. %) NaCl on average for the different deposits. No evidence suggests a significant difference in salinity between ore fluids associated with the base metal-enriched deposits versus those with a smaller base metal concentration. Observations of first melt temperatures (T_e) from one deposit suggest a composition intermediate to the $MgCl_2$-H_2O and $NaCl$-KCl-H_2O systems. Homogenization temperatures of Type 1 inclusions in all the

61

deposits are comparable averaging 270° ±20°C. Pressure estimates based on fluid inclusion data and fluid inclusion data coupled with stable isotope geothermometry range between 210 and 500 bars suggesting relatively shallow emplacement of mineralization.

5.1 Analytical Techniques

A total of 58 doubly polished sections of thicknesses ranging from 100 to 300 μm were prepared from 20 samples of quartz and carbonate vein material from 5 occurrences: Congress, Howard, Lou, Minto, and Olympic. Thirty-seven sections yielded inclusions for microthermometry analyses.

Petrographic study of the inclusion sections was carried out using a Leitz microscope equipped with 10X periplan oculars in combination with 4X, 10X, and 32X EF objectives. Microthermometric analyses were performed using an adapted U.S.G.S. gas-flow, heating-freezing stage mounted on the microscope. The accuracy of the stage using a SCXIN - 020U - 4.5 inch thermocouple with a Doric Digital Trendicator (Model 410A) temperature readout is quoted as ±0.1°C in the range -56.6° to +660.4°C by the manufacturer. The stage was calibrated using liquid nitrogen, ice water, and Merck Standard 9800 (melting point 200°C).

Fluid inclusions suitable for freezing and/or heating tests were mapped in detail at low magnification to determine their spatial and temporal relationships to the total population of inclusions in the sample. Microthermometric measurements were then carried out. Measurements of all melting and homogenization temperatures were repeated at least twice to insure reproducibility. Replicate measurements for the temperature of final melt of CO_2 were within ±1.0°C. Replicate measurements for the the temperature of final melt of ice were within ±1.5°C, as was the reproducibility of homogenization temperatures for CO_2 inclusions. The reproducibility for homogenization of H_2O inclusions was generally less than ±1.0°C.

Phase changes occurring in several inclusions in a field were measured in a single freezing or heating run. Lcw temperature measurements were performed first to avoid the possibilty of high temperature stretching of the inclusion walls and thereby altering the volume of the inclusion (Roedder, 1984). The inclusions were cooled to -100° to -110°C and then warmed to within 5°C of important phase changes . At this point the inclusions were allowed to equilibrate and a subsequent heating rate of from 0.2 to 0.5°C/minute was used until the particular phase change was observed. During high temperature heating runs inclusion chips were heated rapidly to within 20° to 30°C of the temperature of homogenization. At this point the inclusion was then allowed to equilibrate and a subsequent heating rate of from 0.2° to 0.5°C/minute was used until homogenization occurred. Data derived from fluid inclusion measurements are presented in Table 5-1 and summariz ed in Table 5-2.

5.1.1 Description and Classification of Inclusions

Gangue minerals selected for fluid inclusion analysis consisted of rare, subhedral to euhedral quartz and carbonate (ankerite, calcite); more commonly the material was strained and/or highly fractured and crushed. Quartz and carbonate specimens from five of the deposit/occurrences in the study contain fluid inclusions ranging in size from less than 1 to 25 μm in their longest dimension. The majority of inclusions analyzed were in the range of 5 to 10 μm. No useable inclusions were found in any material from the Dauntless prospect. In this study fluid inclusions were classified based on observable phases at room temperature and include:

Type 1: Dilute salt-H_2O inclusions homogenize by expansion of the liquid and disappearance of the vapour bubble upon heating. No evidence for noncondensed gases was observed in these liquid-rich inclusions. The

Table 5-1. Fluid inclusion data. (Notes at end of table.)

Sample/Host	Origin	Inc Size	Inc Shape	Bub Diam	Phase Assem	Vol% H2O	Vol% CO2(l)	Vol% CO2(g)	Te	TmCO2	Fill @ TmCO2	TmICE	ThCO2	Th	Eq Wt % NaCl
CON 16 FI1-C carb	prim	17.0	rect	5.0	L-V	85			-25 to -30			-0.6		295	1 0
	prim	10.0	irr, eq	2.0	L-V	80						: :		256	
	prim	9.0	irr, eq	2.0	L-V	80						: :		251	
CON 16 FI1-C carb	prim	10.0	elong	2.5	L-V	80			-25 to -30			-3.0		282	4 9
	prim	7.5	irr, eq	1.5	L-V	80						-3.0		290	4 9
	sec?	20.0	irr, eq	7.0	L-V	70						: :		271	
CON 16 FI1-D carb	psec	5.0	irr, eq	1.0	L-V	80						-1.4		236	2 4
	psec	8.0	irr, eq	2.0	L-V	80						-1.4		232	2 4
	psec	7.5	elong	1.0	L-V	85			-25 to -30			-1.4		234	2 4
	prim	20.0	elong	5.0	L-V	75			-25 to -30			-2.0		253	3 4
	prim	25.0	irr, elong	8.0	L-V	75						-2.0		260	3 4
	prim	9.0	irr, elong	2.5	L-V	80						-4.1		320	6 6
	prim	8.0	irr, elong	2.5	L-V	70						-1.0		285	1 7
	psec	8.0	eq	2.5	L-V	70						-2.7		238	4 5
CON 16 FI1-A carb	prim	8.0	irr, eq	2.0	L-V	75			-25 to -30			-2.2		266	3 7
	prim	8.0	irr, eq	2.0	L-V	75						-2.3		351	3 9
CON 12 FI1-A carb	prim	15.0	irr, elong	5.0	L-V	70						-2.5		329	4 2
	sec	10.0	neg xtal	1.5	L-V	80						-2.3		226	3 9
	prim	10.0	neg xtal	5.0	L-V	70						-2.1		337	3 5
	prim	15.0	irr, elong	3.5	L-V	80						-2.7		332	4 5
	prim	8.0	neg, xtal	2.0	L-V	75						-2.3		258	3 9

Table 5-1 continued.

Sample/ Host	Origin	Inc Size	Inc Shape	Bub Diam	Phase Assem	Vol% H2O	Vol% CO2(l)	Vol% CO2(g)	Te	TmCO2	Fill @ TmCO2	TmICE	ThCO2	Th	Eq Wt% NaCl
CON 18 FI1-A qz	prim	10.0	eq	3.0	L-V	80			-25 to -30			-1.5		260	2.6
	prim	7.5	eq	2.5	L-V	75						-2.4		301	4.0
	prim	8.0	eq	2.0	L-V	75						-1.6		281	2.7
	prim	10.0	eq			75								298	
	prim	10.0	eq		L-V	75			-25 to -30			-1.2		292	2.1
	prim	7.0	elong	2.0	L-V	70						-2.9		287	4.8
CCN 14 FI1-B qz	sec	6.0	irr, eq	1.0	L-V	75								233	
	prim	8.0	elong	1.5	L-V	75								315	
	prim	6.0	eq	1.0	L-V	70								304	
CON 18 FI1-A qz	prim	11.0	elong	2.0	L-V	80			-25 to -30					265	
	prim	8.0	eq	1.0	L-V	85								273	
CONEX 01 FI1-A qz	sec	10.0	irr, eq	2.0	L-V	95								143	
	sec	8.0	irr, eq	1.5	L-V	80								153	
	sec	10.0	irr, eq	2.0	L-V	85								158	
CONEX 01 FI2-A qz	psec	15.0	irr, elong	4.0	L-V	75						-6.1		274	9.3
	prim	6.0	eq	1.0	L-V	75						-4.6		255	7.3
	prim	10.0	eq	2.5	V	75						lkd		-	
	prim	13.0	eq	5.0	L-V	75						-4.0		266	6.4
CONEX 03 FI1-A qz	sec	10.0	irr, eq	2.5	L-V	80						-0.8		189	1.4
	prim	12.0	elong	3.0	L-V	80						-2.7		272	4.5

Table 5-1 continued.

Sample/Host	Origin	Inc Size	Inc Shape	Bub Diam	Phase Assem	Vol% H2O	Vol% CO2(l)	Vol% CO2(g)	Te	TmCO2	Fill @ TmCO2	TmIce	ThCO2	Th	Eq Wt% NaCl
LOU 03 FI1-B qz	prim	12.0	neg xtal	2.5	L-V	85						-2.5		271	4.2
LOU 03 FI1-C qz	psec?	10.0	irr	2.0	L-V	90						-0.8		147	1.4
	prim	10.0	elong	2.0	L-V	75						-5.0		165	7.9
LOU 01 FI1-A qz	sec?	15.0	rect	5.0	L-V	85						--		220	
	prim	12.0	elong	1.0	L-V	85						--		263	
LOU 15 FI1-A qz	prim	5.0	irr, eq	0.5	L-V	70						--		263	
	prim	5.0	irr, eq	0.5	L-V	70						--		249	
	prim	5.0	irr, eq	0.5	L-V	70						--		259	
LOU 09 FI1-A qz	prim	10.0	irr, eq	2.0	L-V	85						-2.0		270	3.4
	prim	6.0	eq	1.5	L-V	70						-1.6		260	2.7
	prim	8.5	eq	2.0	L-V	80						-2.1		267	3.5
HOW 06 FI1-A qz	prim	10.0	elong	2.5	L-V	80						-2.6		249	4.3
	prim	8.5	irr, eq	2.0	L-V	80						-2.0		253	3.4
	prim	8.0	irr, eq	2.0	L-V	80						--		258	
	prim	8.0	irr, eq	2.0	L-V	75						--		256	
HOW 08 FI1-A qz	prim	6.0	irr, eq	1.0	L-V	70						--		254	
	prim	8.0	irr, eq	1.5	L-V	80						-1.8		263	3.1
	prim	9.0	irr, eq	2.0	L-V	80						-2.0		258	3.4
	prim	6.0	irr	1.0	L-V	70						--		240	
	prim	8.0	elong	1.0	L-V	80						-2.3		252	3.9

Table 5-1 continued.

Sample/ Host	Origin	Inc Size	Inc Shape	Bub Diam	Phase Assem	Vc % H2O	Vol% CO2(l)	Vol% CO2(g)	Te	TmCO2	Fill @ TmCO2	TmICE	ThCO2	Th	Eq Wt % NaCl
HOW 08 FI2-A qz	prim	8.0	irr, eq	2.0	L-V	85						-1.9		266	3.2
	prim	8.0	irr, eq	1.5	L-V	70						-1.9		246	3.2
	prim?	5.0	irr	<1.0	L-V	60						-1.5		232	2.6
	prim	9.0	elong	2.0	L-V	80						-2.2		259	3.7
HOW 08 FI1-C qz	prim	9.0	irr, eq	2.0	L-V	80						-1.6		264	2.7
	prim	8.0	irr, eq	1.5	L-V	75						-2.0		260	3.4
	prim	8.0	irr, eq	1.0	L-V	80						-1.9		258	3.2
HOW 12 FI1-A qz	prim	8.0	irr, eq	1.5	L-V	75						-2.1		269	3.5
	prim	8.0	irr, eq	1.5	L-V	80						-2.0		248	3.4
	prim	10.0	irr, eq	2.0	L-V	75						-2.3		258	3.9
	sec	6.0	irr, eq	1.0	L-V	65						-0.8		214	1.4
MINTO 06 FI2-A carb	prim?	4.0	neg xtal	<1.0	L-V	70								191	
	prim?	4.0	neg xtal	<1.0	L-V	70								192	
MINTO 06 FI2-C carb	sec	6.0	rect	1.0	L	85								206	
MINTO 07 FI1-A carb	prim	5.0	elong	<1.0	L-V	75								313	
	prim	6.0	irr, eq	1.0	L-V	8°								80	
	prim	8.0	irr, eq	2.0	L-V	80								288	
MINTO 06 FI2-A carb	prim	12.0	irr	2.5	L-V	75						-1.3		234	2.2
	prim	6.0	eq	2.0	L-V	80						-1.0		245	1.7
	prim	9.0	elong	4.5	L-V	50						-1.3		281	2.2
	prim	11.0	elong	2.0	L-V	80						-2.1		272	3.5
	prim	12.5	neg xtal	2.0	L-V	70						-1.3		226	2.2

Table 5-1 continued.

Sample/ Host	Origin	Inc Size	Inc Shape	Bub Diam	Phase Assem	Vol% H2O	Vol% CO2(l)	Vol% CO2(g)	Te	TmCO2	Fill @ TmCO2	TmICE	ThCO2	Th	Eq Wt % NaCl
MINTO 07 FI2-A carb	prim	10.0	eq	2.0	L-V	80								284	
	sec?	5.0	eq	<1.0	L-V	70								195	
	prim	9.0	elong	1.0	L-V	80								299	
	prim	5.0	eq	<1.0	L-V	70								306	
MINTO 06 FI1-B qz	prim	13.0	neg xtal	2.5	L-V	70						-2.0		242	3.4
	sec	5.0	elong	1.0	L-V	70						-1.9		210	3.2
	prim	8.0	elong	2.0	L-V	7?						-2.0		222	3.4
MINTO 06 FI2-B qz	psec	9.0	rect	2.0	L-V	80						-1.8		208	3.1
	prim	5.0	elong	1.0	L-V	65						-1.7		270	2.9
	psec?	6.0	elong	1.0	L-V	70								209	
	psec	6.0	eq	1.0	L-V	70								206	
	prim?	12.0	elong	2.5	L-V	85						-1.7		260	2.9
	psec?	5.0	irr, eq	1.5	L-V	70								211	
MINTO 07 FI2-C carb	prim	4.5	eq	1.0	L-V	75						-1.8		257	3.1
	prim	11.0	irr	2.5	L-V	75						-2.0		331	3.4
	prim	11.0	elong	2.0	L-V	75						-2.0		310	3.4
MINTO 07 FI2-D carb	prim	10.0	elong	2.0	L-V	85						-1.7		295	2.9
	prim?	8.0	eq	1.5	L-V	75						-0.5		172	0.9
	psec	11.0	elong	2.0	L-V	80						-2.6		218	4.3
	prim	8.0	eq	2.5	L-V	80						-1.8		304	3.1

Table 5-1 continued.

Sample/Host	Origin	Inc Size	Inc Shape	Bub Diam	Phase Assem	Vol% H2O	Vol% CO2(l)	Vol% CO2(g)	Te	TmCO2	Fill @ TmCO2	TmICE	ThCO2	Th	Eq Wt % NaCl
OLY 08 FI1-A qz	prim	10.0	—	2.5	L-V	80						-1.4		245	2.4
	prim	5.0	—	1.0	L-V	80						-1.3		248	2.2
OLY 08 FI1-B qz	prim	7.5	eq	2.5	L-V	80						-2.4		290	4.0
	prim	10.0	elong	2.0	L-V	75						-1.2		292	2.1
	prim	12.5	eq	5.0	L-V	50						-1.3		293	2.2
	prim	12.5	irr, eq	2.0	L-V	85						-3.1		290	5.1
	prim	12.5	along	3.5	L-V	75						-3.1		287	5.
	prim	17.0	irr, along	5.0	L-V	75						-3.5		290	5.7
	prim	5.0	irr, eq	2.0	L-V	70						-1.6		286	2.7
OLY 08 FI1-B qz	prim	7.0	elong	2	L-V	75						-2.3		270	3.9
	prim	12.5	irr, eq	4	L-V	90								302	
	prim	10.0	irr, eq	4.5	L-V	80								309	2
	prim	15.0	elong	5.0	L-V	70						-0.1		292	
OLY 08 FI1-C qz	prim	12.5	irr	5.0	L-V		10	90		-5.	0.90		30.2(v)		
	prim	10.0	elong	3.0	L-V		15	85		-56	0.85		30.1(v)		
	prim	11.0	irr, eq	6.5	L-V		10	90		-57.1	0.95		28.4(v)		
OLY 08 FI1-A qz	prim	15.0	irr, eq	5.0	L-V	40						1.5		265	2.6
OLY 03 FI1-A qz	prim	12.5	irr, eq	5.0	L-V	75						-1.4		262	2.4
	prim	6.0	elong	1.5	L-V	75						-2.2		267	3.7
	prim	9.0	irr, eq	2.0	L-V	80						-1.8		263	3.1

Table 5-1 continued.

Sample/Host	Origin	Inc Size	Inc Shape	Bub Diam	Phase Assem	Vol% H2O	Vol% CO2(l)	Vol% CO2(g)	Te	TmCO2	Fill @ TmCO2	TmICE	ThCO2	Th	Eq Wt % NaCl
OLY 03 FI1-A qz	prim	10 0	elong	5 0	L-V		50	50		-58 6	0 90		30 0(v)	259	2 9
	prim	14 0	irr, eq	6 0	L-V		50	50		-58 3	0 85		30 2(v)	271	3 1
	prim	10 0	irr, eq	2 0	L-V	75						-1 7			
	psec	11 0	elong	2 5	L-V	85						-1 8			
OLY 03 FI2-A qz	prim	7 0	elong	1 0	L-	65						-1 1		266	1 9
	prim	6 0	irr, eq	2 0	L-V	65						-1 3		270	2 2
	prim	10 0	elong	2 5	L-V	75						-1 6		272	2 7
OLY 03 FI1-A qz	sec?	12 0	elong	2 5	L-V	90						-1 0		184	1 7
	prim	7 5	irr, eq	2 0	L-V	75						-1 6		275	2 7
	prim	7 0	irr, eq	2 ?	L-V	65						-1 7		278	2 9
	prim	8 0	irr, eq	2 0	L-V	85						-1 7		275	2 9
	sec?	10 0	irr, eq	2 0	L-V	85						-1 7		170	? 9
	prim	8 0	elong	2 5	L-V	75						-1 4		275	2 4
	sec?	15 0	irr	3 0	L-V	80						-1 7		lka	2 9
OLY 03 FI2-A	prim	10 0	irr, eq	2 0		75						-2 1		312	3 5
	prim	15 0	eq	3 0		? 5						-2 5		312	4 2
	prim	10 0	irr, eq	3 0		? 5						-1 5		374	2 6
OLY 03 FI1-B qz	prim	7 5	irr	1 5	L-V	65						-3 0		345	4 9
	prim	13 0	irr	2 0		80								310	
OLY 03 FI1-C qz	prim	7 0	irr, eq	2 0	L-V	80						-1 ?		259	2 1
	prim	9 0	elong	2.0	L-V	85						-1 3		258	2 2
	prim	5 0	irr, eq	<1 0	L-V	80						-1 6		300	2 7
	prim	5 0	neg xtal	1 0	L-V	65						-1 8		295	3 1

Table 5-1 continued.

Sample/Host	Origin	Inc Size	Inc Shape	Bub Diam	Pha Asse	%	Vol% CO2(l)	Vol% CO2(g)	Te	TmCO2	Fill @ TmCO2	TmICE	ThCO2	n	Eq Wt % NaCl
OLY 07 FI1-A qz	prim	10.0	irr, elong	7.0	L-V	85	20	80		-57.4	0.90	-2.0	30.4(v)	22?	3.4
	sec?	12.5	irr	2.0	L-V										
	prim	8.0	ov	6.0	L-V		5	95		-57.6	0.95		31.0(v)		
	prim	12.0	irr, elong	11.0	L-V		5	95		-57.3	0.90		30.7(v)		
OLY 07 FI1-A qz	prim	9.0	eq	8.0	L-V		5	95		-57.4	0.95		31.0(v)		
	prim	9.0	irr, elong	9.0	L-V		5	95		-57.3	0.85		30.7(v)		
OLY 08 FI1-B qz	prim	9.0		9.0	L-V	85						-1.4		264	2.4
	prim	6.0	eq	1.0	L-V	75						-1.2		270	2.1
	prim	7.5	rect	1.0	L-V	65						-1.2		319	2.1
	psec?	6.0	rect	0.5	L-V	90								120	
OLY 08 FI1-D qz	psec	7.0	irr, eq	1.0	L-V	85						-3.3		235	5.4
	prim	8.0	elong	2.0	L-V	80						-3.0		257	4.9
	prim	5.0	elong	<1.0	L-V	75						-2.7		242	4.5
	prim	9.0	elong	2.0	L-V	75						-3.0		250	4.9
	prim	5.0	irr, eq	1.0	L-V	75						-2.7		251	4.5
	prim	4.0	irr, eq	<1.0	L-V	65								263	
OLY 08 FI2-A qz	prim	6.0	irr	2.0	L-V	75						-3.1		248	5.1
	prim	10.0	elong	3.0	L-V	75						-.6		260	2.7

Notes

All temperatures in °C
Measured dimensions in microns
Abbreviations   qz - quartz   prm - primary   ? - possible   elong - elonga :   neg xtal - negative crystal form
carb - carbonate   sec - secondary   irr - irregular   ov - oval   (v) - homogenization to vapour phase
psec - pseudosecondary   eq - equant   rect - rectangular   (l) - homogenization to the liquid phase
(g) - homogenization to the gas phase

Table 5-2. Average values derived from fluid inclu ion data.

Deposit/ Occurrence	Vol% H₂O(l)	Vol% CO₂(l)	TmCO₂	Tm_ice	Tm_clath	ThCO₂	Th	Eq.Wt.% NaCl
CONCRESS								
mean	'6			2 6			286	4 2
std dev	4	...		1 3	...	...	28	' 9
no of inc	31			22			30	22

Additional data Te = -25 to -30 (8 measurements)

HOWARD								
mean	77			-2 0			255	3 4
std	6	...	. .	0 ?	...	...	9	0 4
no of inc	19			.			19	15

LOU								
mean	78			-2.1			258	3 5
std dev	8	...	...	0 4	...	...	16	0.6
no of incs	9			4			9	4
							~265° ±20°C	

MINTO								
mean	75			-1.7			276	2 9
std dev	8	...	...	0.3	...	...	31	0.6
no of incs	20			14			20	14

OLYMPIC								
mean	75	93	-57 5	-1.9		30.3	278	3.2
std dev	9	2.5	0 6	0 7	...	0 7	28	1.2
no. of incs	47	10.0	1 0	43		10	46	43
							~280° ±30°C	

All temperature measurements °C.

degree of filling for Type 1 inclusions is between 0.75 and 0.80 (degree of filling - volumetric ratio [liquid / [liquid + vapour]). Type 1 inclusions account for all observed inclusions in Congress, Howard, Lou, and Minto samples, and the majority of the inclusions observed in Olympic sample

Type 2: CO_2 rich inclusions show expansion of the vapour phase during heating of the inclusion. CO_2 solid forms at temperatures of -90° to -105°C and melting of CO_2 solid occurs at -57.5°C on average. The presence of another component, probably CH_4 ($X_{CH_4} \cong 0.05$), is indicated by the depression of the melting point of solid CO_2 by about 0.9°C from -56.6°C (Swanenberg, 1979). Type 2 inclusions were observed in 3 Olympic samples only.

Where possible, fluid inclusions were also classified as primary, secondary, or pseudosecondary, based on the empirical criteria of Roedder (1984, p. 43). Quartz and carbonate samples used in the study had been repeatedly fractured during and following vein formation as evidenced by the many planes of fluid inclusions cross-cutting mineral grain boundaries.

Inclusion shape in the plane of focus ranged from equant to elongate with regular, or more commonly, irregular outlines. Secondary inclusions were equant and regular in character while the larger primary inclusions showed more irregular outlines. Inclusions displaying euhedral negative crystal forms were fairly common in carbonate samples, both in planar arrays of small inclusions along fractures (secondary origin) and as larger (10 μm) isolated inclusions (primary inclusions).

5.1.2 Low Temperature Techniques

Low temperature microthermometry p? ~ uced data of four types: CO_2 final melting temperatures ($TmCO_2$), eutectic minima, or first melt temperatures of brine (T_e), final melting temperature of ice (Tm_{ice}), and CO_2 homogenization temperatures ($ThCO_2$).

Final Melting Temperature of C $\cap$ _. $TmCO_2$

The melting temperature of CO_2 is -56.6°C. Any deviation from this value indicates the presence of another gaseous phase in the system. Roedder (1984) noted that CH_4 is by far the most common gas associated with CO_2 in fluid inclusions. The addition of CH_4 to CO_2 lowers the temperature at which phase changes occur with respect to those in the pure CO_2 system (Swanenberg, 1979). Thus a dep   ion in $TmCO_2$ would indicate the presence of CH_4 or other gases.

Two methods can be applied to determine the mole fraction of CH_4 in the CO_2-CH_4 system. On freezing of the CO_2, CH_4 will be concentrated in the gas phase (Swanenberg, 1979). Swanenberg's (1979) method utilizes the final melting temperature of CO_2, which fixes the composition and the density of both the liquid and gas, thus enabling the bulk composition to be determined from the degree of filling (volumetric ratio liquid / liquid + gas) at $TmCO_2$. A second method was described by Burrus (1981) and derived from the fact that if two independent, two-phase tie lines at different temperatures can be determined for an inclusion, the point of intersection must define the bulk composition and the density of the inclusion. That is, with $TmCO_2$, $ThCO_2$ and appropriate V-T-XCH_4 data, the composition and density of the system can be uniquely defined.

Measurements of final melting temperatures of CO_2 were based on a slight change in translucency o the inclusion contents around $TmCO_2$.

Temperature of Eutectic Point, T_e

Accurate measurement of the temperature of first melting (T_e) is important for the determination of the composition of the system. The initial melting of a frozen inclusion in the $NaCl-H_2O$ system starts at the eutectic temperature for the system (-20.8°C). In brines with more than one dissolved salt the overall eutectic minimum shifts according to the composition of the system (Crawford, 1981).

Final Melting Temperature of Ice. Tm_{ice}

A final melt measurement was obtained by cooling the inclusion then observing Tm_{ice} on heating Final melting temperatures were determined by incremental heating near the melting point. Failure of the vapour bubble to shrink (distort due to freezing of the liquid) after the heating element had been disengaged indicated the final melting temperature had been reached. In dilute brines the last phase to melt is ice and the final melting temperature is a measure of dissolved solids in the inclusion fluid in which no other solutes (*e.g* CO_2, CH_4) are present (Potter *et al.*, 1977). Potter and Clynne (1978) showed that the P-V-T-X properties of naturally occurring brines (*i.e.* in the system Na-K-Ca-Mg-Cl-Br-SO_4-H_2O) can be estimated to within ±1.0% by the properties of a NaCl solution with the same Tm_{ice}. Therefore salinities can be reported in equivalent weight percent NaCl (eq. wt. % NaCl) and are calculated according to the formula provided by Potter *et al* (1977):

$$W = 0.00 + 1.76958T - 4.2384 \times 10^{-2}T^2 + 5.2778 \times 10^{-4}T^3$$

Where W is weight percent NaCl and T is the temperature of final melting of ice in °C.

CO₂ Homogenization Temperature, ThCO₂

Carbon dioxide (Type 2) inclusions yielded homogenizati n temperatures upon expansion of the vapour bubble to fill the entire volume of the inclusion. The process v readily reproducible for each inclusion.

The density of the CO_2 phase in Type 2 inclusions can be calculated with the knowledge of $ThCO_2$, the phase to which the inclusion homogenized, and the P-V- ⁻ XCO_2 data of Angus *et al.* (1976).

5.1 3 High Temperature Techniques

High temperature microthermometry provided measurements of temperatures of homo ni:ation for Type 1 inclusions.

Homogenization Temperature, T_h

Homogenization of an inclusion was determined by cycling temperatures in order to bracket the temperature at which the vapour bubble disappeared. Homogenization to the liquid phase occurred in every case. T_h alues for a fluid define an isochore which maps the loci of constant density in P-T space for the fluid. With reference to simple fluid systems it is possible to derive estimates of the P-V-T-X state of the fluids at the time of trapping. However, because most natural systems are multi-component the estimates are semi-quantitative.

Abbreviations used pertaining to fluid inclusion analyses are defined as follows:

$TmCO_2$ = Temperature of final melting of CO_2 solid.

T_e = temperature of eutectic point for $NaCl-H_2O$ inclusions (first melt).

Tm_{ice} = temperature of final melting of ice.

$Th.CO_2$ = temperature of homogenization of CO_2 liquid and CO_2 gas in CO_2 inclusions.

T_h = temperature of homogenization of H_2O brine and H_2O vapour in NaCl H_2O inclusions.

5.2 Measurements of Phase Changes at Low Temperatures

Final Melting Temperature of CO_2, Tm_{CO_2}

` 1 incl. ns in vein material from the Olympic property provided Tm_{CO_2} measurements. The 10 Type 2 inclusions from Olympic vein material had degrees of filling of 0.9 on average at Tm_{CO_2} (-57.5° ±0.6°C) and all homogenized to the vapour phase at Th_{CO_2} (30.3° ±0.7°C). The two methods were applied to estimate the amount of CH_4 in the system. Both methods yield a possible CH_4 content of ≤ 5 mole %. The density of a binary CO_2-CH_4 inclusion may be expressed in terms of "equivalent CO_2-density" (Swanenberg, 1979), yielding densities of ca. 0.35 g/cm³ This value is comparable to that calculated using the equation of Angus *et al* (1976, p.12) for the CO_2 saturated vapour density in an essentially pure CO_2 system, 0.34 g/cm³.

Temperature of Eutectic Point, ".

A first melt (ice) temperature was recorded for only 8 inclusions from Congress samples. In all other cases the small size of the inclusions, coupled with the presumably small volumes of melt fluid at the eutectic precluded recording T_e. The 8 measurements range from -25° to -30°C. The measurements, which must be considered rough estimates, fall between the eutectic minima for the $MgCl_2$-H_2O and the NaCl-KCl-H_2O systems, -33.6°C and -22.9°C respectively (Crawford, 1981).

Final Melting Temperature of Ice, Tm$_{ice}$

Tm$_{ice}$ measurements were recorded for most of the Type 1 inclusions studied. Histograms of salinities for all Type 1 inclusions are presented in Figure 5-1 and are summarized for comparison in Figure 5-2. Average values for the occurrences fall within the range of 2.9 to 4.2 eq. wt. % NaCl.

The presence of CO_2 in the inclusion fluids can affect the freezing point of the fluid (Collins, 1979; Hedenquist and Henley, 1985). Hedenquist and Henley (1985) make the point that relatively low concentrations of CO_2 in dilute brines may escape detection and contribute up to 1.5°C to the depression of the melting point of the fluid, suggesting apparent salinities higher by as much as 2.0 eq. wt. % NaCl than are actually present. The presence of liquid CO_2 was not indicated in any Type 1 inclusions, including those in Olympic vein material. The lack of a liquid CO_2 phase in Type 1 Olympic inclusions places an upper limit of CO_2 concentration at about 2.2 molal at a 10°C isotherm (Hedenquist and Henley, 1985). At CO_2 concentrations between 0.85 and 2 2 molal (3.7 wt. % CO_2 and 8.8 wt. % CO_2) the formation of CO_2 gas hydrate during freezing will concentrate salts in the residual liquid phase and result in a depression of the ice melting temperature. Although no evidence for a CO_2 hydrate was observed in the inclusions, the salinities calculated from ice melting temperatures should be considered maximum values.

Fluid inclusions in Olympic vein material are considered candidates for potential spurious salinity measurements because of the positive identification of CO_2 in (at least part of) the system.
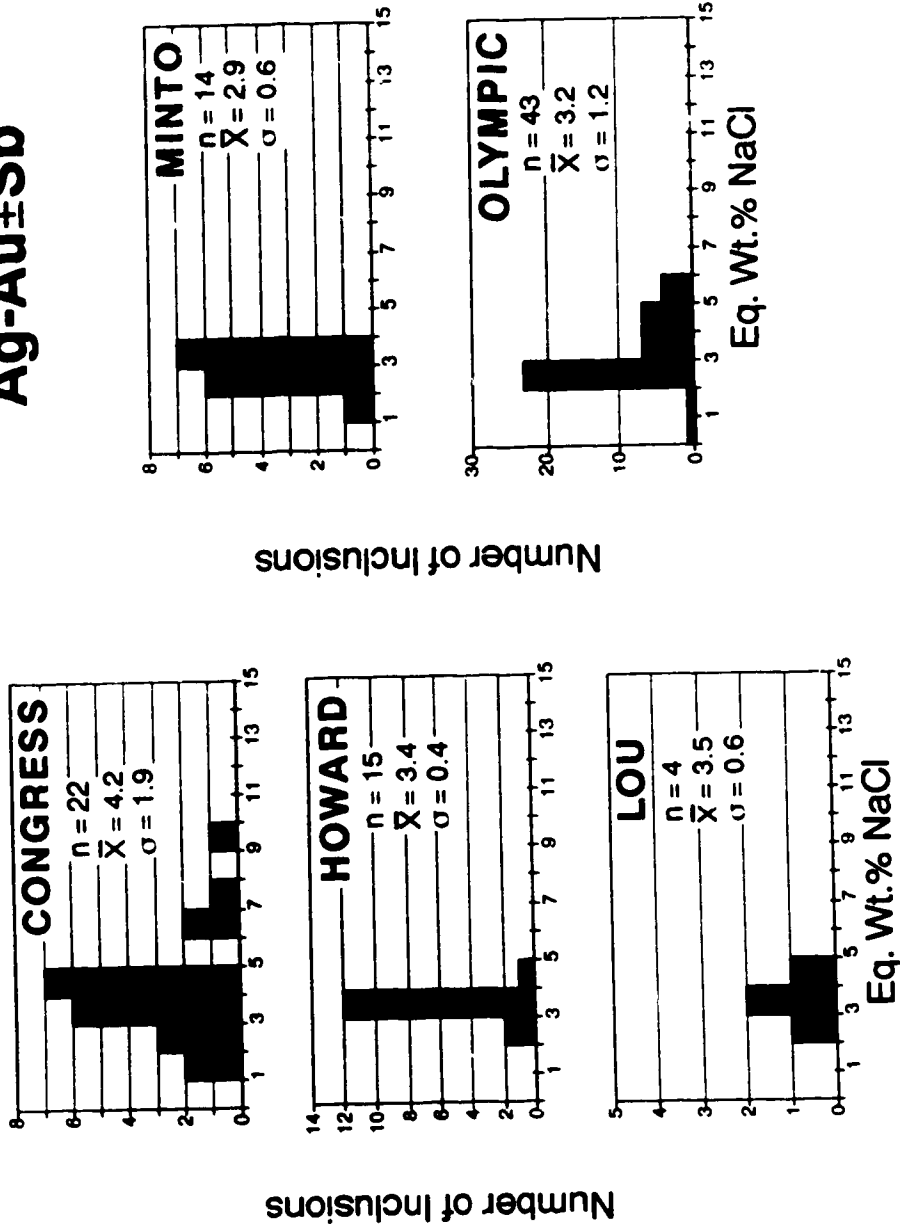
Figure 5-1. Salinities (equivalent weight percent NaCl) as determined from Type 1 inclusions.

Sb-Au-Ag±Hg

CONGRESS

n = 22
$\bar{X}$ = 4.2
σ = 1.9

HOWARD

n = 15
$\bar{X}$ = 3.4
σ = 0.4

LOU

n = 4
$\bar{X}$ = 3.5
σ = 0.6

Base Metal-Enriched
Ag-Au±Sb

MINTO

n = 14
$\bar{X}$ = 2.9
σ = 0.6

OLYMPIC

n = 43
3.2
σ = 1.2
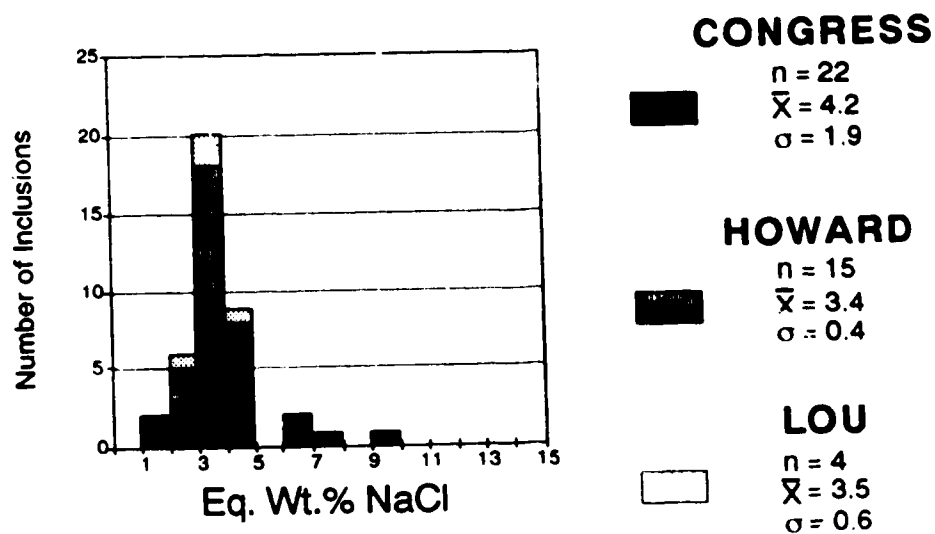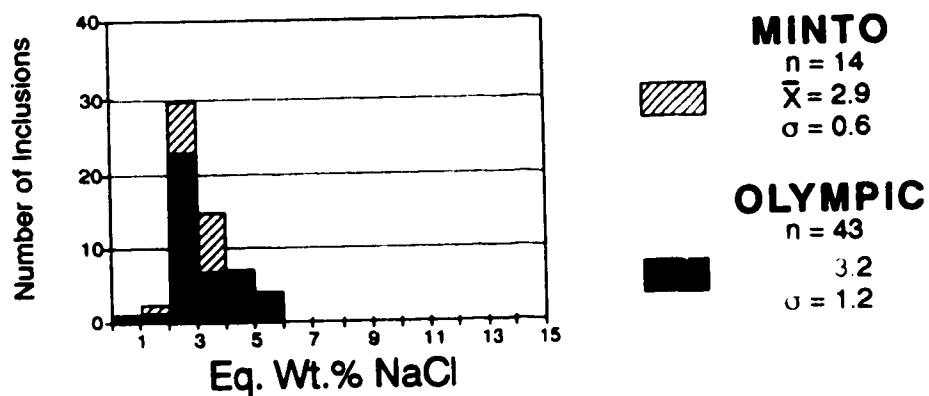
Figure 5-2. Summary and comparison of salinities as determined from Type 1 inclusions.

CO_2 Homogenization Temperature, $Th CO_2$

The 10 Type 2 inclusions from Olympic vein material yielded temperatures of CO_2 homogenization to the vapour phase. The values for $Th CO_2$ range between 28.4°C and 31.0°C with an average of 30.3° ±0.7°C.

The average density for the Type 2 inclusions, assuming pure CO_2, was calculated using the equation of Angus *et al.* (1976; p.12) for CO_2 saturated vapour densities. The value of *ca.* 0.34 g/cm³ is close to the equivalent CO_2 density estimated from the data of Swanenberg (1979) for a CH_4 content ≤ 5 mole % (*cf.* section on $Tm CO_2$).

5.4 Measurements of Phase Changes at High Temperatures

Homogenization Temperature, T_h

Final homogenization temperatures were obtained for most Type 1 inclusions in all material that contained useable fluid inclusions. The results are plotted in Figure 5-3 and summarized for comparison in Figure 5-4. Averages range from 255°C (Howard) to 286°C (Congress) and are notably consistent within first order standard deviations (Table 5-2).

5.5 Discussion of Results

The salinity measurements and homogenization temperature measurements of Type 1 H_2O-NaCl inclusions are considered to be reliable. However, the nature of the Type 2-CO_2 inclusions in Olympic material is suspect; assuming heterogeneous trapping occurred, a wide range of H_2O/CO_2 ratios and degrees of filling should result if entrapment occurred above the H_2O-CO_2 solvus. This was not observed within the inclusion population in Olympic vein material. The argument for immiscibility, and by extension, the determination

Base Metal-Enriched
Ag-Au±Sb

Sb-Au-Ag±Hg
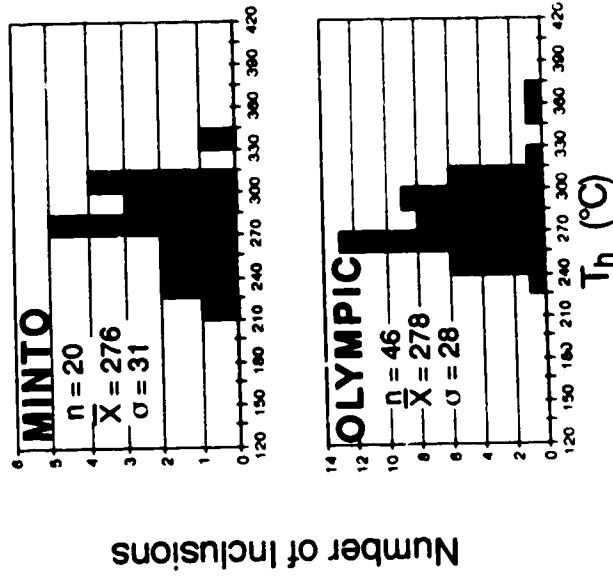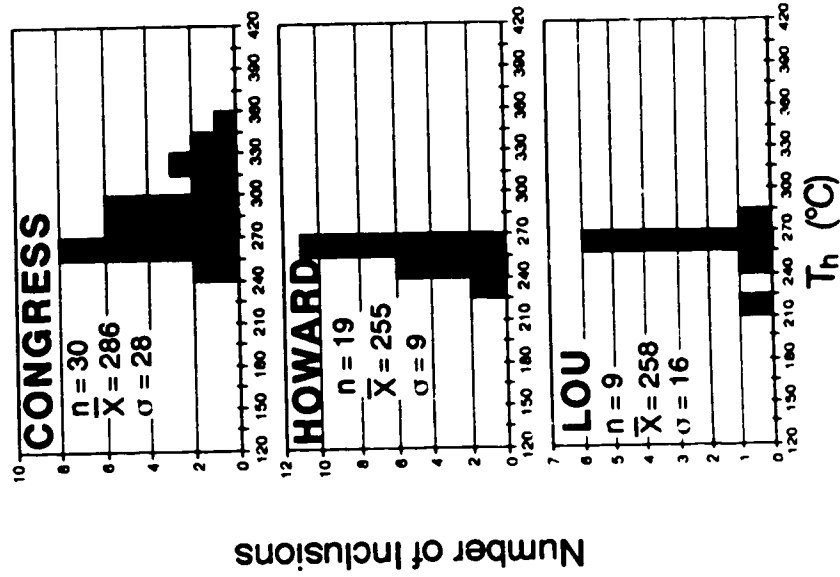
Figure 5-3. Temperatures of homogenization of Type 1 inclusions.

Sb-Au-Ag±Hg

CONGRESS

n = 30
$\overline{X}$ = 286
σ = 28

HOWARD

n = 19
$\overline{X}$ = 255
σ = 9

LOU

n = 9
$\overline{X}$ = 258
σ = 16

Base Metal-Enriched
Ag-Au±Sb

MINTO

n = 20
$\overline{X}$ = 276
σ = 31

OLYMPIC

n = 46
$\overline{X}$ = 278
σ = 28
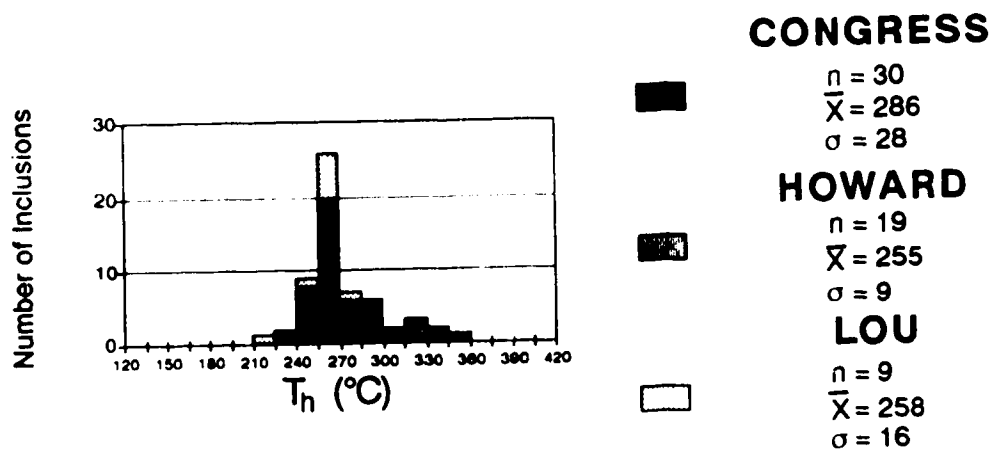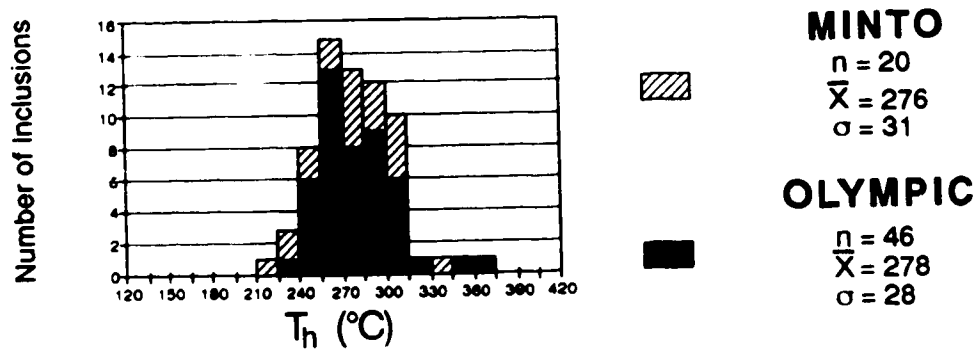
Figure 5-4. Summary and comparison of homogenization temperatures from Type 1 inclusions.

of pressure at trapping (P_t) will be discussed. Geobarometry based on the comparison of T_h in Type 1 inclusions with an independent stable isotope geothermometer will also be discussed.

Salinities of Ore Fluids

Salinity determinations for both subdivisions of the Congress-type deposits are plotted as histograms in Figure 5-2. The salinities for the deposits are comparable in range. Measurments range from 0.2 eq. wt. % NaCl to the highest salinities calculated in inclusions from Olympic (max. 5.7 eq. wt. % NaCl) and Congress (max. 9.3 eq. wt. NaCl) vein material. Average salinities calculated, 3.7 ±1.0 eq. wt. % NaCl and 3.1 ±0.9 eq. wt. % NaCl for Sb-Au-Ag±Hg and base metal-enriched Ag-Au±Sb deposits respectively, are comparable and indicate relatively dilute hydrothermal fluids were involved in ore deposition. These values are also comparable to those obtained from inclusions in northern Cordilleran mesothermal gold lodes (Goldfarb *et al.*, 1986; Murowchick *et al.*, 1986; Nesbitt *et al.*, in press), lode gold deposits in the Foothills Metamorphic Belt deposits of California (Coveney, 1981; Böhlke and Kistler, 1986; Weir and Kerrick, 1987) and Archean lode gold deposits (Spooner, 1981; Colvine *et al.*, 1984; Roedder, 1984a).

Estimation of Pressure and Trapping Conditions

A knowledge of pressure at the time of trapping is important in two respects: 1) the depth of formation is of intrinsic geological significance; and 2) it provides a means of correcting homogenization temperatures to obtain (true) temperatures of trapping (*i.e.* the so-called "pressure correction") (Shepherd *et al.*, 1985). Homogenization temperatures are usually a minimum estimate of trapping temperatures, the difference being a function of

trapping pressure. If the composition and homogenization temperature of a single two phase liquid-vapour inclusion (e.g. Type 1 inclusions in this study) are known, the pressure may be determined from P-V-T-X data on the fluid in the inclusion using a temperature of trapping estimate from an independent geothermometer (Roedder and Bodnar, 1980). Stable isotope fractionations between coeval mineral pairs provide such an independent geothermometer (cf. Chapter 6) to determine the (higher) temperature of formation of the host or associated minerals. The intersection of the appropriate isochore for the given temperature and mode of ho\. , ... with the independently obtained trapping temperature defines the trapping pressure.

The constancy of phase ratios in the two-phase Type 1 inclusions from Congress, Howard, Lou, and Minto mineralization suggests that the host minerals developed from a homogeneous hydrothermal fluid of low salinity in each case. Averages for the salinity of the inclusion fluid in each deposit were determined in a previous section (Table 5-2). The highest recorded is for Congress inclusion fluids at 4.2 eq. wt. % NaCl on average and the lowest is for Minto inclusion fluids at 2.9 eq. wt. % NaCl on average. The volumetric data for the system NaCl-H_2O of 3 eq. wt. % NaCl are used as an approximation of the P-V-T-X properties of the inclusion fluids in all occurrences.

Temperature calculations from several isotopic ($^{18}O/^{16}O$) fractionations between assumed coeval mineral pairs are summarized in Table 5-3. These temperatures have been used as independent estimates of th' temperatures of trapping (formation) in order to limit the pressures of trapping of inclusion fluids and by extension the pressures of formation of the associated minerals. Figure 5-5 illustrates the technique. The range in H_2O-NaCl isochores plotted is based on temperatures of homogenization of Type 1 inclusions in the samples listed in Table 5-3 (270° ±20°C). The range in trapping temperatures plotted (285° ±25°C) is based on stable isotope pair calculated temperatures. Two temperatures calculated from isotope pairs in samples LOU 05 and OLY 01 are significantly higher than the corresponding temperatures of homogenization in fluid inclusions from the same material.

8 6

Table 5-3. Summary of data from the geothermobarometry technique utilizing an independent geothermometer to fix the temperture of formation of the mineral assemblage in order to determine the pressure of trapping (P$_t$) of the inclusion fluids contained within quartz and/or carbonate.

Deposit/ Occurrence	Sample	Mineral Pair[1]	$^{18}O/^{16}O$ (‰) Δ A-B	T Δ A-B[2] (°C)	T F.i.[3] (°C)	P$_t$ (bars)
Congress	CON 05	qz-ser	3.6	291*	270*	~250*
Howard	HOW 07	qz-ser	3.9	265*	254*	-250*
Lou	LOU 03	qz-cal	1.3	297*	271*	~350*
	LOU 03	ank-cal	1.6	286*	271*	~240*
	LOU 05	qz-ser	3.2	332	240	~1100
	LOU 60	ank-cal	1.8	254*	240*	~200*
Minto	MINTO 07	qz-ser	3.3	320*	294*	~350*
Olympic	OLY 01	cal-mag	9.7	378	278	~1300
Avg.				285 ±24	267 ±18	~270 ±60

Notes:

1 Abbreviations: qz = quartz, ser = sericite, cal = calcite, ank = ankerite, mag = magnetite.

2 Isotope pair temperatures calculated using the following expressions: qz-mu and qz-cal, Matsuhisa et al. (1979) and O'Neil and Taylor (1969); ank-cal, Northrop and Clayton (1966); cal-mag, O'Neil et al. (1966) and Bottinga and Javoy (1973).

3 T$_{F.i.}$ = temperature of homogenization of inclusion fluid; In each case the temperature recorded is not necessarily that of the inclusion-bearing mineral used in the isotope pair calculation but can be the T$_h$ of fluids in another sample of the same mineral that yielded better inclusions for analysis.
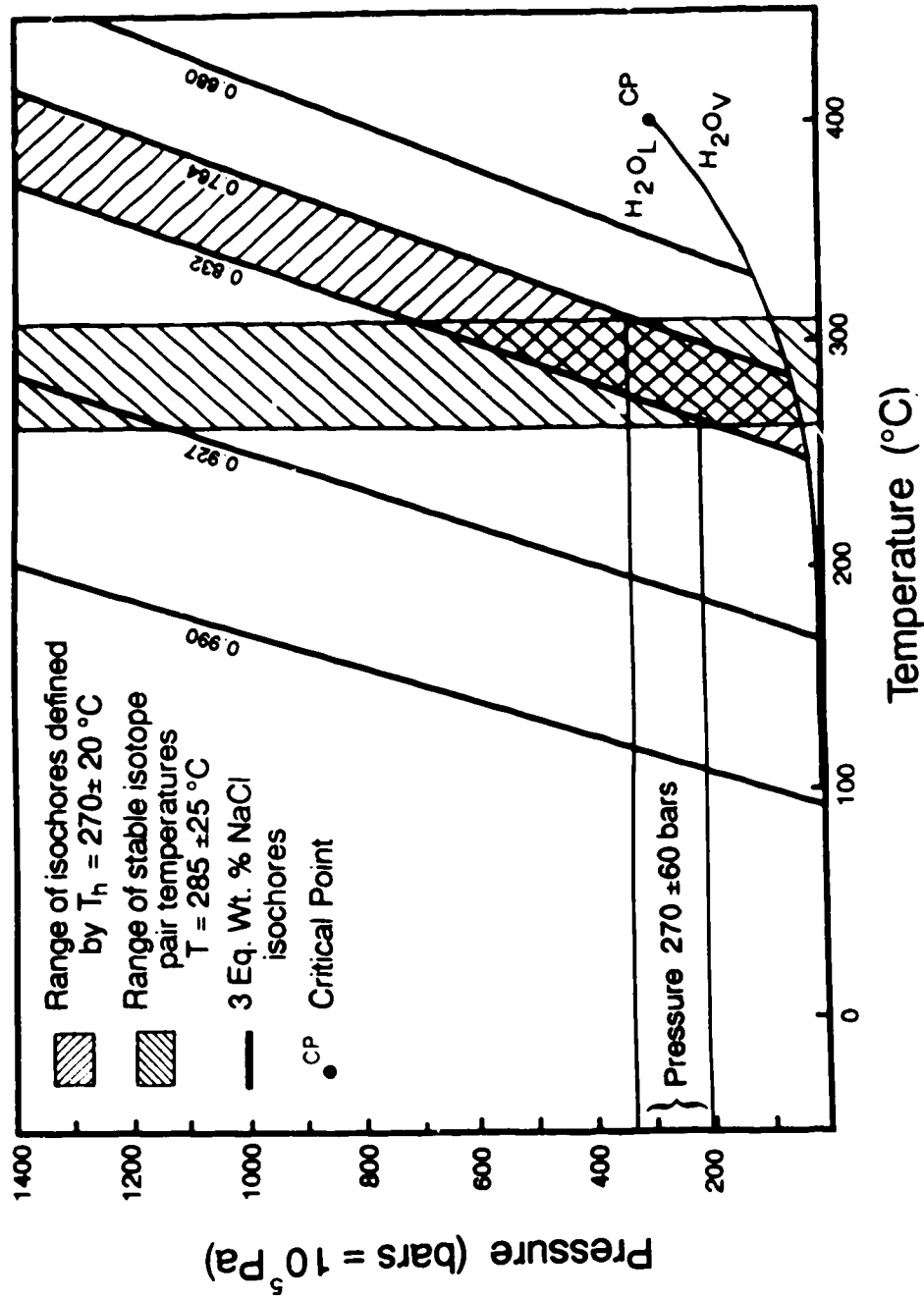
Figure 5-5. Illustration of the fluid inclusion geothermobarometry technique utilizing an independent geothermometer that provides temperatures of trapping, or formation (T_t) (isotope $^{18}O/^{16}O$ mineral pair temperatures) in order to limit pressures of trapping (P_t) of a 3 eq. wt. % NaCl fluid homogenizing to the liquid state. See text for discussion. Data for H_2O-NaCl system isochores from Potter and Brown (1977).

Consequently the pressures of trapping indicated are significantly higher, ~1100 bars (110 MPa) and ~1300 bars (130 MPa) respectively. Several P_t values fall in the range of ~200 to ~350 bars (20 to 35 MPa) and are considered to be representative of trapping conditions. These pressures correspond to a depth of *ca.* 1 kilometre assuming lithostatic conditions apply, and to depths of from about 2 to 3.5 kilometre assuming a hydrostatic regime.

There is a close local association of Type 1-H_2O(l) inclusions with the Type 2-CO_2(v) inclusions in Olympic vein material. The presence of two populations of fluid inclusions of disparate compositions has been interpreted in terms of coexisting immiscible liquid and ("effervescing") vapour trapped separately at the same pressure and temperature conditions (Roedder and Bodnar (1980) and references therein). Ramboz *et al.* (1982) proposed several criteria by which the case for heterogeneous entrapment of fluids may be tested. A very scattered degree of filling, homogenization temperatures, and compositions of the inclusions are considered essential signs of heterogeneous trapping. Inclusions in Olympic vein material do not display these criteria. As well the establishment of unequivocal contemporaneity of trapping of the fluids represented by the two types is difficult. Nevertheless, the implication for geobarometry based on the presence of two distinct inclusion fluids will be discussed.

The values obtained for $ThCO_2$ near -31.1°C show the CO_2 to be nearly pure or at most, to contain a small fraction (X_{CH_4}=0.05) of methane as discussed in a previous section. Kalyuzhni and Koltun (1953) developed the method of geobarometry applicable to separate CO_2 and H_2O inclusions trapped at the same P-T conditions. By plotting the P-V-T diagrams for H_2O and CO_2 in the same plane, the pressure and temperature at trapping are defined by the intersection of the corresponding isochores for each fluid. This method is valid only if the two inclusions were separately trapped as essentially pure components at the same temperature and pressure (Roedder and Bodnar, 1980). These conditions are assumed in the present study for the sake of discussion.

In a previous section it was recorded that the Type 2-CO_2 inclusions in Olympic

material homogenized to the vapour phase with an average density of 0.34 g/cm^3, while the

Type 1-brine inclusions in Olympic material had average salinities of 3.2 eq. wt. % NaCl

and average T$_h$ of 278°C. This average sal... is considered a maximum because of the

possible presence of CO_2 in the system, though none was actually observed in the Type 1

inclusions. A 3.0 eq. wt. % NaCl solution with an average T$_h$ of 278°C defines a density

of ca. 0.79 g/cm^3 (data from Potter and Brown, 1977). Plotting the respective isochores

for the two fluids characterized by Type 1 and Type 2 inclusions (using the data of Potter

and Brown (1977) and Angus et al (1976)) on a common P T diagram, Figure 5-6, gives

an intersection which defines the conditions of trapping of the fluids. The maximum and

minimum isochores for both fluids have been plotted. For Type 1 inclusions the minimum

isochore corresponds to a 0.3 eq. wt. % NaCl solution homogenizing to the liquid phase at

278°C (data from Angus et al., 1976), essentially the pure H_2O 0.750 g/cm^3 isochore. The

maximum isochore (0.800 g/cm^3) used is for a 5 eq. wt. % NaCl solution homogenizing to

the liquid phase at 278°C (data from Angus et al., 1976). For Type 2 inclusions the

minimum isochore used is for a pure CO_2 inclusion homogenizing to the vapour phase at

28.4°C ($\cong$ 0.300 g/cm^3) and the maximum is for the same inclusion homogenizing at

31.0°C (0.420 g/cm^3). The intersections of the maximum and minimum isochore pairs

yield a field of potential trapping conditions; T$_t$ approximately 310° ± 15°C , P$_t$

approximately 400 ±100 bars (40 ±10 MPa). The temperatures are approximately 20° to

50°C higher than the average temperature of homogenization in Olympic Type 1 inclusions.

The trapping pressures correspond to depths of approximately 4 kilometres, assuming

hydrostatic conditions, and 1.5 kilometres, assuming lithostatic conditions.
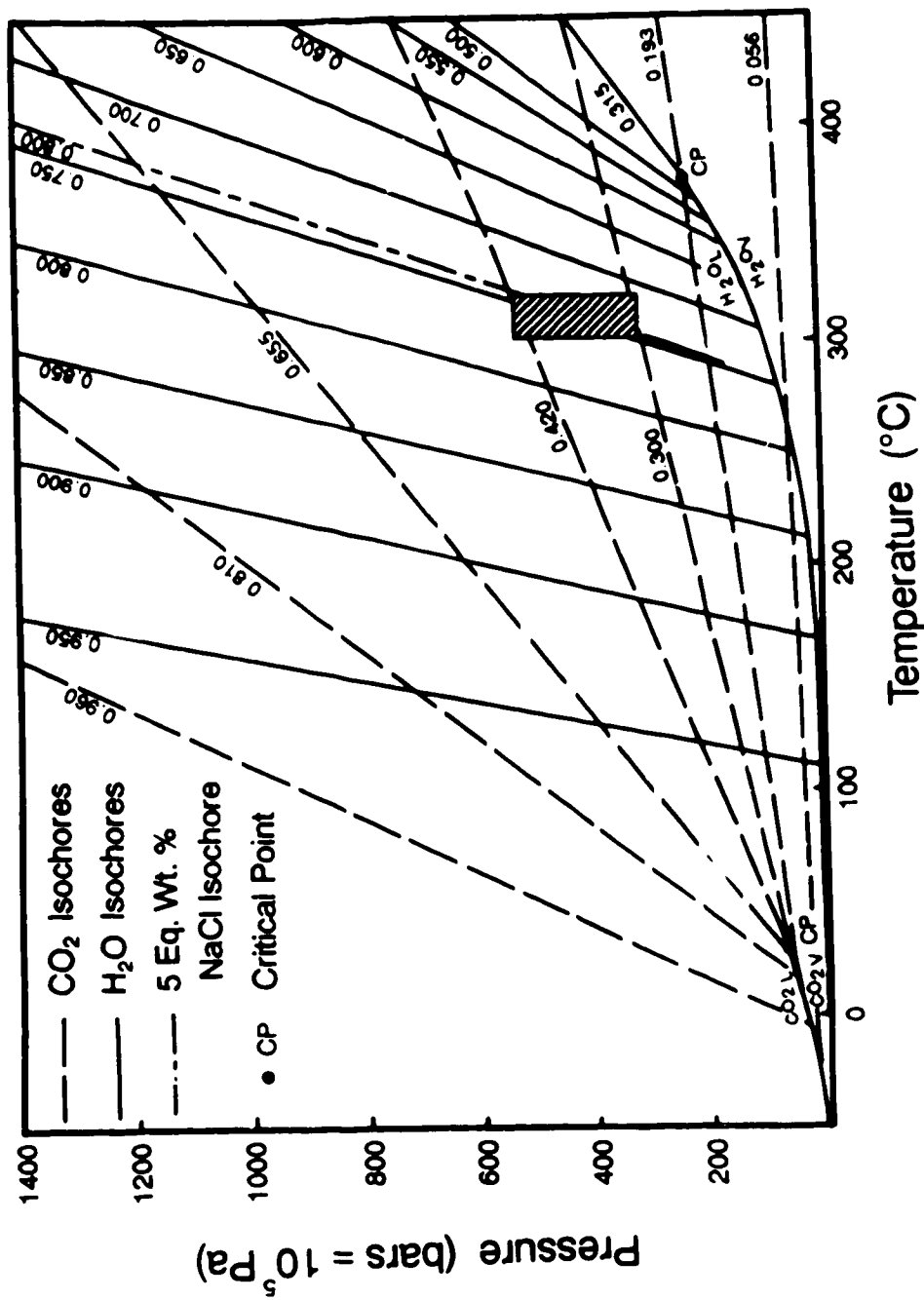
Figure 5-6. Combined P-T diagrams for CO_2 and H_2O illustrating the Kalyuzhnyi and Koltun (1953) method of geothermobarometry using separate CO_2 and H_2O inclusions trapped at the same temperature and pressure. The diagonally patterned field represents the range of common trapping conditions (T_t and P_t) for Olympic Type 1-H_2O and Type 2-CO_2 inclusions. See text for discussion. Diagram modified from Roedder and Bodnar (1980) with data from Fisher (1976), Angus *et al.* (1976), and Potter and Brown (1977).

5.6 Summary

A study of fluid inclusions in quartz and carbonate gangue associated with Sb-Au mineralization in the Bridge River District determined that ore fluids were dilute brines (averages from deposits range from 2.9 to 4.2 eq. wt. % NaCl). Fluids are characterized by low CO_2 contents, possibly up to 5 mol. % on average. However, there is a local population of CO_2 inclusions in base metal-enriched mineralization ($X_{CO_2} \cong 0.95$, $X_{CH_4} \cong 0.05$). Average homogenization temperatures for the main stage of Sb-Au mineralization, uncorrected for trapping pressures, range from 255° ±19°C to 286° ±30°C in five deposits studied.

Trapping conditions were derived from stable isotope equilibrium fractionation relationships among gangue phases associated with Sb-Au-Ag±Hg mineralization (Congress, Howard, Lou). Trapping temperatures indicated are ca. 285° ±25°C with the application of a pressure correction of ca. 20°C. Trapping pressures are in the range of ca. 200 to 350 bars (20 to 35 MPa).

Trapping conditions were determined from the simultaneous trapping of two different fluids during the deposition of base metal-enriched Ag-Au±Sb mineralization (Minto, Olympic). Trapping temperatures of 310° ±15°C were indicated, using a pressure correction of ca. 30°C. Trapping pressures of 300 to 500 bars (30 to 50 MPa) were indicated.

VI. STABLE ISOTOPE STUDY

6.0 Introduction

A stable isotope study of gangue and alteration minerals associated with gold-antimony mineralization in the Bridge River District was undertaken in an attempt to determine the nature and evolution of the ore-forming fluids. The efficacy of stable isotope geothermometry was also investigated with respect to these deposits. A camp-scale stable isotopic survey is included encompassing Au-Ag mineralization in the southwest and Hg mineralization in the northwest to investigate the genetic relationship between the varied deposits in the camp.

Analyses were made of $^{18}O/^{16}O$, $^{13}C/^{12}C$, and D/H ratios in samples of whole rock, serpentinite, magnetite, vein quartz, vein carbonate, hydrothermal sericite, and inclusion fluids in quartz. The results indicate that the fluids responsible for Sb-Au mineralization and the alteration of country rock were highly enriched in ^{18}O.

Furthermore, there is a bimodal distribution of the $\delta^{18}O$ values; quartz and carbonates from base metal-enriched Ag-Au±Sb deposits are not as ^{18}O-enriched as those from Sb-Au-Ag±Hg deposits. The hydrothermal fluids imparted ^{18}O-enriched values to the country rocks in a pattern indicative of decreasing water/rock ratios away from the deposits.

Results from the district-wide isotope survey suggest that the entire region was mineralized by ^{18}O-enriched fluids. Analyses of gangue minerals from various metal deposits and showings reveal a camp scale oxygen isotope trend along a 30 km transect with $\delta^{18}O$ values increasing progressively to the northeast. The analyses of vein quartz and carbonate indicate the deposition of metals from an isotopically unique fluid through a possible geothermal gradient decreasing in a direction away from the Coast Plutonic Complex in the southwest.

Carbon isotope analyses of ankerite and calcite are coincident with crustal carbon values that have undergone minor shifts, possibly in response to local perturbations in redox conditions at the depositional sites, but do not necessarily imply a magmatic origin to CO_2. Carbon analyses also suggest that deposition over a geothermal gradient occurred from a fluid with a unique isotopic carbon signature.

Deuterium analyses of water in sericite associated with Sb-Au-Ag mineralization are indicative of D-enriched hydothermal parent fluid(s). However, D/H measurements of inclusion fluids in ore-stage vein quartz are indicative of meteoric D/H ratios. The results from sericite analyses fit a metamorphically-derived fluid model while those of inclusion fluids corroborate an evolved meteoric fluid model.

Isotopic analyses of vein minerals in the antimony-associated gold deposits provided an opportunity to investigate the efficacy of stable isotope geothermometry. Evidence of isotopic non-equilibrium on a local scale was common in many assemblages. Notable are the wide ranging non-equilibrium ankerite $\delta^{18}O$ values. However, several gangue and alteration mineral assemblages (CON 05, HOW 07, LOU 03, 05, 60, MINTO 01) gave reliable isotopic temperatures providing an estimate of formation temperature independent from fluid inclusion microthermometry.

A synopsis of analytical techniques and results is given. The discussion is organized on two scales. On the deposit-scale the discussion encompasses the isotopic systematics among the Sb-associated Au-Ag deposits in the study. The camp-scale stable isotopic survey places the Sb-associated mineralization in the context of the diverse metallogeny of the Bridge River district. In the context of both scales the discussion includes oxygen, hydrogen and carbon isotope ratio analyses. Particular attention is focused on the nature of the hydrogen isotope ratios in waters from fluid inclusions in quartz and bound water in alteration mica separates from Sb-associated mineralization.

The deuterium data are not only complex but are integral to the discussion of the genesis of the hydrothermal antecedents of the ore fluids. The results are discussed in light

of the current prevailing theories of the genesis of the fluids responsibe for the deposition of precious metal mineralization in mesothermal vein deposits in the North American Cordillera.

Lastly, the data from the district-wide isotopic survey are discussed with respect to a camp-scale model invoking the deposition of metals through a geothermal gradient.

6.1 Analytical Techniques

Mineral separates were obtained by a variety of techniques including hand picking, HCl and HNO_3 acid treatment, gravity settling, and magnetic separation. X-ray powder diffraction analyses of selected separates was used to determine their purity. Oxygen yields (μmol/mg) from oxide and silicate minerals were within 5% of ideal amounts.

Oxygen was liberated from silicates, oxides, and whole rock samples by the reaction of sample material with bromine pentafluoride (BrF_5) at 600° to 650°C (Clayton and Mayeda, 1963). The oxygen was reacted with carbon to form CO_2, which was mass spectromically analysed.

Carbonates were reacted with 100% phosphoric acid (H_3PO_4) at 25°C for periods of from 24 hours (calcite) to 2-3 weeks (ankerite) (McCrea, 1950). In samples containing two carbonates a modification of the method of Epstein et al. (1964) was used taking advantage of the different reaction rates of the carbonates. Collections of evolved CO_2 were made at various times after the start of reaction with H_3PO_4. The early collections contain CO_2 almost completely from the more reactive carbonate, while later extractions contain CO_2 representative of the slower reacting carbonates. The CO_2 was mass spectromically analysed for $^{13}C/^{12}C$ and $^{18}O/^{16}O$ ratios.

Waters collected for D/H analyses were extracted in a method similar to that of Godfrey (1962). Dehydration of 0.3 to 1.0 g separates of hydrous minerals took place under vacuum at 1100°C following at least 12 hours of degassing at 150°C to remove

extraneous water. The same methodology was used to extract waters from fluid inclusions in ~10 gram samples of quartz (0.5 to 1 0 mm size fraction). The quartz samples were carefully selected to maximize the percentage of primary fluid inclusions. Nesbitt *et al.* (1987) found the thermal decrepitation tecnnique used to liberate inclusion fluids is preferred over the crushing technique (Pickthorn *et al.*, 1987) because of the potential presence of CO_2-bearing inclusions relative to H_2O-dominated secondary inclusions. Earlier and more complete decrepitation of the primary inclusions occurs relative to secondary inclusions and consequently there is a higher percentage of the primary ore-forming solution in the extracted fluid. The process is readily confirmed by visual observation of the decrepitation of primary inclusions prior to secondary inclusions during heating on a fluid inclusion heating stage (Nesbitt *et al.* 1987).

Water liberated at the higher temperature of dehydration/decrepitation was reacted with zinc metal at *ca.* 430°C to produce hydrogen gas (Coleman *et al.*, 1982). The hydrogen was subsequently mass spectromically analysed for D/H ratios.

Isotope ratio data are reported in the conventional δ-notation:

$$\delta = (R_{sample} / R_{standard} - 1) \times 1000\%_o$$

where R_{sample} is the isotopic ratio for the sample and $R_{standard}$ is the corresponding ratio for the standard. Results are relative to Standard Mean Ocean Water (SMOW) (Craig, 1961b) for $\delta^{18}O$ and δD and to Pee Dee Belemnite (PDB) (Craig, 1957) for $\delta^{13}C$.

The isotopic fractionation between two phases, A and B is defined :

$$1000\ln\alpha_{A-B} \cong \Delta_{A-B} = \delta R_A - \delta R_B$$

where α_{A-B} is the fractionation factor between the isotopic species in the phases A and B.

Oxygen and carbon analyses were performed using a Micromass 602D Nier-type (Nier, 1947) isotope ratio mass spectrometer with a 6 cm radius analyser, 90° magnetic deflection and double collector arrangement. Hydrogen analyses were performed using a Micromass 602C isotope ratio mass spectrometer with similar specifications.

Most of the δ values reported are the averages of replicate analyses. The measured values of $\delta^{18}O$, $\delta^{13}C$, and δD are within ±0.4‰, ±0.1‰, and ±3.0‰ respectively, of the mean based on the replicate analyses. Twelve $\delta^{18}O$ measurements of United States National Bureau of Standards quartz standard (NBS-28, quartz sand) made during the course of this study average +9.38 ±0.30‰ (SMOW) using a fractionation factor of 1.04070 between oxygen in CO_2 and H_2O at 25°C (Compston and Epstein, 1958). Using a $\alpha_{CO_2-H_2O}$ of 1.04120 (O'Neil and Epstein, 1966) NBS-28 quartz has a $\delta^{18}O_{SMOW}$ value of ca. +9.60‰ (Matsuhisa et al., 1971). Actual measurements of $\delta^{18}O$ were converted to SMOW using a calcite working standard and then calibrated against Vienna-SMOW (VSMOW) and Standard Light Antarctic Precip'ation (SLAP) waters, where $\delta^{18}O_{SLAP/SMOW}$ = -55.5‰ (Coplen, 1988).

Measured oxygen isotope ratios in CO_2 liberated from calcite and ankerite were converted to $\delta^{18}O$ (SMOW) using an empirical calibration curve derived from analyses of the working standard and a fractionation factor of 1.01025 between oxygen in H_3PO_4 and carbonate (Sharma and Clayton, 1965).

Measurements of $\delta^{13}C$ are related to the NBS-20 standard (Solenhofen limestone, $\delta^{13}C$ = -1.06 ‰ PDB) (Craig, 1957).

Measurements of δD were calibrated against a working standard normalized to the SMOW scale using analyses of Greenland Ice Sheet Precipitation (GISP, $\delta D_{GISP/SMOW}$ = -189.9‰; Gonfiantini, 1978), SLAP ($\delta D_{SLAP/SMOW}$ = -428.0‰; Hut, 1987), and SMOW. For intercalibration purposes a sample of U.S. National Bureau of Standards biotite (NBS-30) was analysed and yielded a δD value of -71‰. The reported δD value of NBS-30 normalized on the VSMOW/SLAP scale is ca. -66.5‰ (Hut, 1987).

Equilibrium fractionation expressions used in the study are listed in the Appendix.

6.2 Analytical Results and Equilibrium Relationships

Data obtained from all isotope analyses made during the course of this study are presented in Table 6-1. The data from the analyses of vein and alteration minerals associated with Sb-Au-Ag mineralization in the Bridge River district are averaged and summarized in Table 6-2.

6.2.1 Sb-Au-Ag±Hg Deposits: Congress, Howard, Lou, Dauntless

Figure 6-1 summarizes $\delta^{18}O$ data for these deposits. Oxygen isotopic analyses of vein quartz, carbonate and sericite are plotted on an exchange equilibrium diagram (Figure 6-2) (Rumble, 1978). The diagram may be considered isothermal within the range of 260° to 310°C. In the figure the slopes of tie lines connecting minerals from the same rock are dependent on the temperature of isotopic equilibrium as the slope is directly proportional to $\Delta^{18}O_{A-B}$. As a function of the diagram steeper slopes represent smaller fractionations and therefore higher temperatures of precipitation. Conversely, the shallower the slope of a tie line the larger the fractionation and therefore the lower the temperature of isotopic equilibrium according to the appropriate isotopic equilibrium expression (see Appendix).

The calculated equilibrium tie lines plot as ranges because calculations were performed over the range of formation temperatures based on pressure-corrected fluid inclusion data. Where a tie line between measured analyses of two phases closely parallels the loci of caculated equilibrium tie lines an approach to isotopic equilibrium between the phases is indicated. If the measured tie line slopes are not parallel to the calculated equilibrium tie lines over the formation temperature range, fractionations larger or smaller than equilibrium values are indicated (e.g. Figure 6-2, LOU 38 qz-ank tie line). If tie lines show negative

Table 6-1. Stable isotope data. (Notes and abbreviations at end of table.)

Deposit/ Occurrence Sample No.	Mineral	δD o/oo SMOW	δ18O o/oo SMOW	δ13C o/oo PDB	Mineral Pair A-B	Δ18O A-B	T (°C) Δ18O A-B	T (°C) f.i.T [1]	δ18O fl using min pair T	δ18O fl using f.i.T [1]	δD fl o/oo SMOW [2]
BRALORNE											
BR-53	cal		15.4	-8.7				275		9 0	
BR-54A	qz		18.2		qz-cal	2.1	200			6 6	7 2
BR-54B	cal		16.1	8.3	qz-cal		200	210		6 6	7 1
BR-55	qz		18.9		qz-cal	1.5	270	220		10 9	8 5
	cal		17.4	-9.5	qz-cal		270			10 9	8 9
BR-57	qz		14.4					250		5 5	
BR-58B	qz		20.0					275		12 2	
BR-59	serp°	-75	9.1		serp-mag	6.0	355	275	-9 0		-45
	mag		3.1								
ARIZONA											
ARIZ 03	qz		14.4								
ARIZ 04	serp°	-181	9.0		serp-mag	6.2	340		-9 0		-154
	mag		2.8								
VERITAS											
VER 03	serp°	-72	11.0		serp-mag	6.5	320		-11 0		-44
	mag		4.5								
CONGRESS											
CON 05	qz		21.8		qz-ser	3 6	290	290	14 6	14 6	
	ser	-116	18.2					290	14 6	14 6	-65
		-107									-56
CON 07	ser	-110	13.4					290		9 8	-59
	wr		19.5								
	basalt										
CON 10	qz		23.6					290		16 4	-135
CON 13	qz		21.9					290		14 7	
CON 14	qz		20.5					305		13 8	-134
	ank		28.5	-4.9						19 7	
CON 17	qz 1		22.2					290		15 0	
	qz 2		20.3								
	ank		25.5	-6.3						16 2	
CON 18	qz		20.7					305		14 0	
CON 19	qz		20.6					290		13 4	
	ank		28.9	-5.9						19 6	

Au-Ag±W, As Deposits

Sb-Au-Ag±Hg Deposits

Table 6-1 continued.

Sb-Au-Ag±Hg Deposits

Deposit/ Occurrence Sample No.	Mineral	δD o/oo SMOW	δ18O o/oo SMOW	δ13C o/oo PDB	Mineral Pair A-B	Δ18O A-B	T (°C) 18O/Δ18O A-B	T (°C) f.i.T [1]	δ18O fl using min pair T	δ18O fl using f.i.T	δDfl o/oo SMOW [2]
CON 20	qz		21 0		qz-ser	2 5	430	290	17 6	13 8	-64
	ser	-115	18 5				430		17 6	14 9	
CONEX 01	qz		21 8					285		14 4	
CONEX 05	qz		20 0					250		11 1	
HOWARD											
HOW 01	wr basalt		15 2								
HOW 04	wr gabbro		15 2								
HOW 05	ank		23 2	-8 9				275		14 0	
HOW 06	wr fel p dyke		20 2								
HOW 07	qz 1		24 4		qz 1-ser	3 9	265	275	16 2	16 6	
	qz 2		23 0		qz 1-cal	1 9	220		12 6		
	ser	69	20 2							16 2	-11
		-76	20 5				265		16 2	16 5	-18
	cal		22 5	-6 8			220		14 0	15 4	
	ank		24 ?	-6 7	ank-cal	2 4	185		11 2	14 9	
	carb wr		20 9	-6 9			185		7 2	10 9	
HOW 07B	carb wr		23 6	7 5				275		14 4	
HOW 08	qz		22 8					275		15 0	
HOW 09	qz		22 5					275		14 7	
LOU ZONE											
LOU 01A	wr fel p dyke		17 4								
LOU 01B	wr feld dyke		18 5								
LOU 02	qz		22 4		qz-cal	1 7	240	260	13 0	14 0	
	cal		20 7	-6 0			240		13 0	13 0	
	ank		26 4	-7 2						15 7	
	carb wr		24 0	-7 8						13 3	
LOU 03	qz		25 6		qz-al	1 3	300	290	18 7	18 4	
	cal		24 3	-7 3			300		18 7	17 8	
	ank		25 9	-7 7	ank-cal	1 6	285		17 1	16 6	
	carb wr		23 6	-8 5							
LOU 04	qz		21 2					260		12 8	
LOU 05	qz		21 3		qz-ser	3 2	330	260	15 4	12 9	-118
	ser*	-121	18 1				330		15 4	13 6	-62
LOU 07	qz		24 1					260		15 7	
	carb wr		21 8	-5 5						12 0	

Table 6-1 continued.

Sb-Au-Ag±Hg Deposits

Deposit/ Occurrence Sample No.	Mineral	δD ‰ SMCW	$\delta^{18}O$ ‰ SMOW	$\delta^{13}C$ ‰ PDB	Mineral Pair A-B	$\Delta^{18}O$ A-B	T (°C) $\Delta^{18}O$ A-B	T (°C) f.i.T [1]	$\delta^{18}O$ fl using min pair T	$\delta^{18}O$ fl using f.i.T	δD fl ‰ SMOW [2]
LOU 08	ser	-88	15.5					260		11.0	29
LOU 09	qz		21.5					285		14.1	
LOU 11	wr fel p dyke		20.0								
LOU 12	wr fel p dyke		18.2								
LOU 13	qz 1		19.9								
	qz 2		19.6		qz2-cal	4	170	260	5.9	11.2	
	ank 1		20.0	-10.0						9.3	
	cal 2		17.2	-10.7			170		5.9	9.5	
LOU 14	qz		20.8					260		12.4	
LOU 15	qz		23.3					280		15.7	
	ank		16.3	-8.0						6.4	
LOU 16	qz		20.8					260		12.4	
LOU 17	qz		20.7					260		12.3	
LOU 18	qz		22.6					260		14.2	
LOU 19	wr hbl p dyke		19.0								
LOU 20	wr- above brecciated		24.3								
LOU 21	ank		23.6	-6.7				260		13.8	
LOU 22	wr bx'd basalt		7.4								
LOU 38	qz		21.4			..		260		13.0	
LOU 53	qz		23.0					260		14.6	
LOU 54	qz		22.2			..		260		13.8	
	ank		24.0	-8.5						13.3	
LOU 60	qz 2		19.0			..		260		10.6	
	cal		24.1	-9.3	ank-cal	1.8	255		17.0	16.4	
	ank		25.9	-9.3			255		15.9	15.2	
	carb wr		24.1	-10.2						13.4	
LOU 73	qz		22.8		qz-ser	6.1	145	260	7.0	14.4	
	ser*	-100	16.7				145		7.0	12.2	41
LOU 101	ser	-88	16.9					260		12.4	-30

Table 6-1 continued.

Deposit/ Occurrence Sample No.	Mineral	δD ‰ SMOW	δ^{18}O ‰ SMOW	δ^{13}C ‰ PDB	Mineral Pair A-B	Δ^{18}O A-B	T (°C) Δ^{18}O A-B	T (°C) f.i.T	δ^{18}O fl using min pair T	δ^{18}O fl using f.i.T	δD fl ‰ SMOW
DAUNTLESS											
DAUNT 01	qz		21.5		ank-cal	1.6	285				
	cal		22.5	-6.3	ank-cal		285		6.5		
	ank		24.1	-6.5			285		15.3		
DAUNT 02	qz		2<2				285		14.7		
DAUNT 03	qz		16.7				285		9.2		
	wr argillite		14.9								
DAUNT 04	wr argillite		15.5								
DAUNT 05	qz		21.8				285		14.3		
DAUNT 06	qz		15.5				285		8.1		
	cal		19.5	-8.5			285		13.5		
MINTO MINE											
MINTO 01	qz		17.1					305		10.4	
	cal 2		20.5	-9.4						15.1	
	ank 2		21.3	-9.3						13.2	
MINTO 02	qz		19.8					305		13.1	
MINTO 03	qz		16.4					305		9.7	
MINTO 05	qz		19.5					305		12.8	
	ank		25.0	-10.8						16.9	
MINTO 06	qz 1		19.2					305		12.5	
	qz 2		14.4								
	ank		19.0	-9.8				230		7.9	
MINTO 07	qz		20.1		qz-ser	3.3	320	325	13.9	14.1	
	ser		16.8				320		13.9	14.0	
OLYMPIC											
OLY 01	cal		13.0	-13.3	cal-mag	9.7	380	310	9.4	7.7	
	mag		3.3						10.4		
OLY 03	qz		18.8		qz-cal	1.7	240	310	9.4	12.3	
	cal		17.1	-13.0			240		9.4	1.8	
OLY 04	wr-gabbro		11.4								
OLY 06	wr-gabbro		10.2								
OLY 07	qz		17.4					310		10.9	
OLY 08	qz		18.3		qz-cal	1.5	270	310	10.3	11.8	
	cal		16.8	-11.3	qz-cal		270		10.3	11.5	
	ser	-106	12.7		qz-ser	4.8	205		6.2	9.6	-29

(Left margin vertical labels: "Sb-Au-Ag±Hg Deposits", "Base Metal-Enriched Ag-Au±Sb Deposits")

Table 6-1 continued.

Deposit/ Occurrence Sample No.	Mineral	δD ‰ SMOW	δ18O ‰ SMOW	δ13C ‰ PDB	Mineral Pair A-B	Δ18O A-B	T(°C) 18Δ18O A-B	T(°C) f.i.T	δ18O fl using min pair T	δ18O fl using f.i.T	δDfl ‰ SMOW
OLY 09	serp	9 7									
OLY 13	wr felsic dyke	13 7									
TUNGSTEN QUEEN											
BR-22	serp mag	-99	21 4 12 0		serp mag	9 4	200		20 0 20 0		62
BR-32	cal		27 0	-5 1						18 5	
BR-32C	qz		28 4		qz-cal	2 1	200	200	16 8	16 8	
BR-32E	cal		26 3	-5 0	qz-cal		200		16 8	17 8	
SILVER QUICK											
BR-20A	cal		19 4	-8 7							
BR-20B	cal		24 5	-7 <							
MANITOU											
BR-11	cal		25 3	5 9				200		16 8	
BR 12	cal		24 5	5 5				200		16 0	
BR-14	cal		27 6	-5 9				200		19 1	
BR-15	cal		28 2	-6 0				200		19 7	
BR-17	cal		28 5	-6 1				200		19 5	
RED EAGLE											
BR-01	serp mag	-166	11 9 5 9		serp mag	6 0	355		-11 8		141
BR-02	cal		19 9	-2 3							
BR-06	cal		23 1	-2 5							

(left margin, vertical) Hg Deposits

Notes:

[1] Fluid inclusion temperature (f.i.T) is T_h + appropriate average pressure correction, see Chapter 5.
No pressure corrections applied to Hg deposit fluid inclusion temperatures.

[2] Where a value is quoted for quartz it is δD of inclusion fluid.

* Average of analyses includes analysis by Global Geochemistry Corporation, Canoga Park, California.

° Average of analyses includes analysis by J.R. O'Neil, U.S. Geological Survey, Menlo Park, California.

Abbreviations:

qz = quartz	cal = calcite	ank = ankerite	serp = serpentinite
mag = magnetite	ser = sericite	carb = carbonate	wr = whole rock analysis
hbl p dyke = hornblende porphyry dyke		fel p dyke = feldspar porphyry dyke	

Table 6-2.Summary of stable isotope data from hydrothermal minerals associated with Sb Au-Ag mineralization in the Bridge River District.

All values in ‰	$\delta^{18}O_{SMOW}$ quartz	$\delta^{18}O_{SMOW}$ carbonate	$\delta^{13}C_{PDB}$ carbonate	$\delta^{18}O_{SMOW}$ ser	$\delta^{18}O_{SMOW}$ [1*] fluid	δD_{SMOW} ser	δD_{SMOW} [2*] fluid	δD_{SMOW} [3] inc fl
Sb-Au-Ag±Hg Deposits								
CONGRESS								
n	10	4	6	3	10	4	4	2
x̄	21.4	27.0	-5.0	16 7	14.1	-111	-61	-135
σ	±1.1	±2.0	±2.0	±2.9	±1.4	±4	±4	±1
HOWARD								
n	3	5	5	2	3	2	2	
x̄	23.2	23.0	-7.4	20 4	15.4	-72	-15	n.a.
σ	±1.0	±1.5	±0.9	±0.2	±1.0	±5	±5	
LOU								
n	16	16	16	4	16	4	4	1
x̄	22.1	22.2	-7.8	16.8	13.7	-99	-41	-118
σ	±1.5	±3.7	±2.3	±1.1	±1.8	±16	±15	--
DAUNTLESS								
n	5	3	3		5			
x̄	19.5	22.0	-7.1	n.a.	12.1	n.a.	n a.	n.a.
σ	±3.2	±2.3	±1.2		±3.2			
TOTALS								
n	34	30	30	9	34	10	10	3
x̄	21.6	23.8	-7.1	17.6	13.8	-98	-39	-129
σ	±1.6	±3.2	±1.9	±1.5	±1.4	±9	±9	±9.5
Base Metal-Enriched Ag-Au±Sb Deposits								
MINTO								
n	6	5	5	1	6			
x̄	18.7	22.9	-8.6	16.8	12 1	n.a.	n.a.	n.a.
σ	±1.5	±3.9	±2.8	--	±1 7			
OLYMPIC								
n	3	3	3	1	3	1	1	
x̄	18.2	15.6	-12.5	12.7	11.7	-106	-29	n.a.
σ	+0.7	±2.3	±1.1	--	±0.7	--	--	
TOTALS								
n	9	8	8	2	9	1	1	
x̄	18.5	20.2	-10.1	14.8	12.0	-106	-29	n.a.
σ	±1.2	±3.3	±2.2	±2.9	±1.4	--	--	

Notes:

*Temperatures used to calculate $\delta^{18}O$ and δD of fluid ar those recorded in Table 6-1 for fluid inclusion trapping temperatures (T_t) from vein quartz and carbonate. If no fluid inclusion temperature available oxygen isotopic temperatures were used (Table 6-1).

[1] Calculated from vein quartz analyses.

[2] Calculated from D analyses of sericite.

[3] Measured δD from inclusion fluids in vein quartz.

n.a. = no sample analysed.
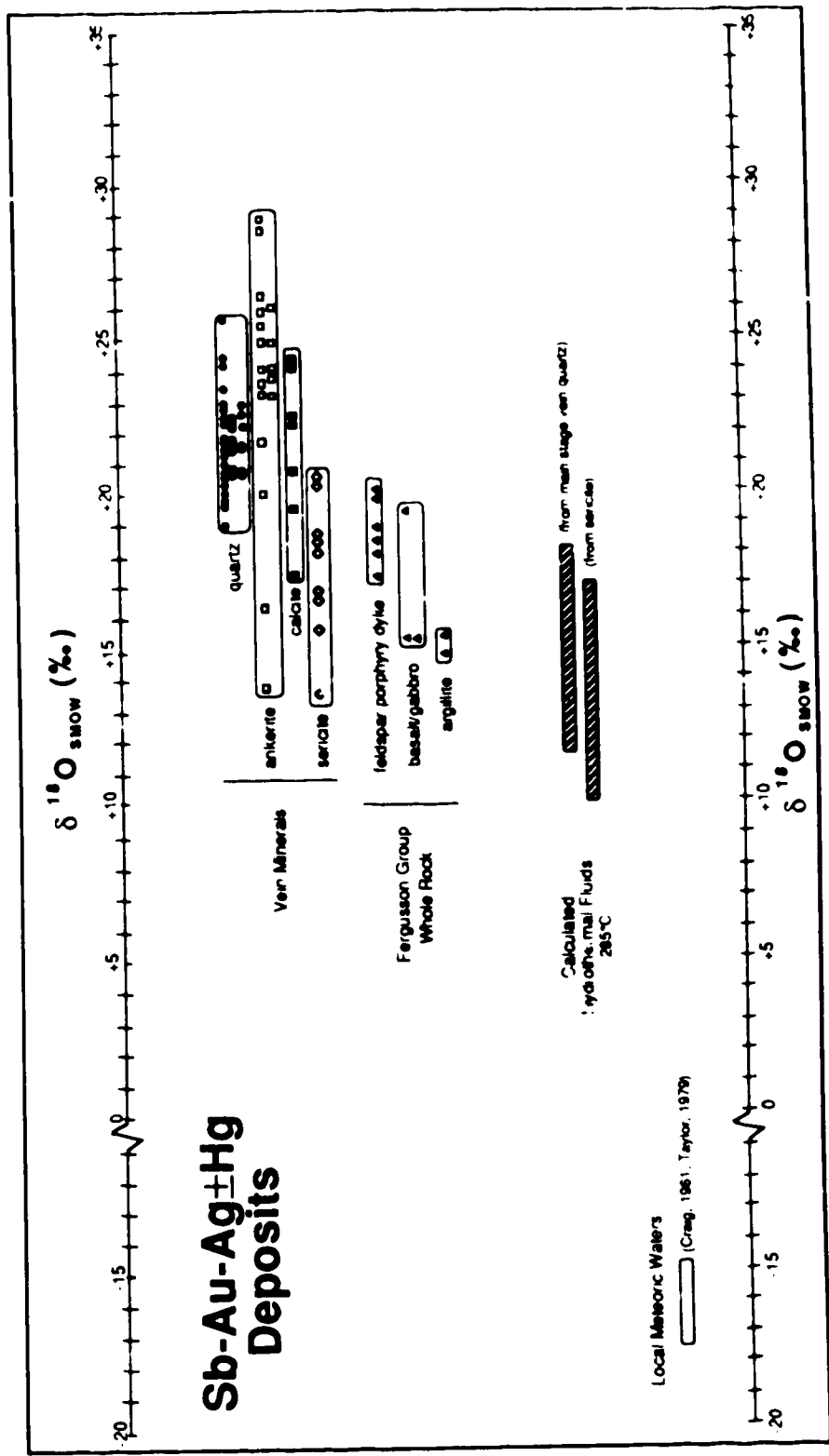
Figure 6-1. Summary of $\delta^{18}O$ data from Sb-Au-Ag±Hg Deposits.
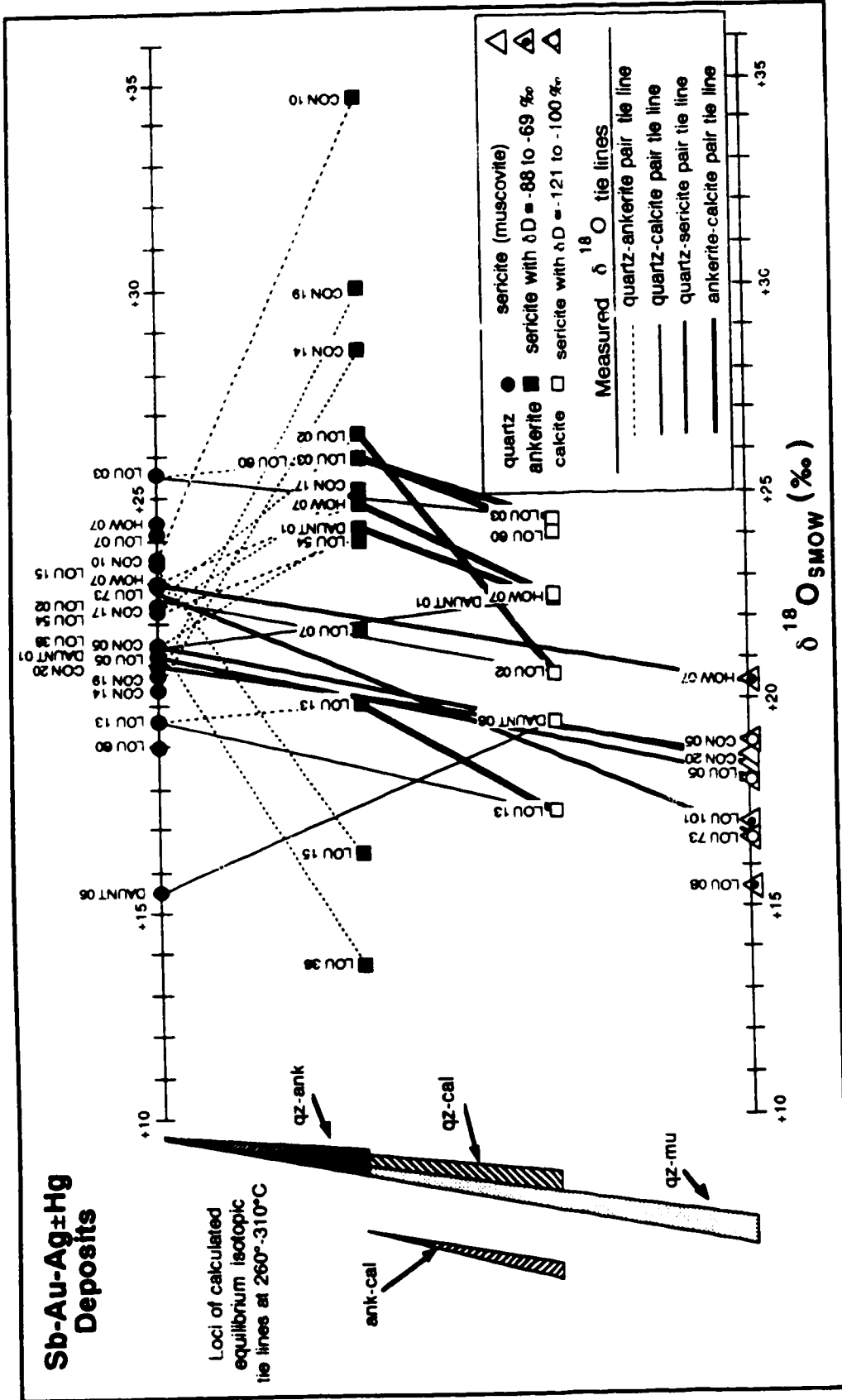
Figure 6-2. Exchange equilibrium diagram of vein mineral assemblages in Sb-Au-Ag±Hg Deposits illustrating isotopic equilibrium-disequilibrium relationships among the minerals that constitute a coeval assemblage based on textural relationships. Isotopic data indicates that many assemblages either are: 1) not in isotopic equilibrium and represent different stages of deposition or; 2) illustrates equilibration of carbonate phases with successive lower temperature events. See text for discussion. Diagram adapted from Rumble (1978).

slopes the fractionations between phases are reversed from those expected at equilibrium (e.g. LOU 13, quartz-ankerite-calcite assemblage: positive slope direction of the qz-cal tie line versus negative slope direction of the qz-ank tie line). In both of the above examples non-equilibrium conditions are indicated.

Most mineral pairs and triplets indicate a lack of isotopic equilibrium in the assemblages. Several mineral pairs show isotopic reversals from the normal $^{18}O/^{16}O$ fractionation. Measurements of Δ_{qz-ank} in particular show abnormally small or negative values. It is necessary to make the point that the calculated equilibrium Δ_{qz-dol} expression has been substituted for Δ_{qz-ank} in this study (appendix) and the fractionation factor for ankerite-water may differ from that of dolo   At present there is little information on the isotopic characteristics of ferroan dolol.   though Rosebaum and Sheppard (1986) in their isotopic study of iron-bearing carbonates at high temperatures reported a close agreement in oxygen fractionation factors between the $\delta^{18}O_{carbonate}$ and that of the acid-extracted CO_2 for dolomite ($\alpha = 1.00913$ at $100°C$) and ankerite ($\alpha = 1.00901$ at $100°C$). However, no carbonate-water equilibrium experiments were conducted by Rosebaum and Sheppard (1986). Furthermore, in the present study ankerite separates were not analysed for their purity beyond powder X-ray diffraction techniques, therefore the data of Rosebaum and Sheppard (1986) may not be wholly applicable. In any case it is felt that any differences resulting from the use of dolomite fractionation expressions in this study are not significant because the total range in measured values is so great (range in $\delta^{18}O_{ank}$ from Sb-Au-Ag mineralization: ca. +14 to +33‰) compared to the possible differences arising from the use of different equilibrium fractionation factors among the carbonate phases.

Vein quartz from the deposits in this group average +21.6 ±1.6‰ and range from +15.5 to +25.6‰. The average for carbonate analyses is +23.8 ±3.2‰, which indicates general isotopic disequilibrium between quartz and carbonate. The high $\delta^{18}O_{carb}$ reflects the contribution by ankerite analyses which average +25.6 ±4.4‰ and range from +13.7 to

+28.9‰. Calcite values average +21.4 ±2.1‰ and range from +17.2 to +24.1‰. In this study $\Delta_{qz\text{-ank}}$ values average -2.4 ±5.5‰, whereas the calculated equilibrium fractionation between quartz and ankerite at the temperatures of formation between 260° and 310°C is +1.2 to +0.54‰ (Figure 6-2). Over the same temperature range the calculated equilibrium $^{18}O/^{16}O$ fractionation between quartz and calcite varies from +1.7 to +1.3‰. Measured $\Delta_{qz\text{-cal}}$ values average 1.8 ±0.4‰.

Similar isotopic relationships between vein quartz and carbonate have been documented in Precambrian mesothermal Au-Ag deposits (Kerrich *et al.*, 1986; Kyser *et al.*, 1986). Carbonate minerals are less resistant than quartz to retrograde oxygen isotope exchange (Clayton *et al.*, 1968) and therefore the wide range in $\delta^{18}O$ of Fe-bearing carbonates could be interpreted to reflect varied degrees of re-equilibration at temperatures lower than those of quartz-carbonate precipitation.

Analyses of $\delta^{18}O$ in separates of hydrothermal sericite (<2 μm size fraction) average +17.6 ±1.5‰ and range from +13.4 to +20.5‰. The 2 μm size fractions contain from ~5 to 20% clay minerals estimated from X-ray diffraction analyses and for this reason the $\delta^{18}O$ values are suspect. Calculated equilibrium quartz-sericite (muscovite) $^{18}O/^{16}O$ fractionations over the temperature range of formation determined from fluid inclusion analyses (260° to 310°C) are between +4.2 and +3.5‰. The observed $\Delta_{qz\text{-ser}}$ between assumed coeval mineral assemblages in this study average +3.9 ±1.4‰ and are compatible with the equilibrium values for $\Delta_{qz\text{-mu}}$ at the same formation temperatures (Figure 6-2).

The $\delta^{18}O$ of fluids in equilibrium with vein quartz and hydrothermal sericite (Figure 6-1) were calculated using T_f of 285° ±20°C (obtained by combining the average $T_h = 265°$ ±20°C from fluid inclusion data, coupled with a pressure correction of 20°C) and the appropriate extrapolated mineral-water fractionation curves. Calculated $\delta^{18}O$ values of fluids in equilibrium with quartz from 265° to 305°C range from +11.3 to +17.6‰. Waters in equilibrium with sericite separates over the same temperatures vary from +9.2 to +15.8‰.

Measurements of D/H ratios in ten sericite separates associated with mineralization range from -121 to -69‰ and average -98 ±9‰. The average for calculated δD values of the hydrothermal fluid is -39 ±9‰. However, three δD values from water in fluid inclusions in quartz range from -135 to -118‰.

Analyses of $^{13}C/^{12}C$ ratios in vein carbonates are notably consistent between early and late mineralizing events within any deposit and between the deposits (Howard avg. $\delta^{13}C$ = -7.4 ±0.9‰, Lou avg. $\delta^{13}C$ = -7.8 ±2.3‰, Dauntless avg. $\delta^{13}C$ = -7.1 +¹ 2‰). Carbonates from Congress mineralization are an exception; $\delta^{13}C$ values average -5.0 ±2.0‰, 2.1‰ greater than the average for all the deposits in the subgroup.

6.2.2 Base Metal-Enriched Ag-Au±Sb Deposits: Minto, Olympic

Figure 6-3 summarizes $\delta^{18}O$ data for the Minto deposit and Olympic occurrences while Figure 6-4 is an exchange equilibrium diagram that illustrates isotopic equilibriuı disequilibrium $\delta^{18}O$ relationships among gangue phases in a manner similar to Figure 6-2.

The $\delta^{18}O$ values for vein phases in these deposits are ^{18}O-enriched, though to a lesser extent than those in the previous group. Quartz values range from +16.4 to +19.8‰ (avg. = +18.5 ±1.2‰). Calcite $\delta^{18}O$ values range from +13.0 to + 20.5‰ (avg. = +16.9 ±3.0‰) and ankerite values range from +19.0 to +28.6‰ (avg. = +23.5 ± 4.2‰). The Δ_{qz-ank} values consistently indicate isotopic disequilibrium with an average value of -4.6 ±3.7‰; calculated equiliorium $^{18}O/^{16}O$ fractionations between quartz and ankerite over the same temperature range (295° to 325°C) are between +0.8 to +0.54‰. Two Olympic Δ_{qz-cal} values indicate an approach to $^{18}O/^{16}O$ equilibrium at the same temperatures of formation (Figure 6-4) with values of +1.7 and +1.5‰; calculated equilibrium $^{18}O/^{16}O$ fractionations between coeval quartz-calcite pairs range from +1.4 to +1.3‰ over the range of 295° to 325°C.
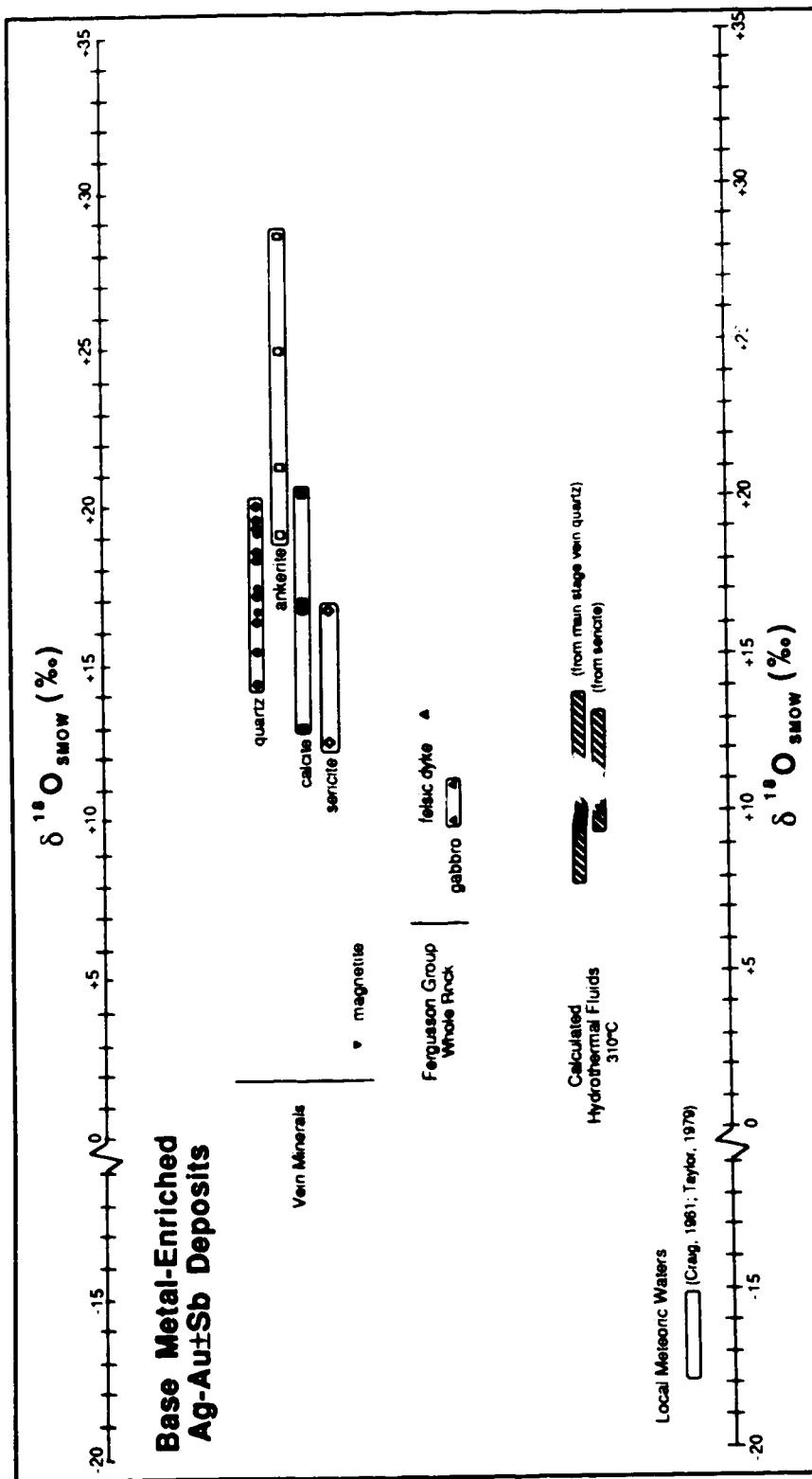
Figure 6-3. Summary of $\delta^{18}O$ data from Base Metal-Enriched Ag-Au-±Sb Deposits.
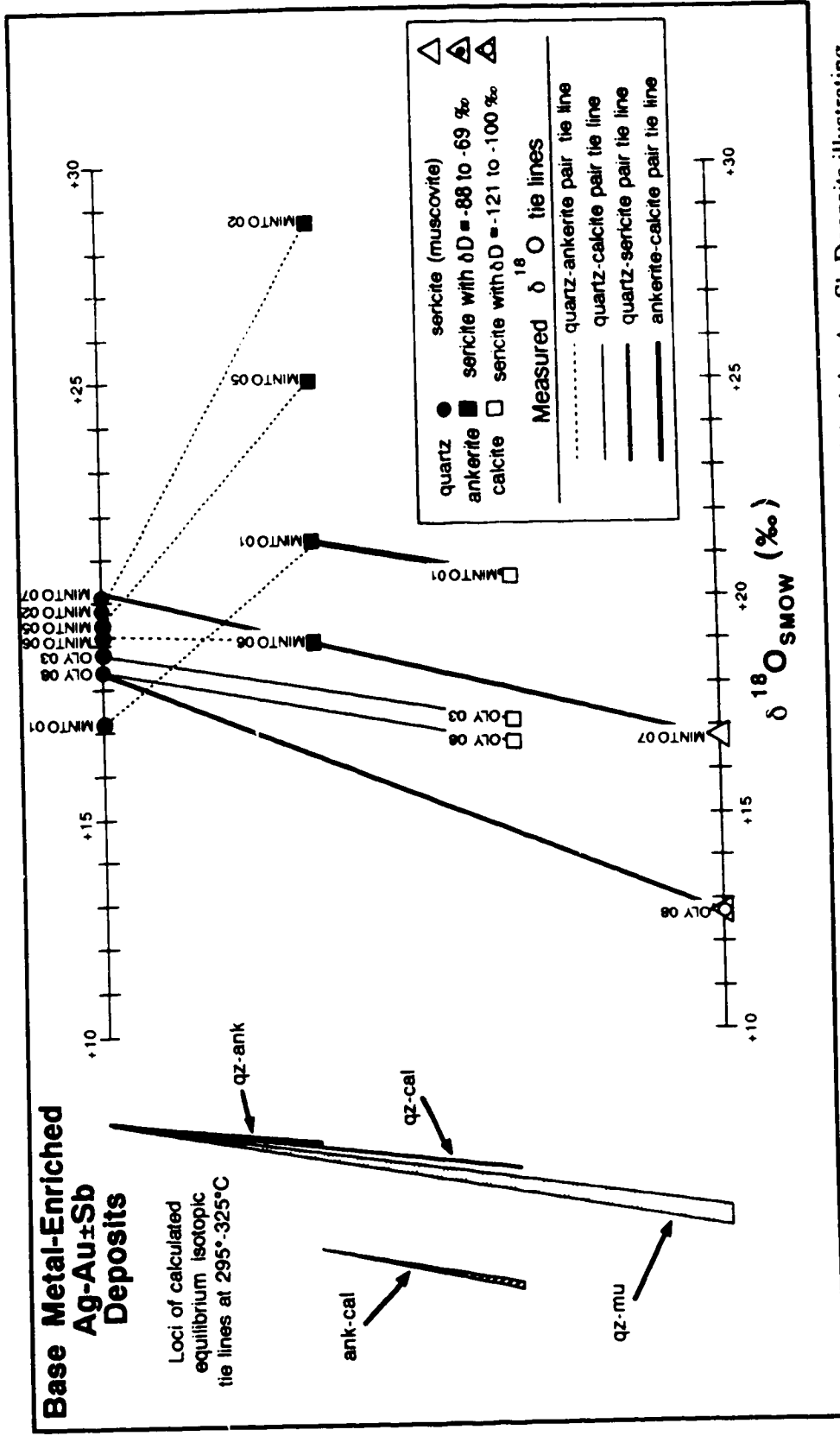
Figure 6-4. Exchange equilibrium diagram of vein mineral assemblages in Base Metal-Enriched Ag-Au±Sb Deposits illustrating isotopic equilibrium-disequilibrium relationships among the minerals that constitute a coeval assemblage based on textural relationships. Isotope data indicates that many assemblages either are: 1) not in isotopic equilibrium and represent different stages of deposition or; 2) illustrates equilibration of carbonate phases with successive lower temperature events. See text for discussion. Diagram adapted from Rumble (1978).

Separates of hydrothermal sericite from Minto and Olympic were analysed for $\delta^{18}O$ (MINTO 07 $\delta^{18}O$ = +16.8‰, OLY 08 $\delta^{18}O$ = +12.7‰). Calculations of Δ_{qz-ser} indicate approximate equilibration; +1.4 to +1.1‰ over the temperature range of 295° to 325°C.

As before, $\delta^{18}O$ of fluids in equilibrium with vein quartz and hydrothermal sericite were calculated using formation temperatures from pressure corrected fluid inclusion data (310° ±15°C) and the appropriate fractionation curves. Results are plotted in Figure 6-3. Temperatures of homogenization in fluid inclusions are comparable or slightly ..gher than those for the Sb-Ag-Au±Hg deposits. Because of similar temperatures in both deposit types, the trend in $\delta^{18}O$ va! ies calculated for the fluids parallels the trend in $\delta^{18}O$ values of the minerals in each group (Figures 6-1 and 6-3).

A single δD value for hydrothermal sericite was obtained from Olympic vein material. The value of -106‰ is comparable to those D/H ratios measured from sericite separates in the more antimony-rich deposits. The calculated δD value for water in equilibrium with the sample is -28‰.

Average $\delta^{13}C$ values of the base metal-enriched Ag-Au±Sb occurrences are depleted in ^{13}C compared to the Sb-Au-Ag±Hg deposits (Table 6-2). Olympic $\delta^{13}C$ values (avg. -12.5 ±1.1‰) negatively weight the combined average as Minto values average only -8.6 ±2.8‰.

6.2.3 Isotopic Relationships in Host Lithologies

Analyses of whole rock samples of several lithologies hosting the deposits mimic the trend outlined by $\delta^{18}O$ measurements of vein minerals. Country rocks associated with Sb-Au-Ag±Hg deposits are more ^{18}O-enriched than those rocks associated with the base metal-enriched deposits yet both deposit groups are hosted by the same lithologies. The isotopic patterns parallel that of vein phases (Figures 6-1 and 6-3) among the two deposit

classifications and indicate that the fluids responsible for mineralization in the respective groupings were also responsible for resetting the isotopic ratios of the host rocks.

Andesite to dacite dykes associated with the antimony-associated Au-Ag deposits have $\delta^{18}O$ values ranging from +17.4 to +20.2‰, about 12 to 13‰ greater than typical primary whole rock values for such lithologies (Taylor, 1968). Analyses of $\delta^{18}O$ in mafic rocks closely associated with the deposits range from +15.2 to +19.5‰. These values are also 10 to 12‰ greater than the range in $^{18}O/^{16}O$ ratios recorded for typical basaltic values (Taylor, 1968). Two samples of argillite from the vicinity of the Dauntless prospect have an average $^{18}O/^{16}O$ ratio of +15.2 ±0.4‰.

6.2.4 Camp Scale Isotope Systematics

A preliminary stable isotope survey of lode gold mineralization to the southwest (Bralorne, Arizona, Veritas) and mercury deposits to the northeast (Manitou, Silver Quick, Tungsten Queen, Red Eagle) was conducted (see Figure 3-1 for locations). Results from the analyses of vein quartz and carbonate as well as several analyses of serpentinite and magnetite associated with these deposits are included in Table 6-1.

A camp scale trend of increasing enrichment emerges over a distance of 30 kilometres in a direction northeast from the Coast Plutonic Complex; from the lode gold deposits in the southwest through the antimony-associated gold deposits to the mercury deposits in the northeast.

Analyses of vein phases from the gold deposits are enr   ·n ^{18}O to a degree comparable to values from the base metal-enriched category   'ein quartz $\delta^{18}O$ range from +14.4 to +20.0‰ (avg. +17.9 ±2.4‰). Calcite - ···· ·τ +15.4 to +17.4‰ (avg. +16.3 ±1.0‰). Measurements of $\delta^{18}O$ in ι ·τ   )sits northeast of the Sb-Au-Ag zone range from +19.4 to +28.5   ±3.7‰). A single analysis of vein quartz yielded a value of +28.4‰.

Serpentinites spatially associated with mineralization in each of the three metallogenetic zones in the district were analysed for $\delta^{18}O$ and δD (Table 6-1). A semi-quantitative determination of the proportions of serpentine polymorphs in the samples were made by powder X-ray diffraction analysis (Whittaker and Zussman, 1956). The compositions range from approximately 100% antigorite (BR-01, ARIZ 04, VER 03) to about 30% antigorite (BR-22). Analysis of sample BR-59 indicates a composition of about 80% antigorite and possibly 20% lizardite-chrysotile, while OLY 09 displays almost an equal proportion of antigorite to lizardite-chrysotile. Lesser amounts of chlorite, kaolinite, talc and possibly brucite are also present in the samples. The Tungsten Queen (BR-22) serpentinite specimen is set apart by the relatively larger proportions of chlorite and talc in the sample.

Three serpentinite samples (<2 μm size fraction separates) from the Bralorne fault zone (Figure 2-3) are associated with lode gold mineralization (BR-59, Bralorne; ARIZ 04, Arizona; VER 03, Veritas). The $\delta^{18}O_{serp}$ values for these rocks are +9.1‰, +9.0‰, and +11.0‰ respectively. The measurements of δD_{serp} are -77‰, -181‰, and -72‰ respectively. A single sample (OLY 09) of serpentinite associated with Sb-Au-Ag mineralization was analysed and yielded a $\delta^{18}O$ value of +9.7‰; no δD value was obtained for this sample. Serpentinite from the Red Eagle mercury deposit (BR-01) yielded values of +11.9‰ for $\delta^{18}O$ and -160‰ for δD. The analyses of BR-22, serpentinite from the Tungsten Queen mercury deposit, are strikingly dissimilar to the values for Red Eagle; $\delta^{18}O$ = +21.4‰ and δD = -99‰.

Magnetite separates were also obtained from the serpentinite specimens and the oxygen isotope analyses of the separates are listed in Table 6-1. The $\delta^{18}O_{mag}$ values from the Bralorne fault zone serpentinites (Bralorne, BR-59; ARIZ 04; VER 03) are +3.1, +2.8 and +4.5‰ respectively. The $\delta^{18}O_{mag}$ values from serpentinites associated with Hg mineralization in the northeast are +5.9 and +12.0‰ respectively, for samples BR-01 (Red

Eagle) and BR-22 (Tungsten Queen). A magnetite separate was not obtained from serpentinite specimen OLY 09.

6.3 Discussion

Deposits similar to the Congress-type have been documented as integral parts of complex metallogenetic systems that deposit Au-Sb-Hg. Antimony-gold deposits can be considered an intermediate component in a vertical metal zonation associated with Cretaceous-Tertiary lode gold mesothermal deposits in the Cordillera and can be linked with mesothermal lode gold mineralization and with mercury vein deposits. Several studies (Woodsworth et al., 1977; Maheux et al., 1987; Leitch et al., 1988) of mineralization in the Bridge River district have proposed genetic links between the different metal deposits. This association has also been documented on a regional scale throughout the Canadian Cordillera by Nesbitt et al. (in press).

Several models have been proposed to explain the source of the fluids and metals in the mesothermal gold deposits, and by extension the antimony and mercury deposits within the metallogenetic continuum. The origin of Cordilleran mesothermal gold deposits and their Precambrian analogues has been accounted for by several hypotheses including: magmatic (Griffis, 1968), lateral secretion (Boyle, 1979), metamorphic degassing (Kerrich and Fryer, 1979; Kerrich and Fyfe, 1981; Kerrich, 1987), mantle degassing-granulitization (Colvine et al., 1984; Fyon et al., 1984), evolved meteoric water circulation (Nesbitt et al., 1986; Nesbitt et al., in press), and multi-stage processes.

In many cases deposits are situated proximal to plutons, but the low-^{18}O meteoric-hydrothermal effects shown by Magaritz and Taylor (1976a, 1976b, 1986) to be typical of these environments in B.C. are missing from the deposits in the district. The data from the present study are discussed in light of the lack of a fresh meteoric signature in any of the

rocks and with respect to the prevalent fluid models for the origin of mesothermal lode gold deposits in the North American Cordillera.

6.3.1 Interaction of Meteoric-Hydrothermal Fluids with Plutonic Rocks

Magaritz and Taylor (1986) extended their study of meteoric-hydrothermal alteration of plutonic rocks in the northern Cordillera (Magaritz and Taylor, 1976b) to southern British Columbia. Their study encompassed a complete section across the Cordilleran batholiths and also cut across the conglomeration of accreted terranes that abut the western edge of the continent. The results of this work are of particular interest to the present study because the Bridge River District falls within their study area.

Analyses of mineral separates from samples of isolated plutons along the eastern margin of the Coast Plutonic Complex provided evidence for the involvement of low-δD (-69 to -130‰) meteoric-hydrothermal fluids along the eastern edge of the Coast batholith. This phenomenon had been previously documented on a large scale farther north along the eastern margin of the Coast Plutonic Complex (Magaritz and Taylor, 1976a) as well as to the south around a group of epizonal granitic plutons in the Idaho batholith (Criss and Taylor, 1983). Whole rock $\delta^{18}O$ values (avg. = +11.0 ±3.0‰) of granitic rocks emplaced in the Bridge River terrane showed the meteoric-hydrothermal alteration effects associated with the granitic plutons to be weak in the Bridge River area and not to extend a great distance into the metamorphic country rocks when compared to the cases to the north and south (Magaritz and Taylor, 1986). Mica schist whole rock $\delta^{18}O$ values ranged from +12.5 to +21.9‰ and the δD values were uniformily between -69‰ and -73‰. Magaritz and Taylor (1986) suggested this pattern implied that the southern Coast Batholith rocks intruded less permeable country rocks or that the southern traverse had sampled a deeper erosional level. It may also be possible that the isotopic signature developed in the rocks were the result of a process other than an epizonal overprint incorporating meteoric water,

or perhaps meteoric waters had a different isotopic signature during operation of the epizonal hydrothermal system.

Overall D/H variations of altered granitic rocks from batholithic terranes in southern British Columbia exhibit decreasing δD values from west to east. The west to east trend closely parallels the trend in present-day meteoric waters in British Columbia but is enriched by 20 to 30‰. This enrichment is compatible with a northward translation of the batholithic terranes. The data are also compatible with an overall shift from a warmer marine environment to a cooler, more continental climate in southern British Columbia during the late Mesozoic and early Cenozoic eras when the meteoric-hydrothermal alteration took place (Magaritz and Taylor, 1986).

If mineralization in the Bridge River district is genetically associated with the Coast Plutonic Complex presumably the ore deposit system should show some evidence of the same meteoric-hydrothermal alteration effects seen in the granitic rocks. More significantly, it would be expected that the deposits were the expression of shallow hydrothermal systems involving large volumes of surface-derived waters. Results from the stable isotope oxygen analyses in this study disprove these scenarios.

6.3.2 Isotope Systematics of the Bridge River Antimony-Associated Au-Ag Deposits

Oxygen

The most striking aspect of the results of this study is the level of ^{18}O-enrichment in all vein phases. Average analyses of vein quartz from the Sb-associated Au-Ag deposits in the Bridge River district fall within the range of +18.2 ±0.7‰ to +23.2 ±1.0‰ and are generally greater than values from other gold-bearing mesothermal deposits (Figure 6-5). The bimodal distribution of $\delta^{18}O$ values for minerals from the antimony-associated Au-Ag deposits in the Bridge River District documents that vein minerals from base metal-enriched
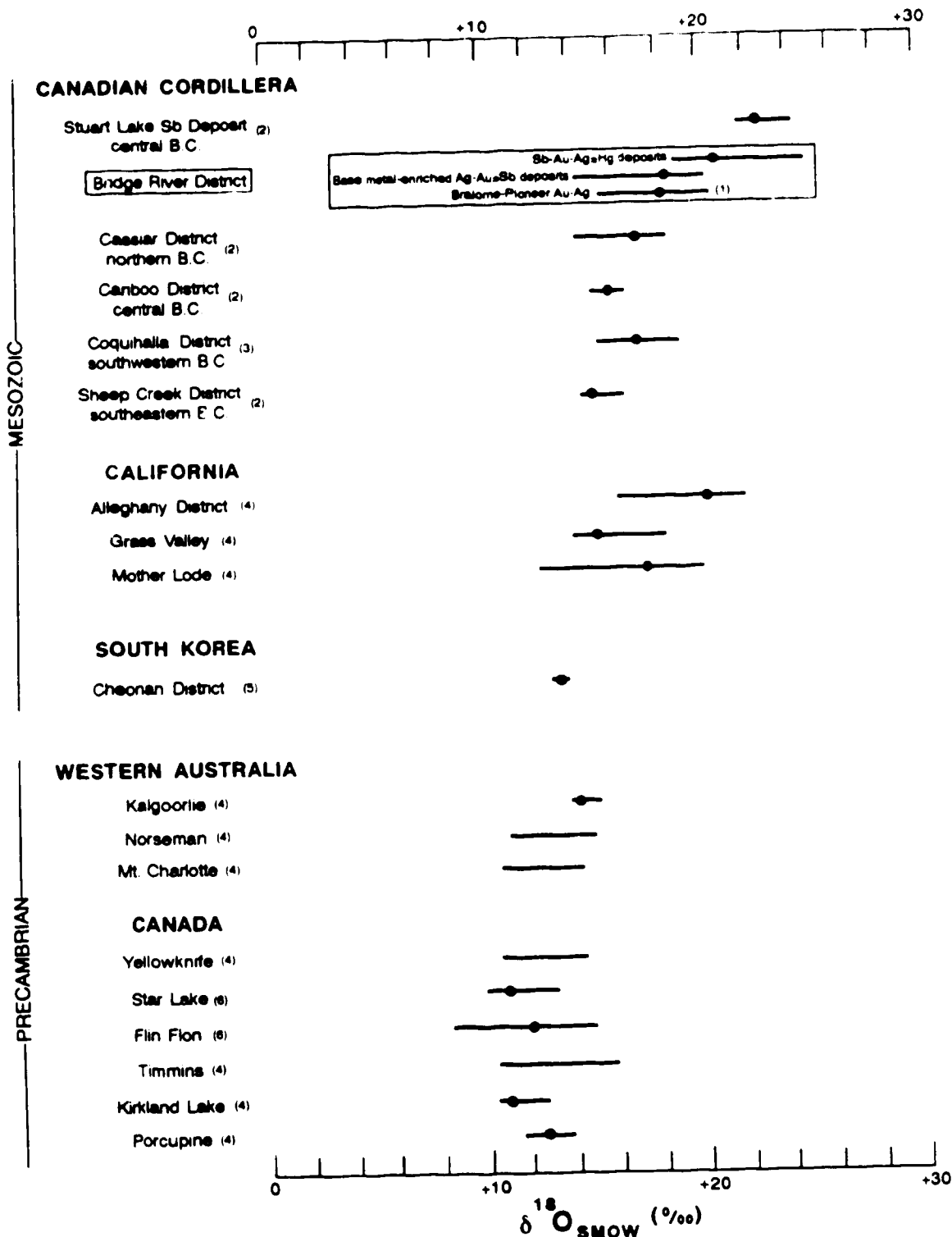
Figure 6-5. $\delta^{18}O$ of vein quartz from selected gold-bearing lode deposits; bar indicates range in values, filled circle indicates average value. Sources of data: (1) Maheux *et al.* (1987); (2) Nesbitt *et al.*, in press; (3) Murowchick *et al.*, 1987; (4) Taylor, 1987; (5) So and Shelton, 1987; (6) Kyser *et al.*, 1986.

Ag-Au±Sb mineralization are not as ^{18}O-enriched as vein minerals from the Sb Au Ag±Hg deposits studied ($\delta^{18}O_{qz}$: +18.5 ±1.2‰ vs. +21.6 ±1.6‰; $\delta^{18}O_{carb}$: +20.2 ±3.3‰ vs. +23.8 ±3.2‰; $\delta^{18}O_{ser}$: +14.8 ±2.9‰ vs. +17.6 ±1.5‰).

This pattern may be the result of initial differences in the isotopic composition of the ore fluids or may be due to differences in the physio-chemical parameters at the site of deposition. A difference in formation temperatures between the two groups of deposits might account for the approximate 3‰ difference in gangue mineral analyses. However, evidence from fluid inclusion microthermometry anlyses and stable isotope thermometry does not support the hypothesis. If an isotopically uniform ore solution for the deposits is assumed, the quartz precipitation temperatures of the Sb-Au-Ag±Hg deposits (Congress, Howard, Lou, Dauntless) should have been higher than in the base metal-enriched deposits (Minto, Olympic). However, the fluid inclusion study indicates comparable temperatures of homogenization for deposits in both deposit categories; 265° ±20°C and 280° ±30°C respectively. Geothermobarometry yielded comparable pressure corrections for the deposits, indicating trapping temperatures of approximately 20°C greater than the homogenization temperatures for Sb-Au-Ag±Hg mineralization and 30°C for base metal-enriched Ag-Au±Sb mineralization. If the differential cannot be explained by depositional temperatures perhaps unique fluids were responsible; yet there is no data at this time that suggests two separate Sb-Au-Ag ore-forming fluids existed, each with its particular $\delta^{18}O$ value. Another mechanism must have been responsible for the differential in isotope values of vein phases between the two groups.

The isotopic pattern revealed by analyses of wall rocks show that the fluids responsible for mineralization were also responsible for the hydrothermal alteration. Furthermore, analyses of $^{18}O/^{16}O$ ratios in host rocks show a $\delta^{18}O$ trend of enrichment which is dependent on the "primary" isotopic signature of the particular lithology, thus indicating a system characterized by low or at least decreasing water/rock ratios operating during the alteration of the host rocks. The relatively uniformly high $\delta^{18}O$ values imply a

corresponding homogeneity to the $\delta^{18}O$ values of the Sb-Au-Ag ore fluids and to some extent, the temperatures of formation.

Carbon

Carbon isotope compositions of carbonates are relatively tightly clustered within the antimony-associated deposits with an overall average of -7.4 ±1.9‰. The respective populations of $\delta^{13}C$ values of ankerite and calcite are statistically indistinguishable ($\delta^{13}C_{cal}$ = -7.6 ±2.2‰; $\delta^{13}C_{ank}$ = -7.6 ±1.8‰). This is to be expected because ^{13}C fractionations between carbonate phases under hydrothermal conditions are small (Sheppard and Schwarcz, 1970).

More enigmatic is the heterogeneity of $\delta^{13}C$ values within the base metal-enriched Ag-Au±Sb deposit subgroup. Minto values average -8.6 ±2.8‰ but the $\delta^{13}C$ values in Olympic carbonates average -12.5 ±1.1‰. The average $\delta^{18}O$ values of carbonate gangue phases from the two deposits differ significantly as well; $\delta^{18}O_{MINTO}$ average +22.9 ±3.9‰ while $\delta^{18}O_{OLY}$ average +15.6 ±2.3‰.

It is well documented that the $\delta^{13}C$ values in vein carbonates are dependent upon the carbon-bearing species in solution, which in turn are dependent upon the temperature, Eh and pH of the fluid (Ohmoto, 1972). Some mechanism or combination of mechanisms must account for the significant depletion in $\delta^{13}C$ and $\delta^{18}O$ values from Olympic material versus Minto material. To account for the differences based on depositional temperature a range of approximately 225°C would be required. If $T_f \cong T_h$ for Minto is ~300°C then $\Delta_{cal-CO_2} \cong$ -2‰ and therefore $\delta^{13}C_{fluid} \cong$ -6.6 ‰. This requires an unreasonable T_f for Olympic carbonate of ~75°C: for $\delta^{13}C_{fluid}$ = -6.6‰ from the Olympic $\delta^{13}C_{cal}$ of -12.5‰ a $\Delta_{cal-CO_2(g)}$ value of -5.9‰ is required ($\Delta_{cal-CO_2(g)} \cong$ -12.5‰ - [-6.6‰]).

These deposits are hosted by the same lithologic units and it is unlikely that the differences in $\delta^{13}C$ values are the result of variations in the carbon isotope compositions of

the source rocks (*e.g.* very negative $\delta^{13}C$ values obtained by oxidation of graphite). Some other mechanism must account for the pronounced negative shift. The most significant carbon isotope fractionations occur not in response to shifts in the pH of a system but near the boundaries between reduced and oxidized aqueous species (Ohmoto, 1972). The carbon-bearing species in the Olympic fluids are CO_2 and CH_4; fluid inclusion analyses of Olympic inclusions documented locally CO_2-rich inclusions with possibly up to a 5 mol. % CH_4 component. Furthermore, the Olympic vein mineral assemb e includes pyrrhotite as a main-stage phase and late-stage magnetite, locally a coeval phase with calcite, su sting an increase in Eh in the Olympic system at the time of deposition of the carbonate. With oxidation at the site of deposition of isotopically light carbon in only a small quantity of CH_4 (< 10 mol. %) above the CO_2/CH_4 buffer a 4‰ negative shift could easily be produced (Fyon *et al.*, 1984).

The source of carbon in the hydrothermal system cannot be unequivocally determined. Other workers have suggested that similar $\delta^{13}C$ values in ferroan dolomites associated with gold deposits indicate mantle degassing as a source for the CO_2 ($\delta^{13}C = -5.5‰$) with shifts to slightly higher or lower values through excursions from the ambient Eh conditions at the site of deposition (Fyon *et al.*, 1984). However, the "magmatic" appearance of the carbon from the Bridge River carbonates is likely coincident. Given the geologic setting of an ophiolitic environment and the nature of carbon isotope systematics, it is more re ic to propose that the evolved hydrothermal fluids acquired carbon isotope compositions any where in the interval encompassing all natural carbon reservoirs (Figure 6-6).
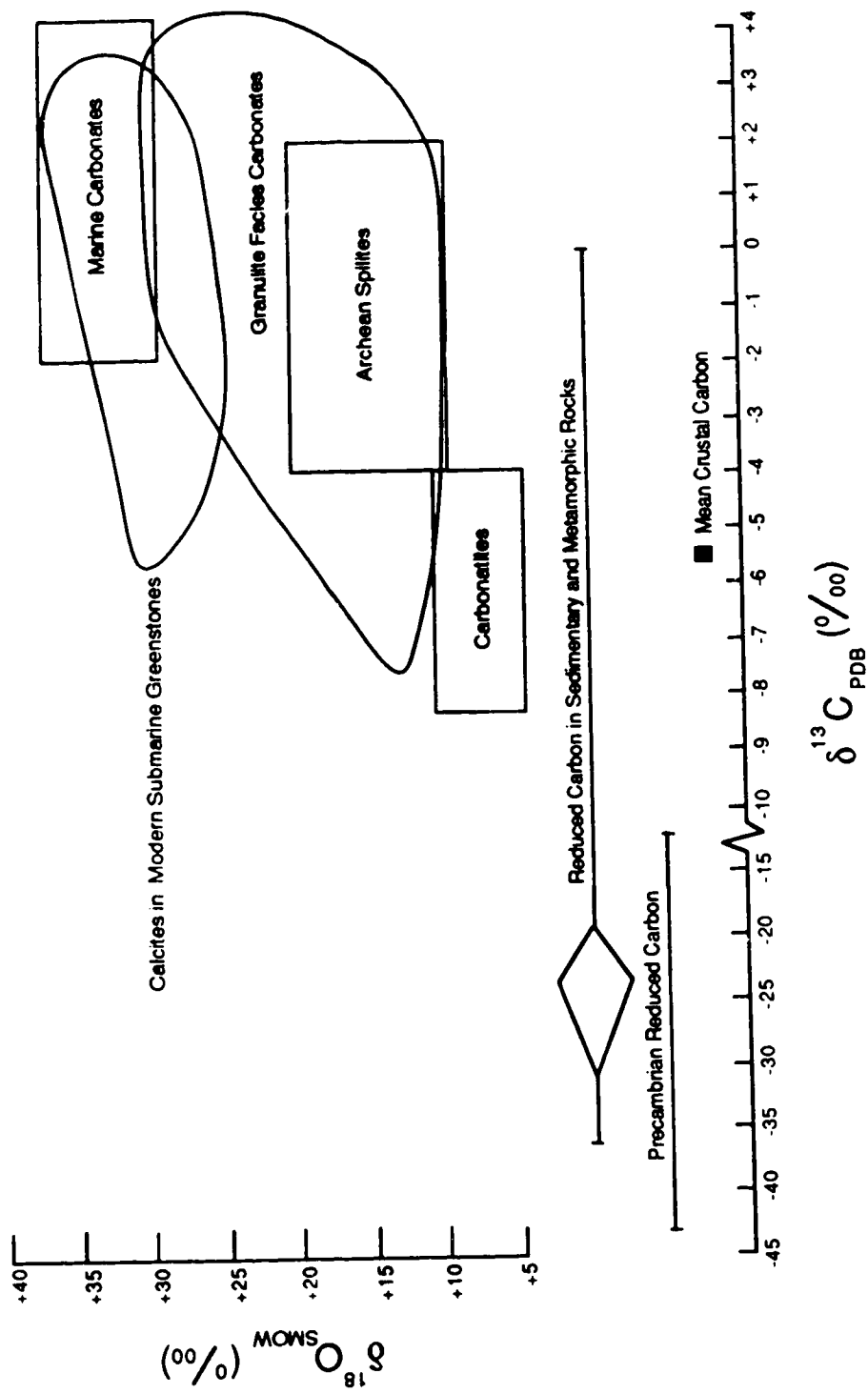
Figure 6-6. The oxygen and/or carbon isotope composition of specified carbon reservoirs. Modified from Kerrich (1987).

Characteristics of the Hydrothermal Fluids: Oxygen, Hydrogen

Suggestions that there are genetic similarities between the mesothermal, Mesozoic Au-Ag deposits of the northern North American Cordillera, the mesothermal Au-Ag deposits of the Sierra Nevada in California, and the Precambrian lode Au deposits of the Canadian Shield have been largely based on the characteristics and source reservoirs of the hydrothermal fluids responsible for mineralization. Light stable isotope studies have been employed to a great extent because of their inherent value as indicators of the origin and evolution of hydrothermal fluids (Marshall and Taylor, 1981; Hodgson *et al.*, 1982; Colvine *et al.*, 1984; Böhlke and Kistler, 1986; Goldfarb *et al.*, 1986; Nesbitt *et al.*, 1986; Kerrich, 1987; Weir and Kerrich, 1987; Nesbitt and Muehlenbachs, 1988).

For identification of the nature and evolution of the hydrothermal fluid it is important to study the D/H ratios of the hydrous phases in the rocks and trapped samples of the fluids in fluid inclusions. The hydrogen isotopes are much less sensitive to small degrees of water/rock interaction th.   : the oxygen isotopes because the hydrogen concentrations in rocks are very small (Taylor, 1977). Therefore hydrogen isotope characteristics, among other geochemical parameters, serve to differentiate the two most prevalent models invoked for the origin of mesothermal lode gold in the North American Cordillera. The oxygen and hydrogen isotope composition of the fluids responsible for Sb-Au-Ag ore deposition in the Bridge River District will be discussed in light of the two models.

Where possible, an estimate of formation temperature was calculated from oxygen isotope fractionations between phases within hydrothermal mineral assemblages in the deposits. Temperature estimates were derived from selected pairs from assemblages of coexisting quartz, sericite, calcite, and ankerite. Triple isotopic concordance is rare among any assemblages of three hydrothermal phases in any sample (Figures 6-2 and 6-4). There is however strong textural evidence for co-precipitation and several isotope pairs yield

calculated temperatures which are reasonable and agree with fluid trapping temperatures from fluid inclusion data. In several instances isotope temperatures provide a reliable estimate of the temperatures of formation of the mineral assemblages that is higher than the estimate of fluid trapping from inclusions (Table 5-3). The isotopic te nperatures (avg. 285° ±25°C) are higher by ca. 15°-20°C on average than fluid trapping temperatures. The differential may be considered to be the pressure correction required because of deposition at elevated pressures; in this case approximately 300 bars (30 MPa) (Chapter 5).

Calculated and measured oxygen and hydrogen isotope compositions of the fluids involved in the Bridge River deposits are plotted in Figure 6-7.

Utilizing temperatures of formation inferred from fluid inclusion analyses and oxygen isotope geothermometry, the $\delta^{18}O$ values of ore-forming fluids were calculated to be in the range of ca. +6 to +18‰. The wide range in values includes those relatively less ^{18}O-enriched fluids calculated to be in equilibrium with vein phases from the base metal-enriched deposits. The $\delta^{18}O$ data provides no evidence for the involvement of any component of fresh meteoric water in the development of the hydrothermal system. The isotope data together with the geothermometry and geobarometry data from fluid inclusion analyses suggest that the antimony-associated gold deposits in the Bridge River district are not epithermal in origin according to the criteria of Heald $et\ al$. (1987).

The range of isotopic composition in the Sb-Au-Ag deposits, their associated host rocks, and other lithologies and vein phases throughout the district, implies some degree of complexity to the system. Some type of mixing, multi-stage partial exchange process, deposition through a thermal gradient in space and possibly time, or a combination of these processes must have been operating.

Hydrogen isotope data from gold deposits in the southern North American Cordillera are compatible with the metamorphic water field (Figure 6-7) suggesting that the fluids were derived from devolatilization reactions during regional metamorphism (B öhlke and Kistler, 1986; Taylor, 1987). The hydrogen isotope analyses are the key to
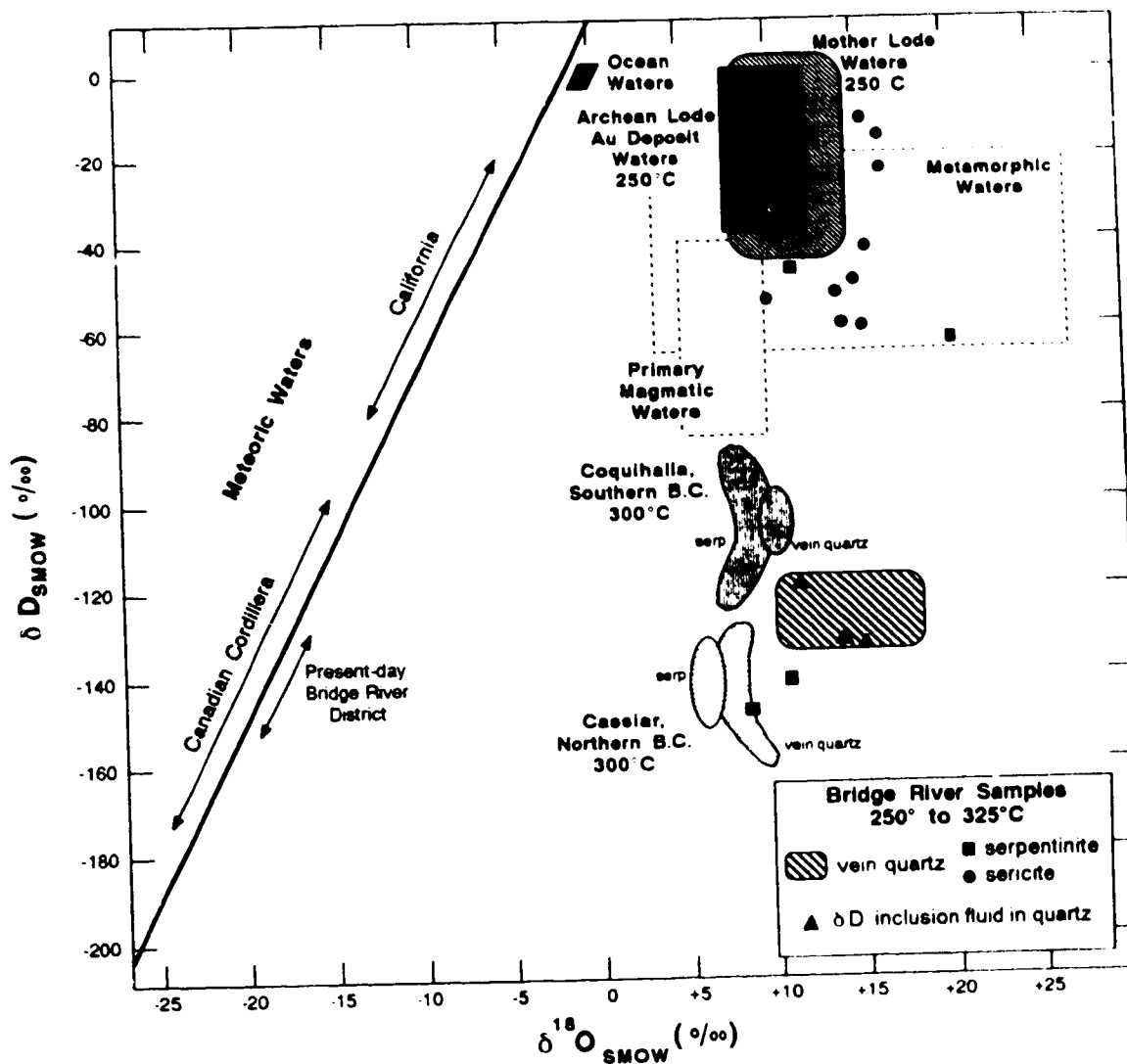
Figure 6-7. Plot of δD vs. δ¹⁸O for calculated waters in equilibrium at temperatures indicated with minerals in lode Au-bearing deposits and for measured inclusion fluids in vein quartz. Isotopic composition of natural fluid reservoirs after Taylor (1974). Other data not this study: Mother Lode; Böhlke and Kistler (1986), Marshall and Taylor (1981), Weir and Kerrick (1987); Coquihalla and Cassiar; Nesbitt *et al.* (1986).

differentiating the sources of the fluids between this model and that of Nesbitt *et al.* (in press) who studied deposits in the northern Cordillera between latitudes 50° N and 61° N. Nesbitt *et al.* (in press) propose that deposits in the Canadian Cordillera developed through the deposition of metals from meteoric waters that underwent extreme ^{18}O-enrichment and minor D-enrichment. The isotopic criteria for distinguishing between aqueous fluids of metamorphic or meteoric origin are especially powerful in northern latitudes because the $^{18}O/^{16}O$ and D/H ratios of surface meteoric waters systematically decrease northward in the northern hemisphere (Craig, 1961a). This variation is borne out by analyses of δD in deposits throughout the Canadian Cordillera (Figure 6-7). The δD values of inclusion fluids and calculated from hydrous silicates in gold deposits vary from -110‰ in the Coquihalla district, southern British Columbia, to -150‰ in the Cassiar district, northern British Columbia (Murowchick *et al.*, 1987; Nesbitt *et al.*, 1986). Nesbitt *et al.* (1986) suggested that these data are evidence that the deposits formed from meteoric fluids that had been enriched in ^{18}O due to extensive water-rock interaction. They argued that these fluids are not a mixture of heavy δD metamorphic fluid contaminated later by meteoric water depleted in D, because δD results would be observed to vary along a line of mixing from metamorphic to meteoric values depending on the proportions of late stage to early stage inclusions sampled. Nesbitt *et al.* (1987) observed no such trend in their results. Even if late stage fluids were included in the analyses they could in all likelihood be part of the mineralizing system as in many of the deposits gold deposition occurs in the waning stages of the hydrothermal event. This was observed in the present study where gold and mercury mineralization followed main-stage antimony mineralization in the Sb-Au-Ag±Hg deposits (Figure 4-1). In the Minto and Olympic deposits gold was again documented to be associated with later quartz vein material and post-dated main-stage sulphide deposition (Figure 4-11). Measured D/H ratios of inclusion fluids in quartz from the present study are in agreement with the hypothesis of Nesbitt *et al.* (1986) (Figure 6-7).

The proponents of metamorphic devolatilization models have criticized the evolved

meteoric fluid model because it is based principally on hydrogen isotope evidence from

extracted inclusion fluids in ore-stage quartz. Pickthorn et al. (1987) note that fluid

extractions from quartz can be mixtures of primary, pseudosecondary, and secondary

inclusions and may not accurately represent the vein-forming fluid. Goldfarb et al. (1986)

in their study of lode gold in south-central Alaska found that progressive crushing of quartz

samples liberated fluids with increasingly heavy δD values (max. ~-60‰), presumably due

to the fact that the original metamorphic quartz-precipitating fluid would have been sampled

by the primary inclusions. Furthermore, they record the analysis of hydrothermal ore-stage

sericite from the Juneau district has a value of -61‰ and propose that the fluids in

equilibrium with the mica ($\delta D \cong$ -20‰ at 300°C) are more representative of the ore-forming

solution. Pickthorn et al. (1987) suggest that the high δD from their work and others in the

Mother Lode District (B öhlke and Kistler, 1986) possibly represent fluids produced

through prograde metamorphic reactions. They note that the small hydrogen content of

hydrous minerals rules out the possibility that meteoric waters could have undergone such a

large deuterium shift by exchange with the country rocks and they stress the importance of

analyzing ore-stage hydrous minerals to establish that the δD values obtained from fluid

inclusion extractions are representative of the ore-forming fluid and not some later

hydrothermal event.

An attempt was made to address this point by analyzing sericite separates from

several of the deposits in the present study. The range of values obtained (-121 to -69‰,

avg. = -100 ±17‰; Table 6-1) when combined with average fluid inclusion trapping

temperatures yield δD values of from -60 to -11‰ (avg. = -38 ±18‰) for the hydrothermal

fluid. These values fall within the metamorphic fluid field defined by Taylor (1974) (Figure

6-7) and appear to corroborate a metamorphic devolatilization origin. However, as

mentioned above inclusion fluids liberated from samples of ore-stage quartz from Sb-Au-

Ag±Hg deposits in the Bridge River district have measured δD values indicative of local

(southern B.C.) meteoric waters with a slight enrichment in δD. The inclusion fluid δD values corroborate the evolved meteoric fluid model as they are intermediate between those of inclusion fluids from Cassiar to the north and Coquihalla to the south. This pattern is expected on the basis of latidudinal variations in δD of meteoric waters, *i.e.* more depleted values in more northerly latitudes.

Based on the data in the present study an unequivocal determination of fluid provenance is not possible. However, the analyses of sericite separates are considered to be somewhat suspect. The separates were not pure, and though texturally appear to be associated with the ore-forming hydrothermal event, their origin remains in doubt.

6.3.3 District-Wide Isotopic Patterns

Oxygen

Maheux *et al.* (1987) noted that the camp scale pattern in ^{18}O suggested a model of mineral deposition from an ^{18}O-enriched fluid under the influence of a decreasing geothermal gradient. Their work supported the temperature dependent district-wide mineral zoning pattern recognized by Woodsworth *et al.* (1977) who suggested high temperature Au-As-W, through intermediate temperature Sb-Ag-Au-As±Hg, to low temperature Hg vein assemblages were generated in the thermal aureole of the Coast Plutonic Complex. Recently Leitch *et al.* (1988) also concluded that all mineralization in the camp is related to a coherent event based on the clustering of lead isotope data from 17 diverse deposits. They proposed that a single, protracted, but episodic mineralizing event coincided with the emplacement of the Coast Plutonic Complex during Late Cretaceous to Early Tertiary time.

If a single, isotopically evolved fluid was the source reservoir the resulting isotopic pattern over the district would reveal progressively increasing fractionations recorded in gangue minerals precipitated at progressively decreasing temperatures. Cursory fluid

inclusion microthermometry data (L. Walton, unpublished data) from quartz and carbonate gangue associated with Bralorne-Pioneer lode gold mineralization (avg. $T_h = 285° \pm 35°C$) and from calcite associated with mercury mineralization in deposits to the northeast (avg. $T_h = 200° \pm 20°C$) do not completely fit the model. The Bralorne-Pioneer formation temperatures should be approximately 30°C higher and mercury deposit temperatures up to 40°C lower to account for the $\delta^{18}O_{mineral}$ values yielded in the present study if deposition was from a single hydrothermal fluid with a unique isotopic composition equal to that calculated for the Sb-Au-Ag deposits (Figure 6-8).

Recent pressure determinations at Bralorne-Pioneer (Leitch and Godwin, 1988) applied to the Bralorne thermometry data give a corrected deposition temperature of ca. 355°, which closely fits the model. In Figure 6-8 temperature data plotted for the mercury deposits are uncorrected for pressure.

Carbon

Carbon isotope data obtained from carbonate gangue in the lode gold deposits in the southwest and in the mercury deposits in the northeast of the district reveal a district-wide pattern as well. The $\delta^{13}C$ values of carbonates in the lode gold deposits average -8.8 $\pm0.6‰$, those of the antimony-associated deposits average -7.4 $\pm1.9‰$, and mercury deposits in the northeast have $\delta^{13}C$ values averaging -5.5 $\pm1.8‰$ (Figure 6-9). The total range of $\delta^{13}C$ in the district is from -13.3 to -2.3‰.

Deposition over a temperature range of ~155°C (gold deposit $T_f = 355° \pm35°C$ to mercury deposit $T_f = 200° \pm20°C$) comes close to accounting for the range in average $\delta^{13}C$ values recorded in the carbonate phases. Using the respective temperatures of formation to calculate the carbon isotopic value of $CO_2(g)$ in the hydrothermal fluid in each deposit type yields average values of approximately -6.4‰, -5.2‰, and -5.1‰ for the lode gold, antimony-associated gold and the mercury deposits respectively (Figure 6-8). Other
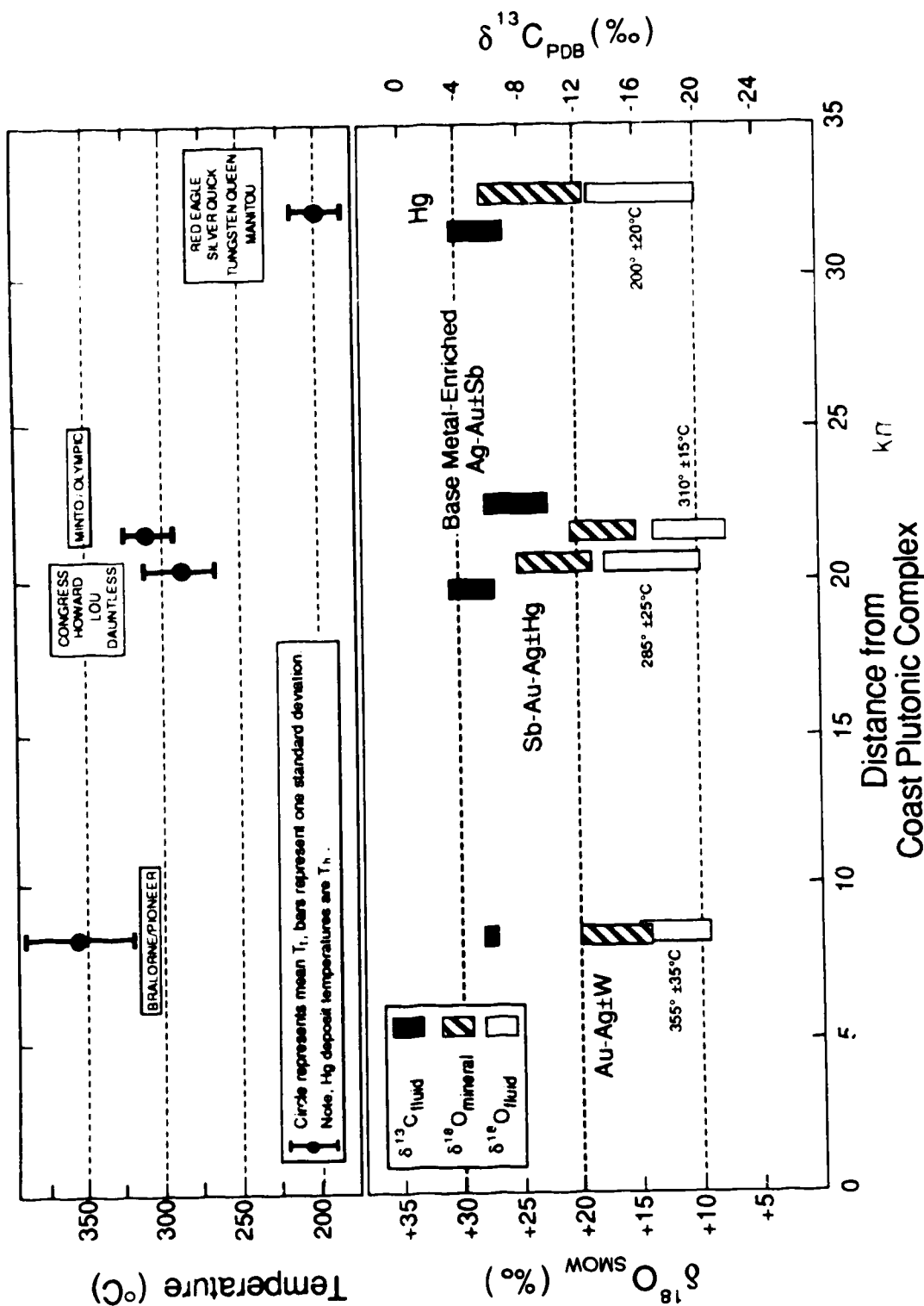
Figure 6-8. Schematic representation of Bridge River District regional carbon and oxygen stable isotope trends among ore deposit gangue minerals and calculated hydrothermal fluids. Isotope data are compared to fluid inclusion microthermometry data corrected for pressure and the distance from the eastern margin of the Coast Plutonic Complex.
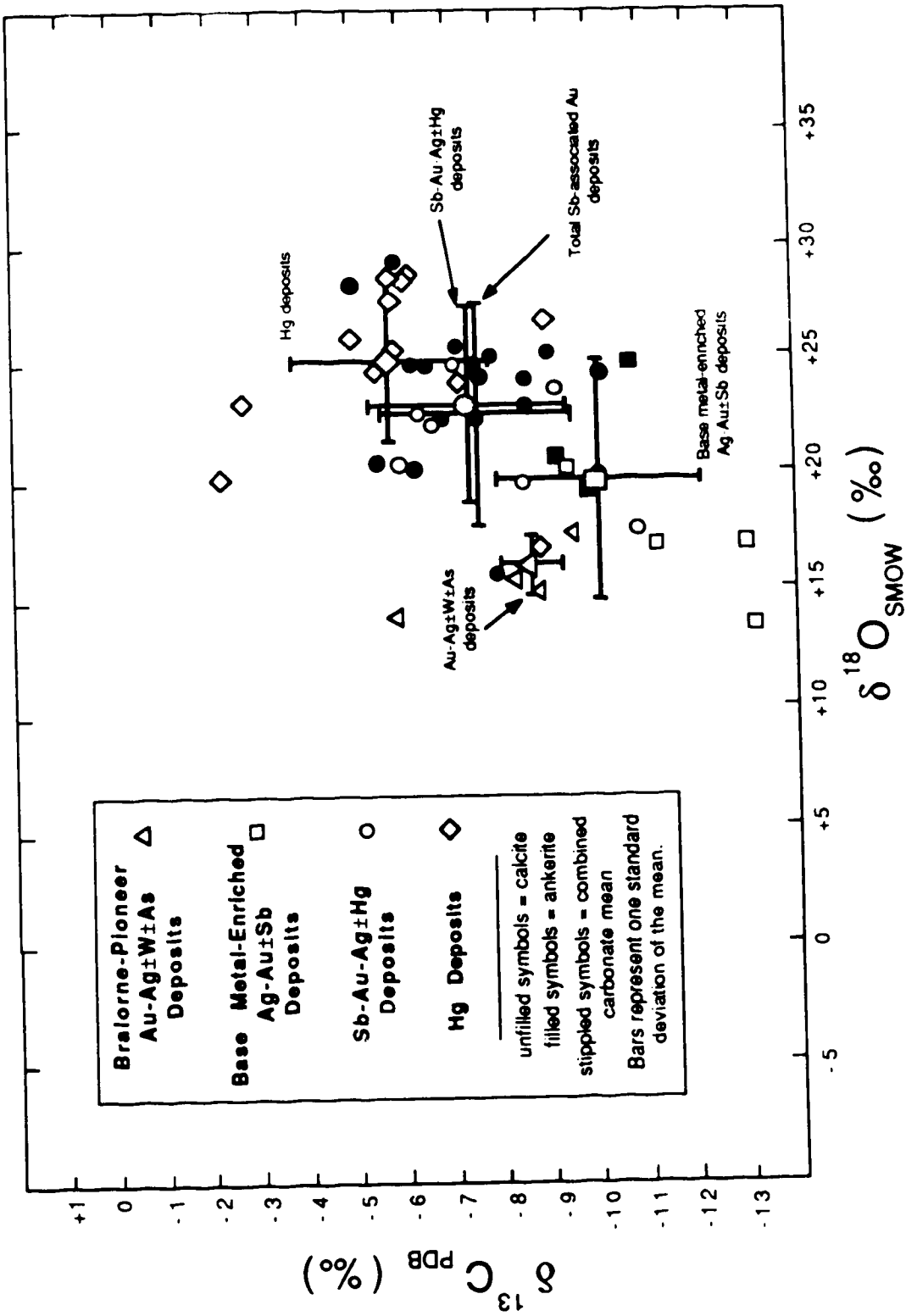
Figure 6-9. Carbon and oxygen isotope compositions of hydrothermal ankerites and calcites from selected deposits in the Bridge River Mining Camp.

mechanisms, such as local changes in the redox state to lower Eh to accomodate positive

shifts in $\delta^{13}C$ values (e.g. mercury deposits); oxidation of carbon sources depleted in the

heavy isotope to account for negativ shifts (e.g. Congress); or variations in pH causing

changes in $\delta^{13}C$ values in alkaline regions where pH-dependent carbon-bearing species are

stable, may be required to account for the inconsistentcies in the district-wide pattern

(Ohmoto, 1972; Kerrich, 1987).

6.3.4 Isotope Characteristics of Bridge River District Serpentinites

In Figure 6-10 the oxygen isotope analyses of serpentine and magnetite from the

serpentinite specimens collected in the present study are plotted for comparison with the

serpentinite data of Wenner and Taylor (1971). The Bridge River antigorites are closest in

oxygen isotopic character to Wenner and Taylor's continental antigorites, however the

$\delta^{18}O$ of the Bridge River serpentines and magnetites are significantly more enriched in the

heavy isotope compared to any of the Wenner and Taylor (1971) analyses and indicate the

influence of the unique ^{18}O-enriched hydrothermal fluids. The analyses of serpentine and

magnetite in BR-22 (Tungsten Queen) are conspicuous by an even greater ^{18}O-enrichment

(+21.4 and +12.0‰ respectively) and suggest the possible involvement of the low

temperature, ^{18}O-enriched hydrothermal fluids responsible for Hg deposition in the

serpentinization process.

In their study Wenner and Taylor (1971) included the category of "anomalous"

lizardite-chrysotile type serpentines (Figure 6-10). This designation was applied to

serpentines that lack consistent $\Delta_{serp-mag}$ values and are characterized by a wide range of

serpentine and magnetite $\delta^{18}O$ values, indicating lack of chemical equilibrium between the

serpentine and magnetite. Furthermore, the chemical heterogeneity and impurity of the

magnetites suggested that chemical, and perhaps isotopic equilibrium was not achieved

between the serpentine and the magnetite (Wenner and Taylor, 1971). In the present study

132

.10   -5   0   +5   +10   +15   +20

"NORMAL" LIZARDITE-CHRYSOTILE TYPE — CONTINENTAL: TIBURON 1 (14.1), TIBURON 2 (13.8), DOM. REPUBLIC 1 (13.7), GUATEMALA 1 (12.9), SAN LUIS OBISPO 8c (15.1); OCEANIC: MID ATLANTIC 70 (43°N) (10.0), MID ATLANTIC 118 (1°N) (12.5)

ANTIGORITE TYPE — CONTINENTAL: VT TALC 1 (4.8), CARLTON QUARRY 3 (8.7), BELVIDERE MT. 9 (8.6), BELVIDERE MT. 5 (6.0), BELVIDERE MT. 8 (6.4), CEDAR HILL 8 (8.6), CEDAR HILL 5 (7.1), SKAGIT 9 (7.0), DEL PUERTO (8.6); OCEANIC: MID ATLANTIC 54 (43°N) (8.2)

"ANOMALOUS" LIZARDITE CHRYSOTILE — JOSEPHINE 1 (10.5), MT. STEWART 1 (6.4), FT. ST. JAMES 1 (6.8), NAHLIN 1 (4.9), CASSIAR 1 (7.4)

BRIDGE RIVER DISTRICT SERPENTINITES — Au-Ag:W: BR-59 (Bralorne) (8.0), ARIZ 04 (Arizona) (6.2), VER 03 (Veritas) (6.5), OLY 09 (Olympic); Pb: BR-01 (Red Eagle) (6.0), BR-22 (Tungsten Queen) (9.4)

● MAGNETITE
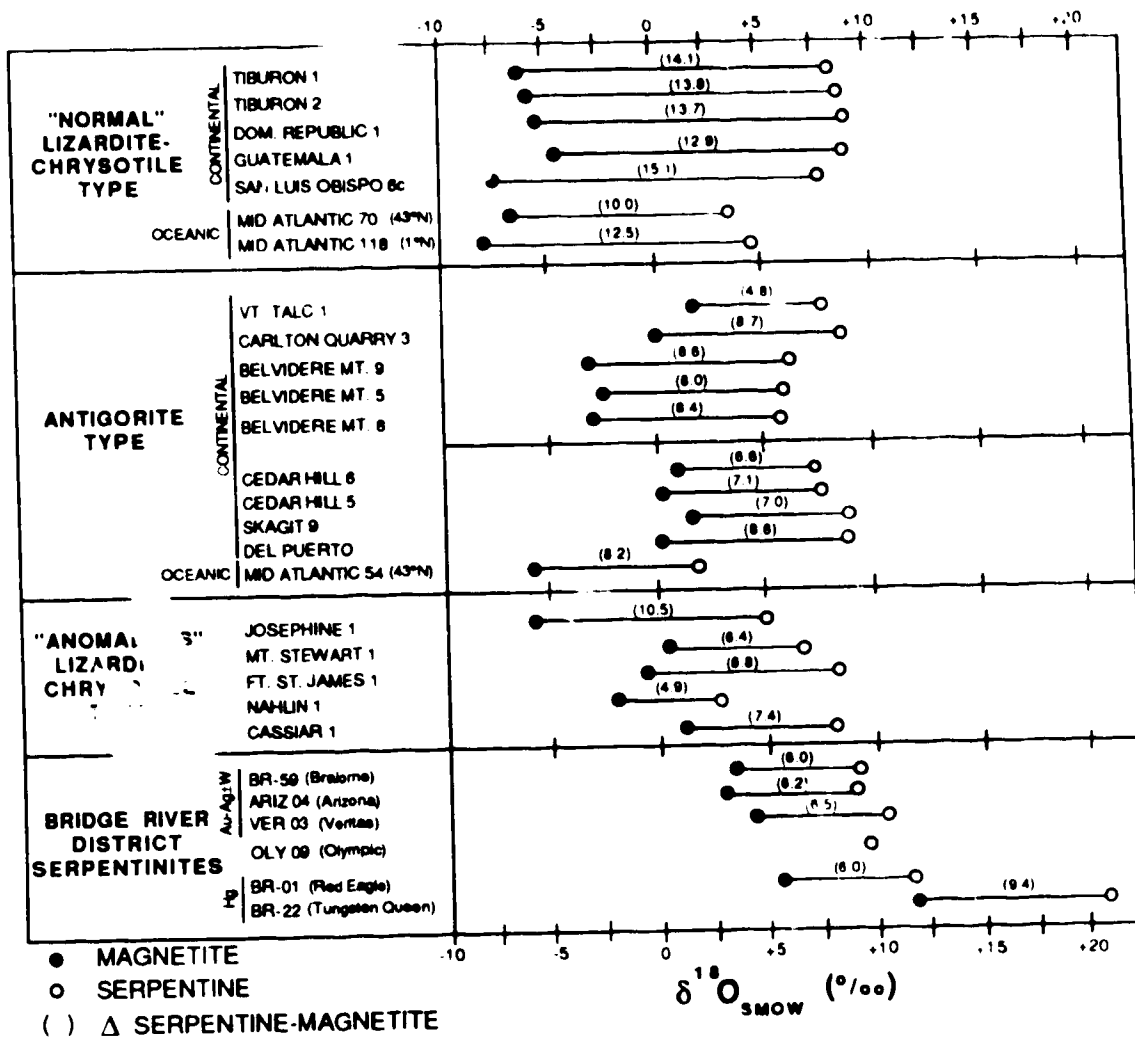○ SERPENTINE
( ) Δ SERPENTINE-MAGNETITE

$\delta^{18}O_{SMOW}$ (°/oo)

Figure 6-10. Plot of measured $\delta^{18}O$ values of serpentine and magnetite from serpentinites in the Bridge River District compared to different types of serpentinites from a wide variety of localities (Wenner and Taylor, 1971). See text for discussion. Diagram after Wenner and Taylor (1971).

the consistency in serpentine and magnetite $\delta^{18}O$ values and $\Delta_{serp-mag}$ values suggest an approach to equilibrium.

The Bridge River antigorites, with the exception of BR-22 (Tungsten Queen), exhibit relatively uniform $\Delta_{serp-mag}$ values ranging from 6.0 to 6.5‰ (Figure 6-10). These values correspond to temperatures of serpentinization of from 320° to 355°C, using the serpentine-magnetite geothermometer proposed by Wenner and Taylor (1971). Figure 6-11 illustrates the geothermometer. The data from serpen   te   the met___genetic zones in the Bridge River District are well grouped and fall within Wenner and Taylor's (1971) continental antigorite data set. An exception is the BR 22 specimen that has a $\Delta_{serp-mag}$ value of 9.4‰, corresponding to a lower temperature of 200°C. This serpentine contained only ca. 30% antigorite but a large fraction of possibly lizardite-chrysotile was recorded in that sample and may account for the somewhat lower temperature of serpentinization (Wenner and Taylor, 1971).

Estimates of the isotopic composition of waters responsible for serpentinization of the Bridge River antigorite samples were made using the equilibrium fractionation curve for serpentine-water proposed by Wenner and Taylor (1973) (see Appendix), and the estimates of temperatures of serpentinization based on measured $^{18}O/^{16}O$ fractionations between coexisting serpentine and magnetite. Ratios of w/r = ∞ are assumed. The values range in $\delta^{18}O$ from ca. +9.0 to +20‰ and in δD from about -45 to -155‰ (Table 6-1) (Figure 6-7; 6-12). Wenner and Taylor's (1969, 1973) data are plotted for comparison to the Bridge River serpentines. Their data from British Columbia serpentines (mostly lizardite-chrysotile) are highlighted. The Bridge River values are significantly more enriched in ^{18}O and in at least one case (BR-22) seem to indicate that low temperature serpentinization involving meteoric water took place. Werner and Taylor (1969) discovered isotopic evidence for low temperature serpentinization ($\delta^{18}O$ of +11.3 to +12.1‰) only for several "deweylite" samples from Pennsylvania and Delaware.
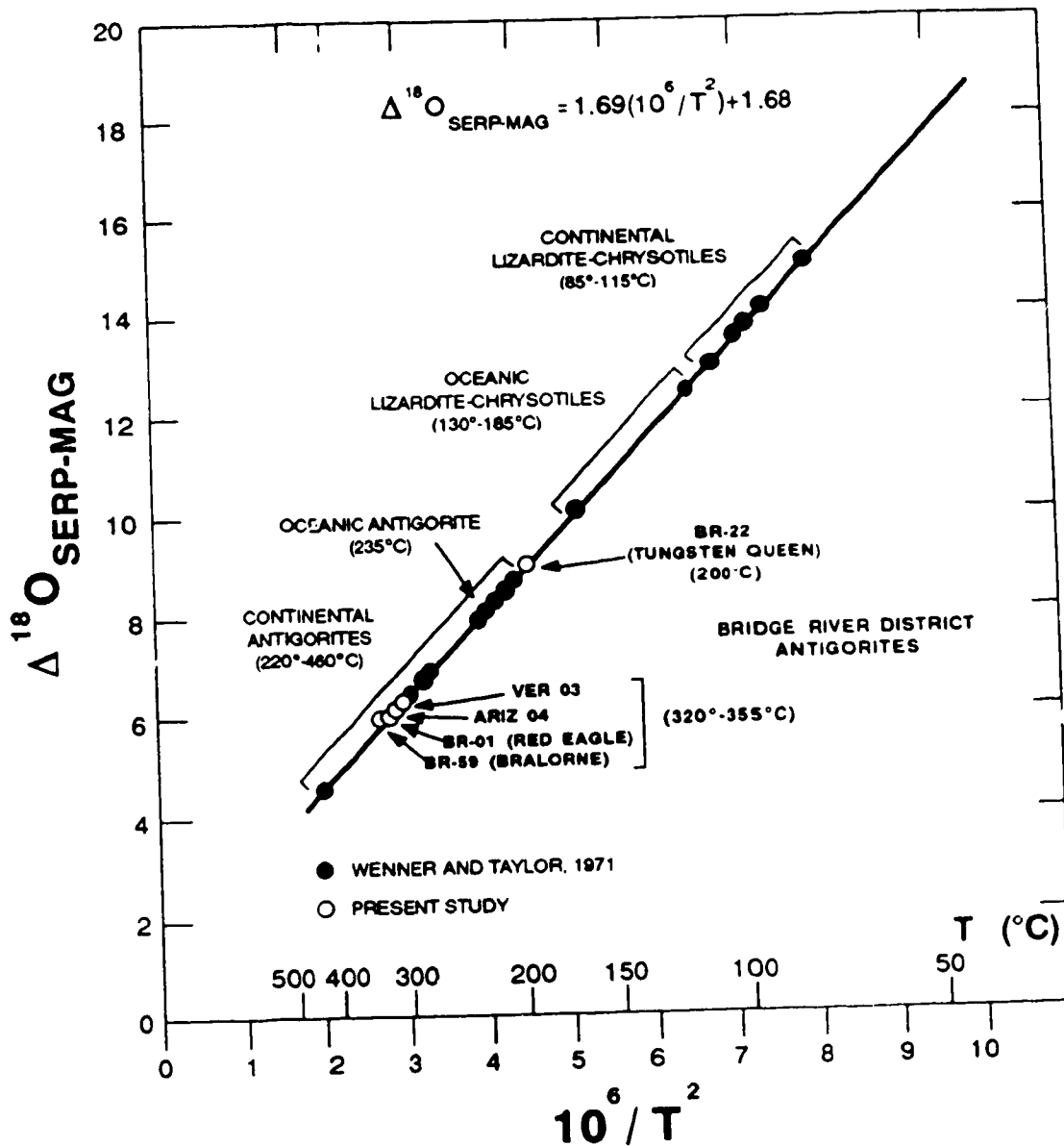
Figure 6-11. Oxygen isotope "temperatures" for serpentine-magnetite mineral pairs analyzed in the present study compared to those analyzed by Wenner and Taylor (1971). The serpentine-magnetite geothermometer is assumed to be identical to the chlorite-magnetite geothermometer (Wenner and Taylor, 1971). The data correspond to serpentine-magnetite pairs in Figure 6-10. The anomalous lizardite-chrysotile types have been omitted. Diagram after Wenner and Taylor (1971).
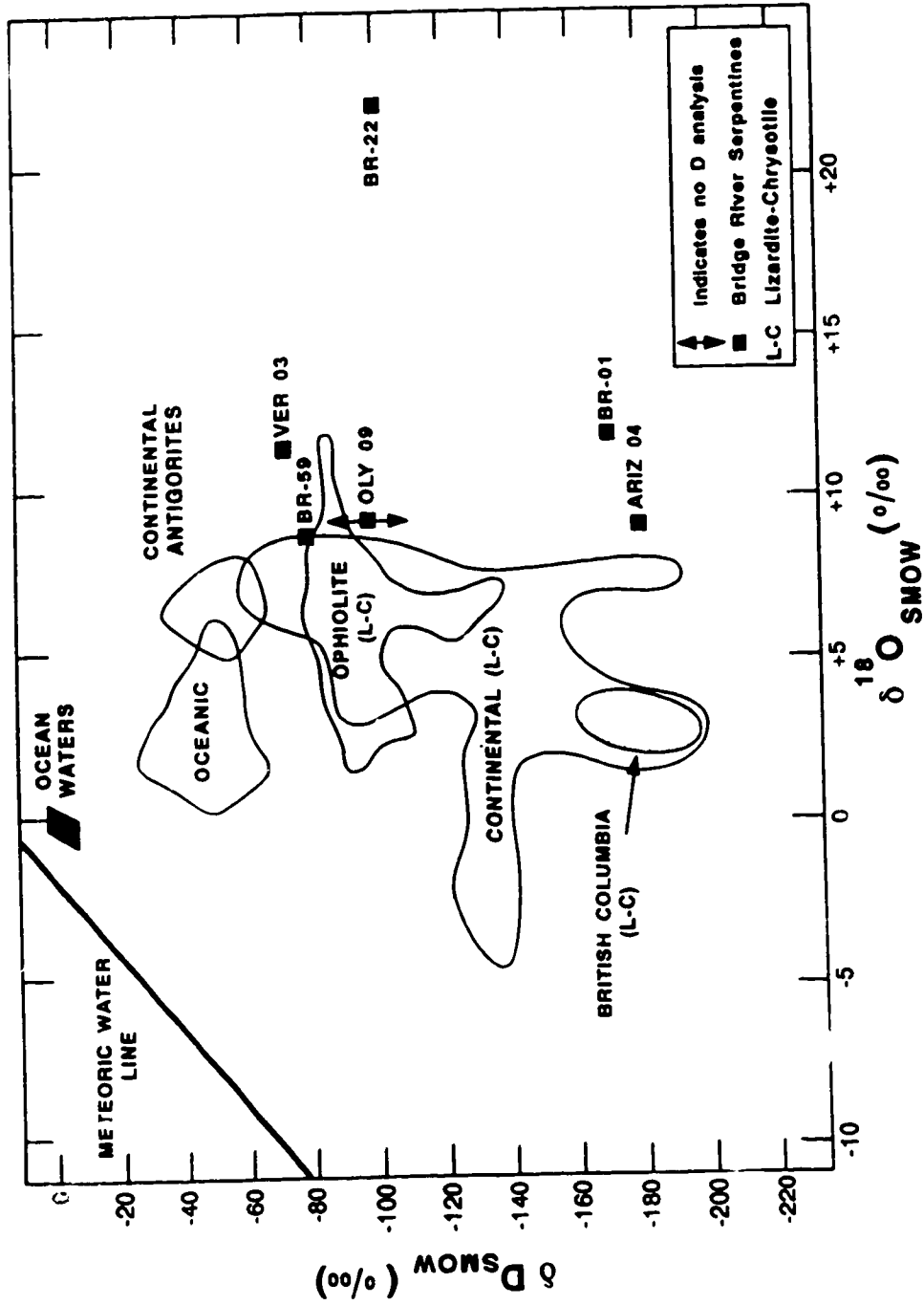
Figure 6-12. Plot of δD vs. δ^{18}O comparing Bridge River serpentines included in the present study with all serpentines examined by Wenner and Taylor (1969, 1973). The position of the meteoric water line and standard mean ocean water are shown for reference. Diagram after Wenner and Taylor (1973).

Based on wide variations in waters that produced the lizardite-chrysotile serpentines of

continental ophiolite bodies Wenner and Taylor (1973) ruled out the possiblity that ocean waters

or "connate" waters were primarily responsible for the observed isotopic compositions of

serpentines from ophiolites (δD, -35 to -115‰; $\delta^{18}O$, -7 to +18‰). They further suggested

that antigorite serpentines associated with ophiolites probably form only in the presence of

metamorphic water. Wenner and Taylor (1971) made a similar conclusion with respect to the

serpentinization of other continental antigorites. Contrary to their conclusions, deep-seated

metamorphic waters are not necessarily responsible for the serpentinization of the Bridge River

specimens. The Bridge River specimens appear to record serpentinization by the same or similar

highly ^{18}O-evolved hydrothermal fluids responsible for the ore deposits in the district.

VII. SUMMARY AND CONCLUSIONS

7.0 Summary: Sb-Associated Au-Ag Mineralization

Two styles of precious metal mineralization that fall within an antimony dominated metallogenetic zone in the Bridge River District have been the focus of this study. Sb-Au-Ag±Hg and base-metal-enriched Ag-Au±Sb mineralization occur in veins and replacement bodies occupying shears within foliated greenstones, gabbro, argillite, chert and serpentinite of the Middle Triassic through Middle Jurassic Bridge River complex. The mineralization is commonly associated with feldspar porphyry dykes of intermediate composition. Each of the mineral occurrences and deposits has a complex structural framework though the dominant regional trend is north to northwest, most likely related to large scale transpressional structures, such as the Yalakom fault system. Local fracture domains are unique however, with variable fracture pattern orientations from dominantly southwesterly (Olympic) to northerly (Congress, Minto).

Mineralization at the Congress Mine , Howard vein deposit and the Lou prospect is characteristic of the Sb-Au-Ag±Hg occurrences. Vein development occurred during two to three stages typically and consists of quartz, ankerite (±calcite) and stibnite with lesser amounts of arsenopyrite and pyrite. The veins are discontinuously banded with comb, vuggy quartz and are commonly brecciated. Other ore minerals include sphalerite, tetrahedrite, marcasite, and cinnabar as irregular concentrations and late vein fillings that partly replace earlier vein material, carbonate altered wall rock, and adjacent dyke rock. Gold is characteristically late stage and associated with stibnite, arsenopyrite and rarely, late open space-filling cinnabar. Rare visible gold occurs in the upper levels of the Howard vein where it is associated with brecciated, locally vuggy, cockscomb quartz-ankerite veins. Typical gold/silver ratios range from 1.2 to 2.0.

The Minto Mine and the Olympic prospect typify the poly-metallic base metal-enriched Ag-Au±Sb mineralization in the area. Greater concentrations of copper, lead, and zinc, as well as lower gold/silver ratios (0.2 to 0.35), among other characteristics, serve to distinguish these ores from those of the Congress and similar deposits The veins contain coarsely crystalline arsenopyrite, pyrite, sphalerite, galena, jamesonite and chalcopyrite with lesser amounts of tetrahedrite and pyrrhotite. Typically three stages of mineralization resulted in banding defined by alternating ore mineral concentrations and quartz-ankerite (±calcite) gangue. Gold deposition occurred during the late main to late stage of mineralization and is most commonly associated with galena, arsenopyrite and jamesonite (Minto). In rare instances gold is closely linked to chalcopyrite deposition in Olympic mineralization.

Wall rock alteration is characterized by rare to abundant ankerite and calcite with lesser amounts of sericite, chlorite and fuchsite.

Hydrothermal fluids responsible for both styles of mineralization were dilute brines ($ca.$ 3 to 4 eq. wt. % NaCl) with low CO_2 contents, possibly up to 5 mole % on average. Locally more CO_2-rich ($XCO_2 \cong 0.95$) fluids were sampled by gangue minerals in base metal-enriched mineralization.

Analyses of gangue minerals from both styles of mineralization are highly enriched in ^{18}O ($ca.$ 20 to 24‰ SMOW, combined quartz and carbonate values) and indicate no significant component of fresh meteoric water to the hydrothermal systems. Isotopic analyses of hydrogen in fluid inclusions liberated from quartz gangue from Sb-Au-Ag±Hg mineralization are depleted in D (avg. -130‰ SMOW) and suggest the ore fluid was derived from meteoric water that subsequently underwent extreme enrichment in ^{18}O. In contrast, deuterium analyses of sericite separates from alteration assemblages suggest metamorphic fluids were responsible for the alteration of wall rock and possibly the deposition of mineralization. The δD values, which range from approximately -30 to -40‰ (SMOW), may in fact record the latest pre-mineralization metamorphic event (Magaritz and

Taylor, 1986). Though textural evidence suggests the sericites are associated with mineralization, their origin was not unequivocally determined.

Analyses of $\delta^{13}C$ in carbonates from the deposits range from -12.5 to -5‰ (PDB). Though the values closely approach "magmatic" values, it is more likely they reflect a more heterogeneous carbon source.

Some contrast in the conditions of formation of the different styles of mineralization is indicated by slight differences in the conditions of trapping of the respective ore fluids. Data from fluid inclusion analyses indicate Sb-Au-Ag±Hg mineralization formed at 285° ±25°C on average and at pressures ranging from 200 to 350 bars (20 to 35 MPa). On the other hand, base metal-enriched Ag-Au±Sb mineralization apparently formed at slightly higher temperatures, 310° ±15°C on average, and higher pressures, 300 to 500 bars (30 to 50 MPa).

The data agree with a model that would place Sb-Au mineralization within a metallogenetic zoning pattern that is well defined by pressure, temperature, and stable isotope and elemental distribution patterns.

7.1 Bridge River Sb-Au Mineralization and the District Ore Deposit Model

The model proposed for camp-scale Au-Sb-Hg systems by Nesbitt and Muehlenbachs (1988) requires convection of meteoric water in the crust to depths of up to 15 kilometres and temperatures of 300° to 400°C. As the fluid moves through the crust it evolves in $\delta^{18}O$ and would become charged with metals for later deposition. The hydrothermal fluids ascend in permeable zones associated with large scale strike-slip faults, depositing quartz, carbonate, sulp   ·< ind Au-Ag at depths of 10 to 8 km and temperatures of ca. 300° to 350°C. Quartz-ι   e lodes with concentrations of Sb±Au, Ag and sulphides would form higher in the   n, possibly at depths of from 2 to 5 km and temperatures of 250° to 300°C. Near the surface Hg and carbonate are deposited at temperatures of ca. 100°C.

Aspects of the model are well illustrated by the formation of the Bridge River Sb-associated Au deposits in the context of a district-wide metal zoning pattern. Data from the present study has illustrated the close link between Sb-Au deposits with the mesothermal Au deposits in the Bridge River district mining camp. Indeed, the Congress *et al.* deposits are more accurately described as mesothermal than epithermal and are more closely related to the Au lodes in the camp than to epithermal mineralization. The most convincing link is the evidence of highly ^{18}O-enriched ore fluids being responsible for the deposition of both ore types. There is no evidence to suggest the development of the deposits in an epizonal, intrusive/subvolcanic environment. Data from fluid inclusions and stable isotope thermometry further corroborate the zonation of metal deposits from higher temperature (300°-350°C) Au lodes to the cooler, more shallowly emplaced Sb-Au deposits at 260°-325°C. Calculated oxygen isotope compositions of the ore fluids throughout the district are in close agreement and further support a common genetic link.

Nesbitt *et al.* (in press) suggest that given the similarity of δD and $\delta^{18}O$ of ore fluids for Sb and Hg deposits to mesothermal lode-Au deposits in a camp such as the Bridge River district, it is likely that all three types of mineralization were deposited from similar fluids. The present study includes isotopic analyses that support the hypothesis. The sequence of decreasing temperature for Au, Sb±Au and Hg deposition with an attendant increase in $\delta^{18}O$ of gangue minerals probably corresponds to decreasing depths of formation from the southwest to the northeast in the Bridge River district.

By way of illustrating the model as it applies to the district, the data from the present study have been incorporated in Figure 7-1. The diagram summarizes the zonation of geochemical parameters in the Au-Sb-Hg system in Cordilleran mesothermal systems (Nesbitt *et al.*, in press). In an ideal system the $\delta^{18}O$ values of the ore fluids would range from *ca.* +5 to +8‰ (Nesbitt *et al.*; in press). In Figure 7-1 the ore fluid isotopic values are higher, up to +20‰, due a larger range in formation temperatures used to calculate the fluid isotopic values. In Figure 7-1 the indicated ranges of depths for Bridge River Sb-associated
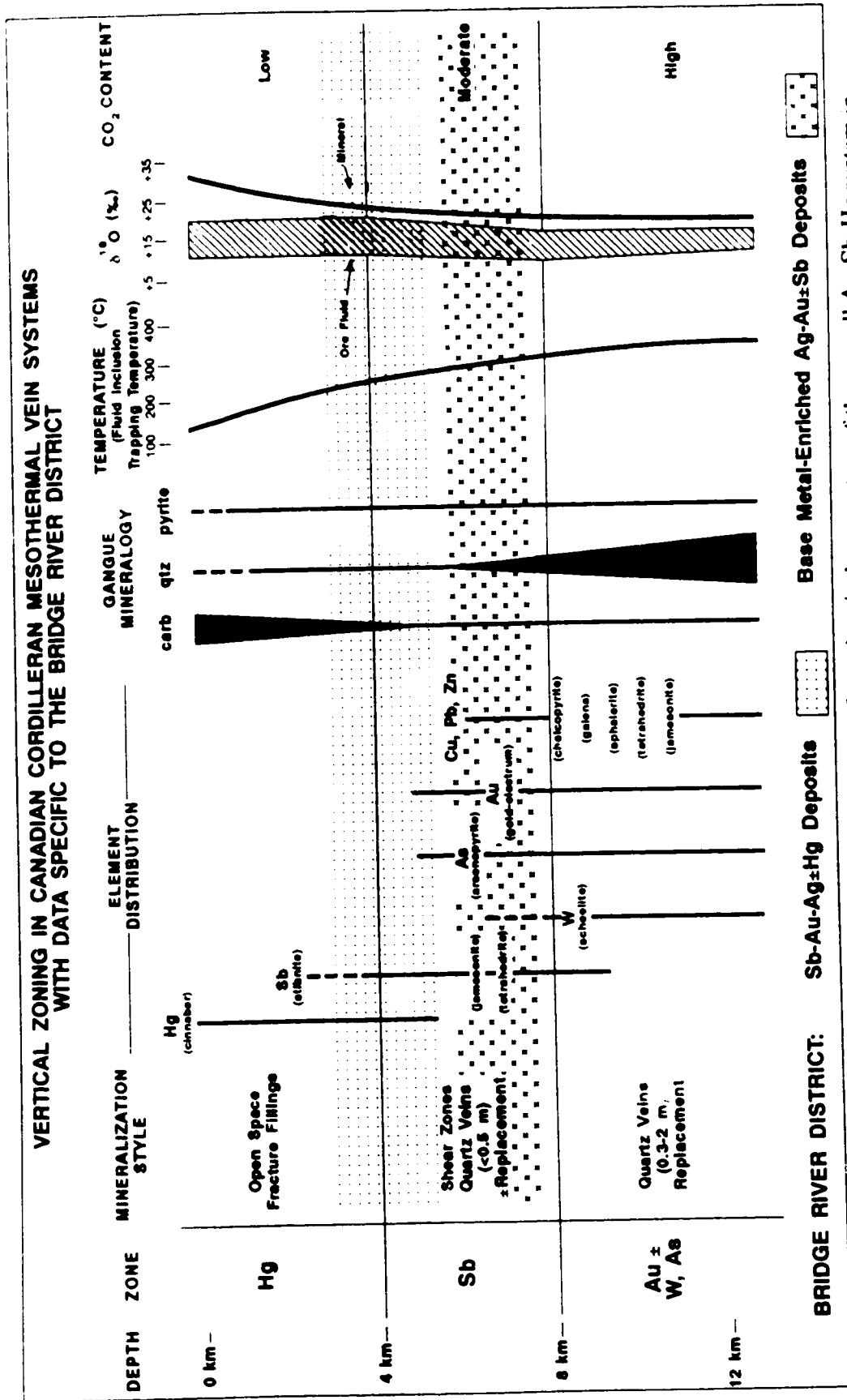
Figure 7-1. Summary diagram illustrating the vertical zonation of geochemical parameters of the overall Au-Sb-Hg system in Cordilleran mesothermal vein systems. The figure incorporates data for the Bridge River district mining camp from the present study. Diagram modified from Nesbitt *et al.* (in press).

Au mineralization that encompass data from the present study are intended as schematic

representations only.

7.2 Bridge River Sb-Au Mineralization Compared to Other Sb-Au Deposits

Though not historically documented as a major source of gold, many lode Sb deposits

throughout the world contain significant economic concentrations of Au. These deposits

bear many similarities to the Bridge River district Sb-associated Au-Ag deposits, which are

good examples of antimony deposits rediscovered for their gold potential. On the other

hand there are examples of Sb-Au vein deposits that have been exploited for their precious

metal content from the outset; these as well are reminiscent of Bridge River mineralization.

Canadian Cordillera

Among the most strikingly similar occurrences to Congress-style mineralization is the

Snowbird Sb-Au deposit in the Stuart Lake region of central British Columbia. The region

is underlain by northwesterly trending and steeply dipping interbedded greenstones and

sedimentary rocks of the Carboniferous to Upper Triassic Cache Creek Group.

Mineralization is closely associated with variably carbonatized and silicified

serpentinite, or listwaenites, in a zone of faulting, shearing and brecciation (Armstrong,

1949). The quartz veins and stringers are mineralized with stibnite, pyrite and gold with

grades of 8 to 10 g/t and up to 10 to 30% antimony over widths of up to 1 metre. Oxygen

isotope analyses of quartz and carbonate reveal ^{18}O-enriched values (+20 to +25‰; Madu,

1988) similar to Bridge River gangue analyses. Furthermore, δD analyses of inclusion

fluids liberated from quartz identify the Snowbird fluids as being originally meteoric in

nature (*ca.* -140‰; Madu, 1988); again similar to the data from the Bridge River Sb-Au mineralization.

Little information is available in the literature regarding other Sb-associated precious metal mineralization throughout the world. Particularly lacking are modern geochemical data that would provide a strong basis for comparison with Bridge River Sb-Au mineralization. However, comparisons can be drawn between Bridge River mineralization and Sb-associated Au deposits in China, Bolivia, Australia and New Zealand.

People's Republic of China

The world's principal resources and reserves of antimony lie in the southern and southwestern parts of the People's Republic of China, particularly in Hunan province (Guilbert and Park, 1986; p 553). The deposits are stibnite-cinnabar lodes and stockworks occupying shear zones in siliceous sedimentary rocks. Gold has not been documented as being found in the ores (Juan, 1946), however not far to the northwest of these deposits are stibnite deposits with associated scheelite and gold-bearing quartz. These are the Wuxi W-Sb-Au mines. The deposits are veins in a folded sequence of sedimentary rocks. The quartz veins are sharply defined along the footwall where gold and stibnite are concentrated. The principal veins are persistent in both strike and dip and in places are as much as 2 metres wide with up to 30% antimony locally. At depth the shoots contract sharply, and stibnite concentrations give way to pyrite. This zonation is suggestive of that in the Congress deposit where Sb decreases at depth while pyrite and arsenopyrite increase in concentration. Little information is available on the morphology of the gold in the deposits but the occurrence of stibnite differs little from Bridge River mineralization and is in veins, irregular veinlets, or lenticular bodies. Open-space filling textures dominate and the deposits have been termed epithermal (Guilbert and Park, 1986; p. 536), though physio-chemical data on these deposits has not been published.

Bolivia

Prominent Sb-Au prospects have been identified in the southern hemisphere as well. In the central and southern part of the Eastern Andean Cordillera of Bolivia more than 500 antimonite deposits are known forming an antimoniferous metallogenetic belt. In many of the deposits gold is a byproduct.

The Eastern Andean Cordillera is formed mainly by lower Paleozoic sedimentary rocks intruded by intermediate to acid batholiths and sub-volcanic rocks of the Permian, Triassic and Tertiary. The Sb-Au deposits are all situated within an Ordivician-Silurian sedimentary sequence of sandstone, siltstone and black shales (Lehrberger, 1988).

A compressive tectonic regime acting during the late Paleozoic resulted in large anticline-syncline structures in the sedimentary basin of the Eastern Cordillera. Faulting of the folded structures was related to compression and the resultant breaks are common loci for the Sb-Au lodes.

The chemical composition of the deposits conforms to the familar pattern dominated by Sb. As. Fe and Au ±Ag, Zn, Pb, Cu. Quartz-carbonate lodes contain antimonite, pyrite, arsenopyrite, jamesonite, sphalerite, chalcopyrite, galena, ±complex sulphosalts. Native gold is always associated with late stibnite (*cf*. Howard), jamesonite (*cf*. Minto), pyrite (*cf*. Congress and Minto), or sphalerite in fractures of quartz or carbonate. Gold typically occurs as complex intergrowths with stibnite or as fracture-fillings in quartz, stibnite and the other sulphides. Anther common occurrence of the precious metal is as minute inclusions in pyrite. Gold-stibnite intergrowths are the most common (*cf*. Figures 4-7 to 4-9 in the present study).

Preliminary fluid inclusion studies have revealed fluids similar to those in the Bridge River Sb-Au deposits. Two types of inclusions dominate; brine-rich inclusions ($T_h = 130°$ to 200°C) and mixed CO_2-H_2O inclusions ($T_h \cong 275°C$).

Australia

The Brunswick Au-Sb Mine in Victoria, Australia, is set in a north-trending shear zone in Lower Silurian siltstones and minor sandstones that have been gently folded Mineralization is thought to be associated wit' magmatic activity during the Upper Paleozoic (O'Shea and Pertzel, 1988). Mineralization consists of pyrite-arsenopyrite-stibnite-gold veining and disseminations within a steep shear zone up to 3 metres thick. Two stages of gold mineralization are present. Early gold is associated with quartz while late, very fine-grained gold is located within stibnite near grain boundaries. Similar to the Congress deposit, individual stibnite crystals exhibit bending and kinking suggesting local dislocations penecontemporaneous with mineralization (cf. Figure 4-4). However, deposition temperatures of 200°C, considerably lower than those for the Bridge River Sb-Au deposits are suggested by current workers (O'Shea and Pertzel, 1988).

New Zealand

In Otago and Marlborough, New Zealand numerous Au-Sb-W quartz lodes occur in the chlorite zone of the Haast Schist, spatially associated with major structural breaks (e.g. Guards Bay Shear: Endeavor Inlet Sb-Au deposit). The Haas Schist is a complexly deformed belt of regionally metamorphosed greywacke with minor mafic volcanic rocks and chert. The Haast Schist belt is interpreted as a composite terrane formed by the Jurassic to early Cretaceous tectonic amalgamation of the Permian-Triassic Caples and Torlesse terranes (Braithwaite, 1988).

The Otago region has long been recognized as an important gold producing province (>2.5 x 10⁵ kg placer, > 9 x 10³ kg lode) (Henley et al., 1976). Hydrothermal lodes are widespread throughout the Haast Schist and the most significant are the gold-quartz and scheelite-quartz lodes of Central Otago. Sporadic stibnite lodes occur in the vicinity of these

deposits. Accessory minerals in all the lodes include stibnite, cinnabar, galena and

sphalerite. Some of the steeply dipping stibnite-bearing lodes appear to have been deposited

at shallower levels (<500 m) than the Au-W lodes as indicated from fluid inclusion studies

(Craw, 1987). Furthermore, there is some suggestion of a metallogenetic zonation as the

base metals become more common to the east of the Central Otago lodes (Henley et al.,

1976).

Paterson (1982) proposed, on the basis of stable isotope distributions in the

Glenorchy scheelite field, that a metamorphic model for the genesis of the Otago Au-Sb-W

lodes, involving derivation of the metals and fluids as a result of metamorphic processes,

was the most reasonable.

The Sb-Au lode at Endeavor Inlet in Marlborough (Pirajno, 1979) was historically an

antimony producer with grades of up to 34% Sb. Recently the deposit has been exploited

for its Au values. Massive stibnite mineralization occurs as sporadic lenticular bodies

within the NW-striking quartz vein. They measure from a few metres to 80 metres in length

and up to 0.6 m wide.

The banded structure of the mineralized veins indicate that at least two stages of quartz

emplacement were separated by sulphide deposition. The three principal ore minerals are

arsenopyrite, pyrite and stibnite. Trace amounts of gold, marcasite and tetrahedrite

accompany the main minerals (cf. ore mineral parageneses of Congress, Lou, Howard;

Figure 4-1). A mineralogical zonation is defined by massive stibnite in the upper levels

passing to discontinuous stibnite veinlets ±arsenopyrite. Stibnite is clearly later than

arsenopyrite (Pirajno, 1979).

The geochemical association of Au with arsenopyrite-pyrite implies that the element

occurs as inclusions in the sulphides in a manner similar to the Congress deposit. Grades

are as high as 7 g/t, particularly in the middle-lower levels of the deposit (Pirajno, 1979).

Pirajno (1979) interpreted the vertical zoning pattern at the Endeavor Inlet deposit to

be the result of variations in the physio-chemical parameters of the ascending ore fluids.

With changing temperature and pressure arsenopyrite and pyrite-marcasite predominate at depths of 250-400 m, gold and tetrahedrite are more common between 300-400 m and scheelite is found in the restricted interval of 200-280 m. Stibnite (±gold) is mainly developed at depths of from 150 m to the surface.

Pirajno (1979) concluded that the mineralization at Endeavor Inlet appeared to have formed within an "epi-mesothermal" hydrothermal stibnite-arsenopyrite-pyrite-gold-quartz vein system, restricted to a zone of shearing in the schist rocks, associated with the Guards Bay shear zone. No isotopic studies were carried out though Pirajno (1979) speculated that the source of the metals and the sulphur (and presumably the hydrothermal fluids themselves) may be related to the metamorphic event that produced the Marlborough Schist. This conclusion is not unlike that drawn by Henley et al. (1976) for the Au-W-Sb lodes in the Haast Schist at Otago.

Comparing the characteristics of these deposits with those of the Bridge River Sb-Au deposits, it would not be improbable to suggest a similar origin for the New Zealand deposits. That is, the convective rise of hydrothermal fluids derived from "connate" waters through the sedimentary pile postulated by the New Zealand workers for the origin of the deposits may in fact involve the convective rise of highly exchanged meteoric-derived waters along major crustal breaks in a fashion similar to the Canadian Cordilleran Au-Sb-Hg lodes. A thorough stable isotope study of the New Zealand lodes would be timely and could potentially lead to the development of lode Au target areas in the vicinity of the Sb-Au lodes.

7.3 Summary Statement

A study of Bridge River District Sb-Au mineralization has served to illuminate most aspects of the role these types of deposits play in the larger context of mesothermal gold

depositing Cordilleran lode systems. The elementally, isotopically and physio-chemically zoned nature of these syst... well illustrated by the deposits in the Bridge River camp.

The model developed at the University of Alberta (Nesbitt and Muehlenbachs, 1988; Nesbitt et al., in press) for the genesis of Cordilleran Au-Sb-Hg lode systems cannot be applied as a rigid template to the observed geological and geochemical characteristics of the Sb-Au, as well as Au and Hg, deposits of the Bridge River district. However, many aspects of deposits, particularly the ore-fluid chemistry, indicate a clear genetic link between mineralization types and suggest that the model calling for convecting, evolved meteoric waters ultimately depositing metals in a well recognized camp-scale pattern in mesothermal-hydrothermal systems is the most applicable.

The value in understanding the origin and morphology of these deposits lies not only in the immediate application to exploration for similar ores in Cordilleran tectono-stratigraphic environments, but also as a window on the genesis of the larger Precambrian anologues of these vein systems.

REFERENCES

Angus, S., Armstrong, B., de Reuck, K.M., Altunin, V.V., Gadetskii, O.G., Chapela, G.A., and Rowlinson, J.S., 1976, Internation thermodynamic tables of the fluid state, v. 3, carbon dioxide: Pergamon Press, Oxford, England, 385 p.

Armstrong, J.E., 1949, Fort St. James map-area, Cassiar and Coast Districts, British Columbia: Geol. Sur. Can., Memoir 252, p. 186-189.

Bacon, W.R., 1978, Lode gold deposits in Western Canada: Can. Inst. of Mining Metal. Bull., v. 71, no. 795, p. 96-104.

Barnes, H.L., 1979 Solubilities of ore minerals: in Barnes, H.L., ed., Geochemistry of Hydrothermal Ore Deposits, 2 ed., John Wiley and Sons, New York, p. 404-460.

Bateman, A.M., 1912, Exploration between Lillooet and Chilko Lake, British Columbia: Geol. Sur. Can., Summary Report for 1912, p. 177-210.

Becker, R.H., 1971, Carbon and oxygen isotope ratios in iron formation and associated rocks from the Hammersly Range of Western Australia and their implications: Univ. Chicago, unpublished Ph.D. thesis, 138 p.

Böhlke, J.K., and Kistler, R.W., 1986, Rb-Sr, K-Ar, and stable isotope evidence for the ages and sources of fluid components of gold-bearing quartz veins in the northern Sierra Nevada foothills metamorphic belt, California: Econ. Geol., v. 81, p. 296-322.

Bottinga, Y., 1968, Calculation of fractionation factors for carbon and oxygen isotope exchange in the system calcite-carbon dioxide-water: J. Phys. Chem., v. 72, p. 800-808.

Bottinga, Y. and Javoy, M., 1973, Comments on oxygen isotope geothermometry: Earth Planet. Sci. Lett., v. 20, p. 250-263.

Boyle, R.W., 1979, The geochemistry of gold and its deposits: Geol. Sur. Can., Bull. 280, 584 p.

Braithwaite, R.L., The tectonic setting and control of gold deposits in New Zealand: in Bicentennial Gold '88, Extended Abstracts Poster Programme, v. 2, Geol. Soc. Australia Abstracts Series, No. 23, compiled by A.D.T. Goode, E.L. Smyth, W.D. Birch and L.I. Bosma, p. 191-196.

Burrus, R.C., 1981, Analysis of phase equilibria in C-O-H-S fluid inclusions: in Hollister, L.S., and Crawford, M.L., eds., Fluid inclusions: applications to petrography, Min. Assoc. Can. Short Course Handbook 6, p. 39-74.

Cairnes, C.E., 1937, Geology and mineral deposits of the Bridge River mining camp, British Columbia: Geol. Sur. Can., Memoir 213, 140 p.

Cairnes, C.E., 1943, Geology and mineral deposits of Tyaughton Lake map area, British Columbia: Geol. Sur. Can., Paper 43-15, 39 p.

Camsell, C., 1911, Geology of a portion of Lillooet Mining Division, Yale District, British Columbia: Geol. Sur. Can., Summary Report for 1911, p. 111-115.

Church, B.N., 1987, Geology and mineralization of the Bridge River mining camp (92 J/15, 92 O/2, 92 J/10): in Geological Fieldwork, 1986, Paper 1987-1, B.C. Min. of Ener. Mines and Petrol. Res., p. 23-29.

Church, B.N., Gaba, R.G., Hanna, M.J. and James, D.A.R., 1988, Geological reconnaissance in the Bridge River mining camp (92J/15, 16, 10; 92O/02): in Geological Fieldwork, 1987, Paper 1988-1, B.C. Min. of Ener. Mines and Petrol. Res., p. 93-100.

Clayton, R.N. and Mayeda, T.K., 1963. The use of bromine pentafluoride in the extraction of oxygen from oxides and silicates for isotopic analyses: Geochim. Cosmochim. Acta, v. 27, p. 43-52.

Clayton, R.N., Muffler, L.J.P. and White, P.E., 1968, Oxygen isotope study of calcite and silicates of the River Ranch No. 1 well, Salton Sea geothermal field, California: Am. J. Sci., v. 266, p. 968-979.

Collins, P.L.F., 1979, Gas hydrates in CO_2-bearing fluid inclusions and the use of freezing data for estimation of salinity: Econ. Geol., v. 74, p. 1435-1444

Coleman, M.L., Shepherd, T.J., Durham, J.J., Rouse, J.E. and Moore, G.R., 1982, Reduction of water with zinc for hydrogen isotope analysis: Analytical Chem., v. 54, p. 993-995.

Colvine, A.C., Andrews, A.J., Cherry, M.E., Durocher, M.E., Fyon, A.J., Lavigne, M.J., Jr., MacDonald, A.J., Marmont, S., Poulsen, K.H., Springer, J.S., and Troop, D.G., 1984, An integrated model for the origin of Archean lode gold deposits: Ont. Geol. Sur., Open-File Report 5524, 98 p.

Compston, W. and Epstein, S., 1958, A method for the preparation of carbon dioxide from water vapor for oxygen isotope analysis: EOS, Amer. Geophys. Union Trans., v. 39, p. 511.

Coney, P.S., Jones, D.L., and Monger, J.W.H., 1980, Cordilleran suspect terranes: Nature, v. 288, p. 329-333.

Cooke, B.J., Sketchley, D.A. and Aelicks, B.T., 1986, Exploration report of diamond drilling, underground sampling and geological compilation on the Congress property near Goldbridge, British Columbia: Unpublished company report, Cooke Geological Consultants Ltd., 45 p.

Coplen, T.B., 19.3, Normalization of oxygen and hydrogen isotope data: Chem. Geol., v. 72, r, 293-297.

Coveney, R. M., Jr., 1981, Gold quartz veins and auriferous granite at the Oriental Mine, Alleghany District, California: Econ. Geol., v. 76, p. 2176-2199.

Craig, H., 1957, Isotopic standards for carbon and   en and correction factors for mass-spectrometric analysis of carbon dioxide   ochim. Cosmochim. Acta, v. 12, p. 133-149.

Craig, H., 1961a, Isotopic variations in meteoric waters: Science, v. 133, p. 1702-1703.

Craig, H., 1961b, Standard for reporting concentrations of deuterium and oxygen-18 in natural waters: Science, v. 133, p. 1833-1834.

Craw, D., 1987, Gold mineralization in East Otago: in Annual conference field trips, Geol. Soc. New Zealand, Misc. Pub. 37B, p. 87-101.

Crawford, M.L., 1981, Phase equilibria in aqueous fluid inclusions: in Hollister, L.S., and Crawford, M.L., eds., Fluid inclusions: applications to petrography, Min. Assoc. Can., Short Course Handbook, v. 6, p. 75-100.

Criss, R.E. and Taylor, H.P., 1983, $^{18}O/^{16}O$ and D/H study of Tertiary hydrothermal systems in the southern half of the Idaho batholith: Geol. Soc. Amer. Bull., v. 94, p. 640-663.

Deines, P., Langmuir, D. and Harmon, R.S., 1974, Stable carbon isotope ratios and the existence of a gas phase in the evolution of carbonate ground waters: Geochim. Cosmochim. Acta, v. 38, p. 1147-1164.

Drysdale, C.W., 1915, Bridge River map-area, Lillooet mining division: in Geol. Sur. Can., Summary report for 1914, p. 75-85.

Drysdale, C.W., 1917, Bridge River map-area, Lillooet mining division: in Geol. Sur. Can., Summary report for 1916, p. 45-54.

Eldridge, C.S., Bourcier, W.L., Ohmoto, H. and Barnes, H.L., 1988, Hydrothermal inoculation and incubation of the chalcopyrite disease in sphalerite: Econ. Geol., v. 83, p. 978-989.

Epstein, S., Graf, D.L. and Degens, E.T., 1964, Oxygen isotope studies on the origin of dolomites: in Craig, H., Miller, S.L. and Wasserburg, G.J., eds., Isotopic and Cosmic Chemistry, North Holland, p. 169-180.

Fisher, J.R., 1976, The volumetric properties of H_2O - A graphical portrayal: U.S.G.S., J. Res., v. 4, p. 189-193.

Friedman, I. and O'Neil, J.R., 1977, Compilation of stable isotope fractionation factors of geochemical interest: in Fleischer, M., ed., Data of geochemistry, Sixth Edition: U.S.G.S., Prof. Paper 440-KK, 64 p.

Fyon, J.A., Schwarcz, H.P. and Crocket, J.H., 1984, Carbonization and gold mineralization in the Timmins area, Abitibi greenstone belt: genetic links with Archean mantle CO_2-degassing and lower crust granulitization: Geol. Assoc. Can., Program with Abstracts, v. 9, p. 65.

Gabrielse, H., 1985, Major dextral transcurrent displacements along the Northern Rocky Mountain Trench and related lineaments in north-central B.C.: Geol. Soc. Amer. Bull., v. 96, p. 1-14.

Godfrey, J.D., 1962, The deuterium content of hydrous minerals from the east-central
Sierra Nevada and Yosemite National Park: Geochim. Cosmochim. Acta, v. 26, p.
1215-1245.

Goldfarb, R.J., Leach, D.L., Miller, M.L., and Pickthorn, W.J., 1986, Geology,
metamorphic setting, and genetic constraints of epigenetic lode-gold mineralization
within the Cretaceous Valdez Group, south-central Alaska: in Keppie, J.D., Boyle
R.W., and Haynes, S.J., eds., Turbidite-hosted gold deposits, Geol. Assoc. Can
Special Paper 32, p. 87-105.

Goldfarb, R.J., Leach, D.L., Pickthorn, W.J. and Patterson, C.J., 1988, Origin of lode
gold deposits of the Juneau gold belt, southeastern Alaska: Geology, v. 16, p. 440-
443.

Gonfiantini, R., 1978, Standards for stable isotope measurements in natural compounds:
Nature, v. 271, p. 534-536.

Griffis, A.T., McIntyre Porcupine Mines Limited, in Geology and ore deposits of Tisdale
Township: Ontario Dept. Mines, Geol. Rept. 58, p. 122-130.

Guilbert, J.M. and Park, C.F., Jr., 1986, The Geology of Ore Deposits: W.H. Freeman
and Co., New York, 985 p.

Harrop, J.C. and Sinclair, A.J., 1986, A re-evaluation of production data Bridge River-
Bralorne camp (92J): in Geological Fieldwork 1985, B.C. Min. of Ener., Mines and
Petrol. Res., Paper 1986-1, p. 303-310.

Heald, P., Foley, N.K. and Hayba, D.O., 1987, Comparative anatomy of volcanic-hosted
epithermal deposits: acid-sulfate and adularia-sericite types: Econ. Geol., v. 82, p. 1-
26.

Hedenquist, J.W. and Henley, R.W., 1985, The importance of CO_2 on freezing point
measurements of fluid inclusions: evidence from active geothermal systems and
implications for epither   ore deposition : Econ. Geol., v. 80, p. 1379-1406.

Henley, R.W., Norris, R.J. and Patterson, C.J., 1976, Multistage ore genesis in the New
Zealand geosyncline, a history of postmetamorphic lode emplacement: Mineralium
Deposita, v. 11, p. 180-196.

Higgins, N.C. and Kerrich, R., 1982, Progressive ^{18}O depletion during CO_2 separation
from a carbon dioxide-rich hydrothermal fluid: evidence from the Grey River
tungsten deposit, Newfoundland: Can. J. Earth Sci., v. 19, p. 2247-2257.

Hodgson, C.J., Chapman, R.S.G. and MacGeehan, P.J., 1982, Application of
exploration criteria for gold deposits in the Superior Province of the Canadian Shield
to gold exploration in the Cordillera: in Precious metals in the Northern Cordillera,
Assoc. Explor. Geochem., p. 173-206.

Hut, G., 1987, Consultants' group meeting on stable isotope reference samples for
geochemical and hydrological investigations: Vienna, 16-18 September, 1985:
International Atomic Energy Agency, Report to the Director General, 42 p.

Irving, E., Woodsworth, G.J., Wynne, P.J., and Morrison, A., 1985, Paleomagnetic evidence for the displacement from the south of the Coast Plutonic Complex, British Columbia: Can. J Earth Sci., v.22, p. 584-598.

Jouhin, F.R., 1948, Bralorne and Pioneer Mines in Structural Geology of Canadian Ore Deposits, Can. Inst. Mining Metall., Spec. Vol., p. 168-177.

Juan, V.C., 1946, Mineral resources of China: Econ. Geol., v. 41, p. 399-474.

Kalyuzhnyi, V.A., and Koltun, L.I., 1953, Some data on pressures and temperatures during formation of minerals in Nagol'nyy Kryazh, Donets Basin: Mineral. Sb. Lvov Geol. Obshch., v. 7, p. 67-74.

Kerrich, R., 1987, The stable isotope geochemistry of Au-Ag vein deposits in metamorphic rocks: in Stable isotope geochemistry of low temperature processes, Min. Assoc. Can., Short Course Handbook, v. 13, p. 287-336.

Kerrich, R. and Fryer, B.J., 1979, Archean pecious-metal hydrothermal systems, Dome Mine, Abitibi greenstone belt: II. REE and oxygen isotope isotope relations: Can. J. Earth Sci., v. 16, p. 440-458.

Kerrich, R. and Fyfe, W.S., 1981, The gold-carbonate association: source of CO_2, and CO_2 fixation reactions in Archean lode deposits: Chem. Geol., v. 33, p. 265-294.

Kerrich, R., Strong, D.F., Andrews, A.J. and Owsiacki, L., 1986, The silver deposits at Cobalt and Gowganda, Ontario: III. hydrothermal regimes and source reservoirs - evidence from H, O, C and Sr isotopes and fluid inclusions: Can. J. Earth Sci., v. 23, p. 1519-1550.

Kleinspehn, K.L., 1985, Cretaceous sedimentation and tectonics, Tyaughton-Methow basin, southwestern British Columbia: Can. J. Earth Sci., v. 22, p. 154-174.

Kyser, T.K., 1987, Standards and techniques: in Short course in stable isotope geochemistry of low temperature fluids, Kyser, T.K., ed., Min. Assoc. Can., Short Course Handbook, v. 13, p. 446-452.

Kyser, T.K., Janser, B.W., Wilson, M.R. and Hattie, I., 1986, Stable isotope geochemistry related to gold mineralization and exploration in the Western Shield, Clark, L.A., ed., Can. Inst. Mining Metall., Special Volume 38, p. 470-498.

Lehrberger, G., 1988, Gold-antimonite deposits in marine sediments of the Eastern Cordillera of the Bolivian Andes: in Bicentennial Gold '88, Extended Abstracts Poster Programme, v. 2, Geol. Soc. Australia Abstracts Series, No. 23, compiled by A.D.T. Goode, E.L. Smyth, W.D. Birch and L.I. Bosma, p. 319-321.

Leitch, C.H.B., Dawson, K.M. and Godwin, C.I., 1988, Late Cretacrʒus-Early Tertiary gold mineralizaticr A galena lead isotope study of the Bridge River Minig Camp, southwestern British Columbia, Canada: in Bicentennial Gold '88, Extended Abstracts Poster Programme, v. 2, Geol. Soc. Australia Abstracts Series, No. 23, compiled by A.D.T. Goode, E.L. Smyth, W.D. Birch and L.I. Bosma, p. 448.

Leitch, C.H.B. and Godwin, C.I., 1987, The Bralorne golr   leposit: an update (92J/15): in Geological Fieldwork, 1986, B.C. Min   ʒ   M   ies and Petrol. ʌes., Paper 1987-1, p. 35-38.

154

Leitch, C.H R. and Godwin, C.I., 1988, Isotopic ages, wall rock chemistry and fluid
inclus   data from the Bralorne gold vein deposit (92J/15W): in Geological
Fieldwork, 1987, B.C. Min. of Ener. Mines and Petrol. Res., Paper 1988-1, p. 301
324.

Madu, B.E., 1988, Petrographic, fluid inclusion and stable isotope study of the Snowbird
mesothermal Au-Sb occurrence near Stuart Lake, British Columbia: Unpublished
B.Sc. thesis, Univ. of Alberta, 43 p.

Magaritz, M. and Taylor, H.P., Jr., 1976a, $^{18}O/^{16}O$ and D/H studies along a 500 km
traverse across the Coast Range batholith and its country rocks, central British
Columbia: Can. J. Earth Sci., v. 13, p. 1514-1536.

Magaritz, M. and Taylor, H.P., Jr., 1976b, Isotopic evidence for meteoric-hydrothermal
alteration of plutonic igneous rocks in the Yakutat Bay and Skagway areas, Alaska:
Earth Planet. Sci. Lett., v. 30, p. 179-190.

Magaritz, M. and Taylor, H.P., Jr., 1986, $^{18}O/^{16}O$ and D/H studies of plutonic granitic
and metamorphic rocks across the Cordilleran batholiths of southern British
Columbia: J. Geophys. Res., v. 91, p. 2193-2217.

Maheux, P.J., Muehlenbachs, K. and Nesbitt, B.E., 1987, Evidence of highly evolved ore
fluids responsible for sulfide-associated gold mineralization in the Bridge River
District, B.C.: Geol. Assoc. Can., Program with Abstracts, v. 12, p. 70.

Marshall, B. and Taylor, B.E., 1981, Origin of hydrothermal fluids responsible for gold
deposition, Alleghany District, Sierra County, California: in Silberman, M.L. and
Field, C.W., eds., Proceedings of the symposium of mineral deposits of the Pacific
Northwest, U.S. Geol. Sur., Open-File Report 81-355, p. 281-291.

Matsuhisa, Y., Goldsmith, J.R. and Clayton, R.N., 1979, Oxygen isotopic fractionation
in the system quartz-albite-anorthite-water: Geochim. Cosmochim. Acta, v. 43, p.
1131-1140.

Matsuhisa, Y,, Matsubaya, O. and Sakai, H., 1971, BrF_5 technique for the oxygen
isotopic analysis of silicates and water: Mass Spec., v. 19, p. 124-133.

McCann, W.S., 1922, Geology and mineral deposits of Bridge River map-area, British
Columbia: Geol. Sur. Can., Memoir 130, 115 p.

McCrea, J.M., 1950, On the isotopic chemistry of carbonates and a paleotemperature scale:
J. Chem. Physics, v. 18, p. 849-857.

Monger, J.W.H., 1984, Cordilleran tectonics: a Canadian perspective: Bull. Soc. Géol.
France, 1984, no. 2, p. 255-278.

Monger, J.W.H., Price, R.A., and Tempelman-Kluit, D.J., 1982, Tectonic accretion and
the origin of the two major metamorphic and plutonic welts in the Canadian
Cordillera: Geology, v. 10, p. 70-75.

Murowchick, J.B., Muehlenbachs, K. and Nesbitt, B.E., 1987, Nature of ore fluids in the Coquihalla gold belt: in Elliot, I.L. and Smee, B.W., eds., Geo/Expo '86: Exploration in the North American Cordillera: Assoc. Explor. Geochem., p. 160-167

Neir, A.O., 1947, A mass spectrometer for isotope and gas analysis: Rev. Sci. Instr., v. 18, p. 398-411.

Nesbitt, B.E. and Muehlenbachs, K., 1988, Genetic implications of the association of mesothermal gold deposits with major strike-slip fault systems: in Kisvarsanyi, G. and Grant, S.K., eds., Proceedings of North American conference on tectonic control of ore deposits and the vertical and horizontal extent of ore systems, University of Missouri at Rolla, p. 57-66.

Nesbitt, B.E., Mueh.enbachs, K. and Murowchick, J.B., in press, Genetic implications of stable isotope characteristics of mesothermal Au deposits and related Sb and Hg deposits in the anadian Cordillera: Econ. Geol.

Nesbitt, B.E., Muro. chick, J.B. and Muehlenbachs, K., 1986, Dual origin of lode gold deposits in the Canadian Cordillera: Geology, v. 14, p. 506-509.

Nesbitt, B.E., Murowchick, J.B. and Muehlenbachs, K., 1987, Reply to a comment on "Dual origins of lode gold posits in the Canadian Cordillera": Geology, v. 15, p. 473-474.

Northrop, D.A. and Clayton, R.N., 1966, Oxygen isotope fractionations in systems containing dolomite: J. Geology, v. 74, p. 174-196.

Ohmoto, H., 1972, Systematics of sulfur and carbon isotopes in hydrothermal ore deposits: Econ. Geol., v. 67, p. 551-578.

Ohmoto, H. and Ry, R.O., 1979, Isotopes of sulfur and carbon: in Barnes, H.L., ed., 2 ed., Geochemistry of hydrothermal ore deposits, John Wiley and Sons, New York, p. 509-567.

O'Neil, J.R. and Epstein, S., 1966, A method for oxygen isotope analysis of milligram quantities of water and some of its applications: J. Geophys. Res., v. 71, p. 4955-4961.

O'Neil, J.R. and Taylor, H.P., Jr., 1969, Oxygen isotope equilibrium between muscovite and water: J. Ge phys. Res., v. 74, p. 6012-6022.

O'Neil, J.R., Clayton, R.N.and Mayeda, T.K., 1969, Oxygen isotope fractionation in divalent metal carbonates: J. Chem. Phys., v. 51, p. 5547-5558.

O'Shea, P.J. and Pertzel, B.A., 1988, The Brunswick gold-antimony mine, Costerfield, Victoria: in Bicentennial Gold '88, Extended Abstracts Poster Programme, v. 2, Geol. Soc. Australia Abstracts Series, No. 23, compiled by A.D.T. Goode, E.L. Smyth, W.D. Birch and L.I. Bosma. .. 282-284.

Paterson, C.J., 1982, Oxygen isotopic evidence for the origin and evolution of a scheelite ore-forming fluid, Glenorchy, New Zealand: Econ. Geol., v. 77, p. 1672-1687.

Paterson, C.J., 1986, Controls on gold and tungsten mineralization in metamorphic-hydrothermal systems, Otago, New Zealand: in Turbidite hosted gold deposits, eds. Keppie, J.D., Boyle, R.W. and Haynes, S.J., Geol. Assoc. Can., Special Paper 32, p. 25-39.

Pearson, D.E., 1976, Mineralization in the Bridge River camp: Geology in British Columbia, 1975, B.C. Min. of Ener. Mines and Petrol. Res., p. G57-G63.

Pickthorn, W.J., Goldfarb, R.J. and Leach, D.L., 1987, Comment on "Dual origins of lode gold deposits in the Canadian Cordillera": Geology, v. 15, p. 471-472.

Pirajno, F., 1979, Geology, geochemistry and mineralisation of the Endeavor Inlet antimony-gold prospect, Marlborough Sounds, New Zealand: New Zealand J. Geol. Geophys., v. 22, p. 227-237.

Potter, C.J., 1983, Geology of the Bridge River Complex, southern Shulaps Range, British Columbia: a record of Mesozoic convergent tectonics: Unpublished Ph.D. thesis, Univ. of Washington, Seattle, Washington, 192 p.

Potter, C.J., 1986, Origin, accretion, and postaccretionary evolution of the Bridge River Terrane, southwest British Columbia: Tectonics, v. 5., no. 7, p. 1027-1041.

Potter, R.W., and Brown, D.L., 1977, The volumetric properties of aqueous sodium chloride solutions from 0° to 500°C at pressures up to 2000 bars based on a regression of available data in the literature: U.S.G.S., Bull. 1421-C, 36 p.

Potter, R.W. and Clynne, M.A., 1978, Solubility of highly soluble salts in aqueous media - Part 1, NaCl, KCl, CaCl₂, NaSO₄, and K₂SO₄ solubilities to 100°C: U.S. Geol. Sur., J. Res., v. 6, p. 701-705.

Potter, R.W., Clynne, M.A., and Brown, D.L., 1977, Freezing point depression of aqueous sodium chloride solutions: Econ. Geol., v. 73, p. 284-285.

Price, R.A., Monger, J.W.H., and Muller, J.E., 1981, Cordilleran cross-section; Calgary to Victoria: in Field guides to geology and mineral deposits, Calgary '81, Geol. Sur. Can., Min. Assoc. Can., Can. Geophys. Union Annual Meeting, p. 261-334.

Price, R.A., Monger, J.W.H. and Roddick, J.A., 1985, Cordilleran cross-section; Calgary to Vancouver: Geol. Soc. Am. Cordilleran Section guidebook, p. 3-1 to 3-85.

Ramboz, C., Pichavant, M., and Weisbrod, A., 1982, Fluid immiscibility in natural processes: use and misuse of fluid inclusion data II. Interpretation of fluid inclusion data in terms of immiscibility: Chem. Geol., v. 37, p. 29-48.

Roddick, J.A. and Hutchison, W.W., 1973, Pemberton (East-half) map area, British Columbia: Geol. Sur. Can., Paper 73-17, 21 p.

Roedder, E., 1984a, Fluid inclusion evidence bearing on the environments of gold deposition: in Symposium Proceedings, Gold '82, Geol. Soc. Zimbabwe, Spec. Pub. 1, A.A. Balkema, Rotterdam, The Netherlands, p. 129-163.

Roedder, E., 1984b, Fluid Inclusions: Reviews in Mineralogy, v. 12, Min. Soc. Amer., 644 p.

Roedder, E. and Bodnar, R.J., 1980, Geologic pressure determinations from fluid inclusion studies: Ann. Rev. Earth Planet. Sci., v. 8, p 263-301.

Rosebaum, J., and Sheppard, S.M.F., 1986, An isotopic study of siderites, dolomites and ankerites at high temperatures: Geochim. et Cosmochim. Acta, v. 50, p. 1147-1150.

Rubinson, M. and Clayton, R.N., 1969, Carbon-13 fractionation between aragonite and calcite: Geochim. Cosmochim. Acta, v. 33, p. 997-1002.

Rumble, D., 1978, Mineralogy, petrology, and oxygen isotopic geochemistry of the Clough Formation, Black Mountain, western New Hampshire, U.S.A.: J. Petrol., v. 19 Part 2, p. 317-340.

Rusmore, M.E., 1985, Geology of the Upper Triassic Cawallader Group and its bounding faults, southwestern British Columbia: Unpublished Ph.D. thesis, Univ. of Washington, Seattle, Washington, 174 p.

Rusmore, M.E., 1987, Geology of the Cadwallader Group and the Intermontane-Insular superterrane boundary, southwestern British Columbia: Can. J. Earth Sci., v. 24, p. 2279-2291.

Sharma, T. and Clayton, R.N., 1965, Measurement of $^{18}O/^{16}O$ ratios of total oxygen of carbonates: Geochim. Cosmochim. Acta, v. 29, p. 1347-1353.

Shepherd, T.J., Rankin, A.H. and Alderton, D.H.M., 1985, A practical guide to fluid inclusion studies: Chapman and Hall in association with Methuen Inc., New York, 239 p.

Sheppard, S.M.F. and Schwarcz, H.P., 1970, Fractionation of carbon and oxygen isotopes and magnesium between metamorphic calcite and dolomite: Contrib. Mineral. Petrol., v. 26, p. 161-198.

So, Chil-Sup and Shelton, K.L., 1987, Stable isotope and fluid inclusion studies of gold- and silver-bearing hydrothermal vein deposits, Cheonan-Cheonyang-Nonsan Mining District, Republic of Korea: Cheonan Area: Econ. Geol., v. 82, p. 987-1000.

Suzuoki, T. and Epstein, S., 1976, Hydrogen isotope fractionation between OH-bearing minerals and water: Geochim. Cosmo. Acta, v. 40, p. 1229-1240.

Swanenberg, H.E.C., 1979, Phase equilibria in carbonic systems and their applications to freezing studies of fluid inclusions: Contrib. Mineral. Petrol., v. 68, p. 303-306.

Taylor, B.E., 1987, Stable isotope geochemistry of ore-forming fluids: in Stable isotope geochemistry of low temperature fluids, Kyser, T.K., ed., Min. Assoc. Can., Short Course Handbook, v. 13, p. 337-445.

Taylor, H.P., Jr., 1968, The oxygen isotope geochemistry of igneous rocks: Contrib. Mineral. Petrol., v. 19, p. 1-71.

Taylor, H.P., Jr., 1974, The application of oxygen and hydrogen isotope studies to problems of hydrothermal alteration and ore deposition: Econ. Geol., v. 69, p. 843-883.

Taylor, H.P., Jr., 1977, Water/rock interactions and the origin of H_2O in granitic
batholiths: J. Geol. Soc. Lon., v. 133, p. 509-558.

Taylor, H.P., Jr., 1979, Oxygen and hydrogen isotope relationships in hydrothermal
mineral deposits: in Barnes, H.L., ed., Geochemistry of Hydrothermal Ore Deposits,
2 ed., John Wiley and Sons, New York, p. 236-277.

Tempelman-Kluit, D.J., 1979, Transported cataclasite, ophiolite and granodiorite in
Yukon: Evidence of arc-continent collision: Geol. Sur. Can., Paper 79-14, 27 p.

Tipper, H.W., 1984, The allochthonous Jurassic-Lower Cretaceous terranes of the
Canadian Cordillera and their relation to correlative strata of the North American
craton: in Jurassic-Cretaceous biochronology and paleogeography of North America,
Westerman, G.E.G., ed., Geol. Assoc. Can., Special Paper 27, p 113-120.

Tipper, H.W., Woodsworth, G.J., and Gabrielse, H., co-ordinators, 1981, Tectonic
assemblage map of the Canadian Cordillera: Geol. Sur. Can. Map 1505A, scale
1:2,000,000.

Weir, R.H., Jr., and Kerrick, D.M., 1987, Mineralogic, fluid inclusion, and stable isotope
studies of several gold mines in the Mother Lode, Tuolumne and Mariposa counties,
California: Econ. Geol., v. 82, p. 328-344.

Wenner, D.B. and Taylor, H.P., Jr., 1969, δD and $\delta^{18}O$ studies in serpentinization of
ultramafic rocks: Geol. Soc Amer., Abstracts with programs, Atlantic City, p. 234-
235.

Wenner, D.B. and Taylor, H.P., Jr., 1971, Temperatures of serpentinization of ultramafic
rocks based on $^{18}O/^{16}O$ fractionation between coexisting serpentine and magnetite:
Contr. Mineral. Petrol., v. 32, p. 165-185.

Wenner, D.B. and Taylor, H.P., Jr., 1973, Oxygen and hydrogen isotope studies of the
serpentinization of ultramafic rocks in oceanic environments and continental ophiolite
complexes: Am. J. Sci., v. 273, p. 207-239.

Whittaker, E.J.W. and Zussman, J., 1956, The characterization of serpentine minerals by
X-ray diffraction: Mineralogical Mag., v. 31, p. 107-126.

Woodsworth, G.J., 1977, Geology of Pemberton (92J) map-area: Geol. Sur. Can., Open
File Map 482, scale 1:250,000.

Woodsworth, G.J., Pearson, D.E., and Sinclair, A.J., 1977, Metal distribution patterns
across the eastern flank of the Coast Plutonic Complex, south-central British
Columbia: Econ. Geol., v. 72, p. 170-183.

Zhang, X., Nesbitt, B.E. and Muehlenbachs, K., in press, Gold mineralization in the
Okanagan Valley, southern British Columbia: Fluid inclusion and stable isotope
studies: Econ. Geol., 36 p.

APPENDIX

The following equilibrium fractionation expressions have been used throughout this study. Mineral pair fractionation curves are derived from combinations of these expressions, except where noted.

For $\delta^{18}O$:

$\Delta_{qz\text{-}H2O} = 3.34(10^6/T^2) - 3.31$ $250°$ to $500°C$ Matsuhisa *et al.*, 1979.

$\Delta_{cal\text{-}H2O} = 2.78(10^6/T^2) - 2.89$ $0°$ to $500°C$ O'Neil *et al.*, 1969.

$\Delta_{dol\text{-}H2O} = 3.20(10^6/T^2) - 1.50$ $300°$ to $510°C$ Northrop and Clayton, 1966.

(This expression substituted for $\Delta_{ank\text{-}H2O}$.)

$\Delta_{dol(ank)\text{-}cal} = 0.45(10^6/T^2) - 0.40$ $100°$ to $650°C$ Sheppard and Schwarcz, 1970.

$\Delta_{mu\text{-}H2O} = 2.38(10^6/T^2) - 3.89$ $400°$ to $650°C$ O'Neil and Taylor, 1969.

(This expression substituted for $\Delta_{ser\text{-}H2O}$.)

$\Delta_{mag\text{-}H2O}$ $0°$ to $800°C$ Curve given by Becker, 1971 (Figure 8, p. 81).

$\Delta_{chl\text{-}H2O} = 1.56(10^6/T^2) - 4.70$ $500°$ to $800°C$ Wenner and Taylor, 1971.

(This expression was extrapolated to lower temperatures and substituted for $\Delta_{serp\text{-}H2O}$.)

$\Delta_{serp\text{-}mag} = 1.69(10^6/T^2) + 1.68$ $0°$ to $500°C$ Wenner and Taylor, 1971.

$\Delta_{qz\text{-}dol(ank)} = 0.9(10^6/T^2) - 2.2$ $300°$ to $510°C$
(Calculated from $\Delta_{qz\text{-}H2O}$ of Bottinga and Javoy (1973) and $\Delta_{dol\text{-}H2O}$ of Northrop and Clayton (1966).)

APPENDIX (Continued)

For δD:

$$\Delta_{mu\text{-}H_2O} = 22.1(10^6/T^2) - 19.1 \qquad 450° \text{ to } 850°C \qquad \text{Suzuoki and Epstein, 1976.}$$

(This expression substituted for $\Delta_{ser\ H_2O}$ and extrapolated to lower temperatures.)

$\Delta_{serp\text{-}H_2O}$: curve given by Wenner and Taylor, 1973 (Figure 7, page 219).

For δ¹³C:

$$\Delta_{dol\text{-}cal} = 0.18(10^6/T^2) + 0.17 \qquad 100° \text{ to } 650°C \qquad \text{Sheppard and Schwarcz, 1970.}$$

(This expression substituted for $\Delta_{ank\text{-}cal}$.)

$$\Delta_{CO_2\text{-}cal} = -2.9880(10^6/T^2) \qquad 0° \text{ to } 700°C \qquad \text{Bottinga, 1968.}$$
$$+ 7.6663(10^6/T) - 2.4612$$